Alma Mater Studiorum – Università di Bologna

DOTTORATO DI RICERCA IN

Biologia cellulare e molecolare

Ciclo: *XXX*

Settore Concorsuale: 05/D1

Settore Scientifico Disciplinare: BIO/09 FISIOLOGIA

AGC-1 deficiency, a rare genetic demyelinating and neurodegenerative disease: a study on oligodendrocyte precursor cells in cell lines, a mouse model and human iPS-derived brain cells.

Presentata da: **Sabrina Petralla**

Coordinatore Dottorato

Prof. Giovanni Capranico

Supervisore

Prof.ssa Barbara Monti

Co-supervisore

Dott. Luis Emiliano Peña-Altamira

Esame finale anno 2018

TABLE OF CONTENTS

ABSTRACT

AGC1 deficiency is a rare genetic neurodegenerative disease caused by defects in the SLC25A12 gene encoding for Aralar/AGC1, a mitochondrial aspartate-glutamate carrier that plays an important role in the metabolism of brain amino acids and myelin synthesis. In patients, AGC1 mutations lead to drastic reduction of carrier activity, which results in severe hypotonia, developmental delay, intractable epilepsy and cortical atrophy with altered myelin formation in the CNS, most likely due to a dramatic reduction of N-acetyl aspartate (NAA) levels in the brain[1,2]. AGC1 deficiency mechanisms are not yet clear and currently there is no therapeutic treatment. The aim of this PhD thesis was to study the molecular mechanisms underlying AGC1 deficiency in appropriate *in vitro* and *in vivo* disease models, in particular by focusing on oligodendrocyte precursor alterations to better define pathogenetic mechanisms that could potentially lead to identify new potentially interesting therapeutic targets.

Studies were performed on immortalized mouse oligodendrocyte precursor cells, Oli-Neu cells (kind gift from Dr. Trotter), where we partially silenced AGC1 expression in order to obtain a reduction of AGC1 carrier activity down to about 30-40% compared to control cells, as observed in mitochondria from human patients. Then, the obtained results were validated in an AGC1 deficiency *in vivo* model represented by SLC25A12 heterozygous knockout mice ($AGC1^{+/-}$ C57BL6/N background), a good model for the study of AGC1 deficiency, since patients with this disease are characterized by reduced carrier activity rather than total loss of carrier activity.

Furthermore, our study focused on the evaluation of Neural Stem Cells (NSCs) proliferation and differentiation in neuronal and glia cells, both astrocytes and oligodendrocytes, in $AGC1^{+/+}$ and $AGC1^{+/-}$ neurospheres derived from the subventricular zone (SVZ) of our mouse model. Lastly, preliminary experiments have been performed on NSCs derived from induced Pluripotent Stem (iPS) cells from AGC1 deficiency patients and healthy controls, in order to further validate our data in human cells

All our results showed a proliferation deficit of oligodendrocyte precursor cells that was not due to mitochondrial biochemical alterations, but rather associated with an alteration of trophic factors essential for maintaining the balance between oligodendrocyte proliferation and differentiation[3], mainly PDGFα and TGFβ. These results supported that alterations

induced by AGC1 reduced activity could impair the physiological cross-talk mediated by growth factors between neurons and OPCs necessary for OPCs proliferation and neuronal survival. The importance of this study lies also on the fact that mitochondrial dysfunction is at the basis not only of AGC1 deficiency, but also of other neurodegenerative and demyelinating diseases, some of which are rare, while others are widely spread, such as multiple sclerosis[4-6]. Thus, the obtained results could be useful to understand disease mechanisms and give hope for the treatment of many human demyelinating diseases.

1. INTRODUCTION

1.1. AGC1 deficiency

AGC1 deficiency is a recessive autosomal genetic disease caused by SLC25A12 gene mutations, which codes for the mitochondrial Aspartate Glutamate Carrier 1 (AGC1)/Aralar[1,2], characterized by neuronal degeneration and global white matter hypomyelination due to reduced activity of the mitochondrial transporter in the central nervous system (CNS). The first human case of AGC1 deficiency was reported in 2009 in a three-year old Swedish girl, who five months after birth showed delayed psychomotor development, severe muscular hypotonia, poor control of head support, and epilepsy. Following SLC25A12 gene sequencing, the first AGC1 mutation represented by a c.1769A → G transition in exon 17 was identified, causing a missense Q590R mutation, which leads to a leak of carrier activity (Fig. 1.1).

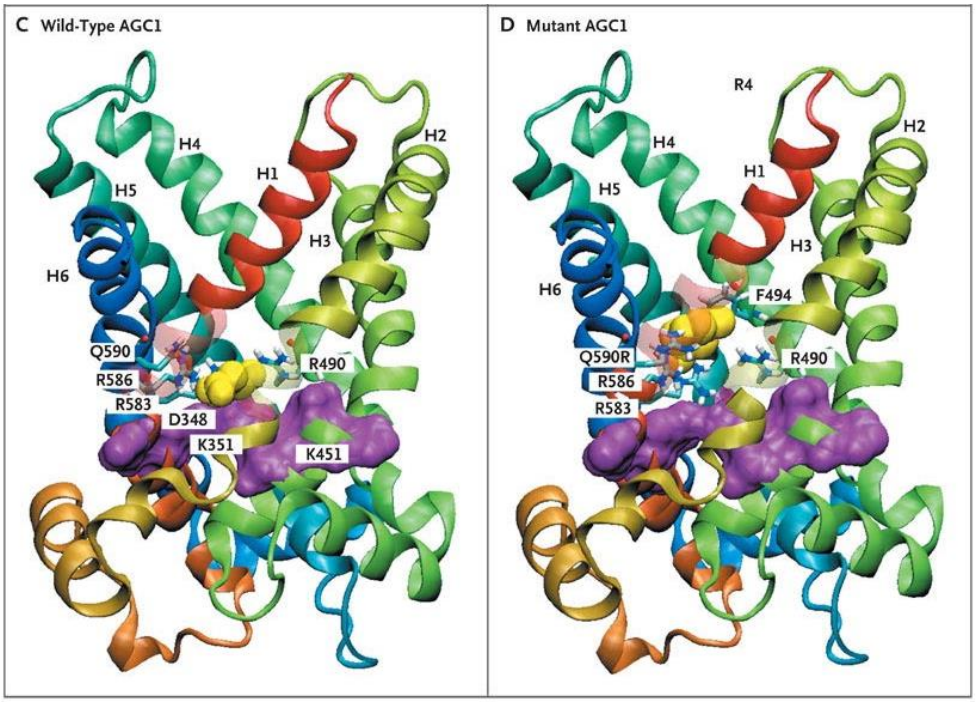

Figure 1.1: *Wild-type AGC1 and Q590R-mutant AGC1 crystallographic structures. Aspartate binding (shown in yellow) in the wild-type AGC1 (panel C) and Q590R-mutant AGC1 (panel D) is shown laterally. Sticks represent some residues found within 4 Å of the substrate. Parts of helices I and II and portions of the salt-bridge network (only in panel C) are rendered transparent to facilitate the viewing of the substrate and lateral chains of some amino acids. Purple surfaces show salt-bridges between residues D348 and K451, E448 and K543*[2].

In fact, residue Q590, highly preserved in the aspartate-glutamate mitochondrial carrier family, is located above the substrate-binding site and, as a result from this mutation, the arginine residue at position 590 appears to move away from the binding site, which is required to maintain the substrate-protein interaction.

Recently, a second mutation in the SLC25A12 gene was identified in a pair of Indian-origin twins[1] which consists in a c.1058G → A transition causing the R353Q mutation in exon 11. Just as for the c.1769A → G transition, this mutation results in a reduction of the mitochondrial carrier activity. However, studies in Escherichia coli CO214 (DE3) on reconstituted liposomes containing mutant (Q590R) and wild-type recombinant AGC1 proteins showed that mutant AGC1 proteins are still able to integrate at the internal mitochondrial membrane as wild-type AGC1.

Initially identified by Wibom as mainly a demyelinating disease due to oligodendrocyte dysfunction[2], Magnetic Resonance Imaging analysis (MRI) on patient brain (Fig. 1.2) showed a progressive reduction in brain volume with the formation of prominent cortical loci, ventricle enlargement, and global myelination loss which led to the hypothesis that AGC1 deficiency may be a neurodegenerative disease due to primary dysfunction of neuronal metabolism and consequent impairment of the myelination process and white matter. However, the cellular and molecular mechanisms of neurodegeneration and demyelination in AGC1 deficiency still remain to be clarified.

Figure 1.2: *MRI of an AGC1 deficiency patient. Panel A shows the 8-month and 16-month MRI brain images of the patient. In both images, a progressive reduction in brain volume is shown with the formation of prominent cortical grooves and ventricle enlargement; development loss of a low age-correlated signal in the cerebral hemisphere white matter was also measured (as opposed to what expected in the myelination process during development). Panel B, shows the patient MRI image at 2 years and 9 months of age with a persistent high signal in the white matter, consistent with ongoing hypomyelination. The analysis shows that hypomyelination persists in the periphery of the frontal, occipital and temporal lobes; however, normal myelination was observed in the cerebellum and brainstem whereas the pale globe and putamen show a slight decrease in volume[2].*

1.2. AGC1 is a member of Calcium-binding mitochondrial carriers (CaMCs)

Calcium-binding Mitochondrial Carriers (CaMCs) are a family of carriers containing six transmembrane helices localized at the internal mitochondrial membrane. Their secondary structure is characterized by a C-terminal domain that corresponds to the MC homologous region of 300 amino acids, and an N-terminal domain containing four calcium-binding EF-hand motifs, localized at the intermembrane space[7] (Fig. 1.3).

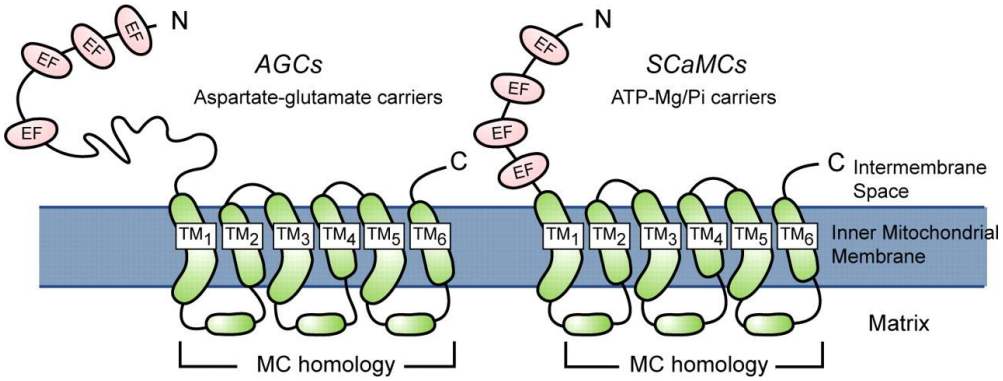

Figure 1.3: *Ca^{2+}- dependent mitochondrial carrier (CaMC) secondary structure. The C-terminal domain corresponds to the MC homology region consisting of 6 transmembrane helices (TM1-6), while the N-terminal domain contains the Ca^{2+}-binding EF-hand motifs. 3 small propellers in the loops between TM 1-2, TM 3-4 and TM 5-6 protrude into the mitochondrial matrix and are parallel to the membrane surface. The MC region forms a basket that opens into the intermembrane space, with a funnel cavity ending near the surface of the matrix[7].*

Two types of CaMCs, aspartate-glutamate carriers (AGCs) and ATP-Mg/Pi carriers, have been distinguished. Concerning AGCs, two isoforms have been identified: Aralar/AGC1[8], expressed in the central nervous system and skeletal muscle, and Citrin/AGC2[9,10] expressed mainly in liver, kidney and heart, with a sequence homology of 77.8% and encoded respectively by genes on chromosomes 2q31[11] and 7q21[12]. Another AGC homolog, Agc1p, has also been identified at the mitochondrial level in yeast, but it differs from the previous isoforms because it does not contain any calcium binding domains[13].

SLC25A12 mutations cause AGC1 deficiency whereas mutations in the SLC25A13 gene, encoding for AGC2, cause the adult-onset type 2 citrullinemia (CTLN2) and neonatal intrahepatic cholestasis (NiCCD)[14]. While NiCCD leads to citrullinemia, bilirubinemia, poor growth, intrahepatic cholestasis and cirrhosis and most of the affected newborns have a spontaneous resolution of symptoms within one year, adult-onset CTLN2 is characterized by hypoproteinemia, hyperammonemia, citrullinemia, neuropsychiatric symptoms, coma, brain

edema, pancreatitis and hepatic steatosis. In CTLN2 patients, the lack of cytosolic aspartate and inhibition of the malate-aspartate NADH shuttle (MAS; as a consequence of the inhibition of cytosolic NADH oxidation) causes hyperlipidemia and fatty liver disease, carbohydrate aversion, preference for high-protein diets, inhibition of alcohol metabolism and inhibition of the argininosuccinate synthetase (ASS) reaction due to the lack of cytosolic aspartate provided by mitochondria[14].

1.3. AGC1 physiopathological role in the Central Nervous System (CNS)

The AGC1 carrier is encoded by the SLC25A12 gene and is the largest AGC isoform expressed in the CNS, mainly in the gray matter. In situ hybridization studies[15] have shown that the expression of the Aralar/AGC1 carrier in adult mouse brain is restricted to areas rich in neurons and undetectable in white matter (Fig. 1.4). In addition, AGC1 mitochondrial levels were significantly higher in neuronal cultures than in glial cultures and also increased with maturation of neurons in culture, providing further confirmation for its predominantly neuronal localization[15].

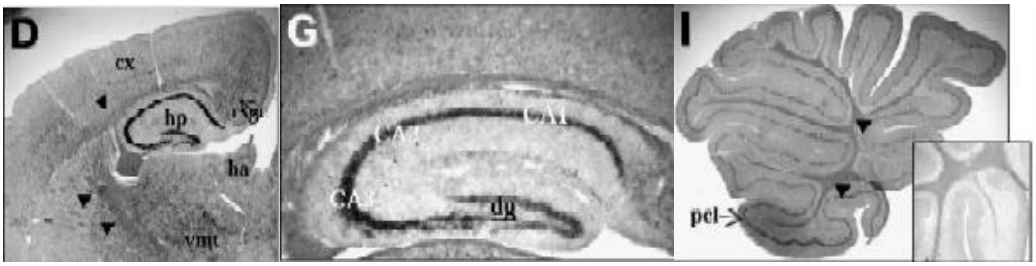

Figure 1.4: *Distribution of Aralar/AGC1 transcript in adult mouse brain. For identification, sections were hybridized with a probe labeled with digoxigenin specific for the SLC25A12 gene. The images show a high expression of AGC1 in brain regions particularly rich in neurons: cortex (D), hippocampus (G), cerebellum (I)[15].*

The first report concerning the activity of AGCs dates back to 1979 following studies on metabolite transport at the mitochondrial membrane[16]. AGC1 play a crucial role in myelin synthesis by oligodendrocytes since they catalyze a unidirectional transport reaction by exchanging aspartate from the mitochondrial matrix to the intermolecular space in exchange for glutamate and a proton. This transport is regulated by the membrane proton gradient and is stimulated by calcium, acting at the intermembrane space where 4 EF-hands are located[17]. Aspartate in the intermembrane space is then transported into the cytoplasm, where it

undergoes the action of N-acetyl transferase (Asp-NAT), which transfers an Acetyl-CoA molecule to form NAA (N-acetylaspartate), precursor of the myelin lipid synthesis[18-21]. NAA is then introduced through the transposon into the oligodendrocyte cytoplasm by NaDC3[22], where it becomes a substrate for aspartocylase (ASPA), which converts NAA into fatty acids and steroids needed for myelin synthesis. After myelination, during the postnatal development of the CNS, NAA is involved in myelin lipid turnover, and has also a role in neuronal mitochondria[23].

The two AGCs are also members of the malate-aspartate NADH shuttle (Fig. 1.5). The MAS is the main way to transfer NADH produced by glycolysis from the cytosol within the mitochondrial matrix during the oxidative phosphorylation process, thus favoring ATP synthesis by avoiding a blockage of the glycolytic process at the level of glyceraldehyde-3-phosphate[24]. Consequently, genetic variations that alter Aralar/AGC1 expression or its insertion into the internal mitochondrial membrane can lead to alterations in MAS function, aspartate synthesis by neuronal mitochondria or N-acetylaspartate production, leading to the involvement in the onset of diseases affecting the central nervous system.

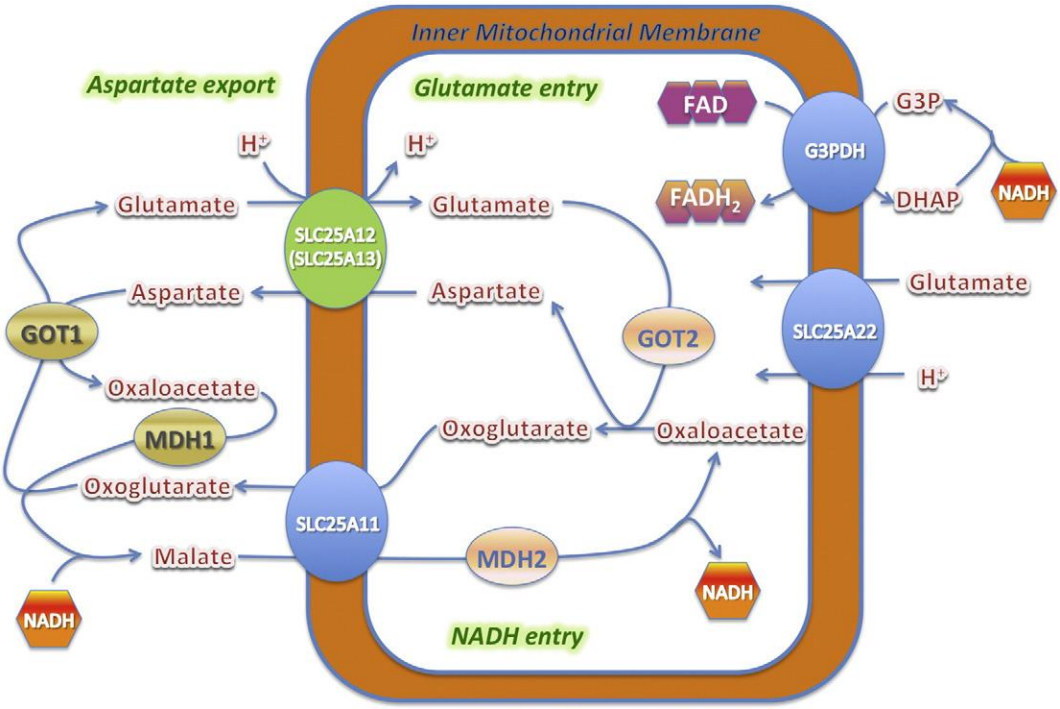

Figure 1.5: *Role of AGC1 in the synthesis of N-acetylaspartate (NAA) and malate-aspartate NADH shuttle (MAS)[14].*

In addition to its role in metabolism and myelin synthesis in the CNS, AGC1 is also involved in psychiatric disorders such as autism spectrum disorder (ASD) and schizophrenia. Autism, originally called Kanner Syndrome, is considered a neuropsychiatric disorder that affects

brain function. Given the variety of symptoms and complexity to provide a coherent and unified clinical definition, the use of Autistic Spectrum Disorder, more properly, has recently been adopted and includes a variety of pathologies or common-feature syndromes. Polymorphisms identified in the SLC25A12 gene seem to be associated with autism despite not achieving a significant genomic incidence, however this has led to hypothesize the involvement of AGC1 in susceptibility to autism[25-28], although some studies suggest the opposite[29,30]. In post-mortem brain, AGC1 is overexpressed in the lateral frontal cortex of autistic patients[28].This means that expression changes may be considered as a consequence of the disorder, and not that AGC1 activity is associated with autism. A valid hypothesis might be that gene defects are compensated by up-regulation or functional redundancy in certain tissues, whereas in the brain the lack of compensatory mechanisms could cause increased sensitivity to respiratory deficiency. AGC1 also seems to be associated with schizophrenia, as shown by studies on schizophrenic patients through magnetic resonance revealing a reduction of NAA levels in large regions of the brain[31]. Moreover, NAA levels decreased in schizophrenic patients in the absence of hippocampal volume differences, which could mean that neuronal loss alone is not enough to explain the reduction in NAA levels but rather could be due to cellular dysfunction interfering with NAA metabolism[32]. In fact, NAA metabolism seems to be compromised by AGC1 *in vivo* as shown by MRI and *post-mortem* samples where reduced myelination was detected[33]. Nevertheless, no correlation has been demonstrated between SLC25A12 and schizophrenia, although NAA levels may play a role in the disease as observed in schizophrenic brains at the prefrontal, temporal cortex, and hippocampal level[34].

1.4. AGC1 deficiency *in vivo* model

The use of functional *Knockout* AGC1 mice as AGC1 deficiency *in vivo* models has been reported in the literature. One of the first reports dates back to 2005; Jalil and colleagues developed homozygous mutant mice through gene trapping by inserting a targeting vector containing a premature stop codon at exons 13-14 in ES SVJ129 cells. Chimeric mice were generated by implanting SLC25A12 mutant cells into C57BL murine blastocysts. SLC25A12/Aralar$^{+/-}$ hybrids were crossed to produce homozygous SLC25A12/Aralar$^{-/-}$ mice expressing a truncated AGC1 protein[35]. According to protein sequence analysis (www.uniprot.org) the truncated protein contained one catalytic site for aspartate, called Solcar-1, therefore a mutant protein with residual activity was produced.

Another SLC25A12 KO mouse model[24] was created by inserting a construct containing a premature stop codon at 1 exon in ES C57BL/6 embryonic stem cells. This AGC1 protein product was a fully inactive truncated protein containing no AGC1 catalytic sites. Clones containing the targeting vector were identified and used to develop chimeric mice and then crossed with C57BL/6Tac females. The first generation was then screened to identify SLC25A12 heterozygous mice ($AGC1^{+/-}$) crossed with an $AGC1^{+/-}$ or $AGC1^{+/+}$ parent mice to obtain homozygous SLC25A12 KO line ($AGC1^{-/-}$). Phenotypically, AGC1 KO mice showed delayed growth, were smaller than $AGC1^{+/+}$ and $AGC1^{+/-}$ mice and displayed a much lower lifespan of 22-23 days[35]. Moreover, at postnatal day 15, AGC1 KO mice manifested tremors and motor coordination problems. In addition, while KO mice were initially indistinguishable from wild-type and heterozygous mice, after some days they were recognized due to their smaller size and growth retardation. Moreover, no AGC1 KO mice survived longer than four weeks after birth. By examining SLC25A12 KO mouse brains, a decrease in brain size and myelination, myelin galactose-cerebroside lipid and N-acetylaspartate (NAA) and aspartate levels were observed, suggesting a role for AGC1 in myelin synthesis. Specifically, immunohistochemical studies found that the major differences between KO mice compared to wild-type mice at postnatal days 13 and 14 (P13 and P14) were a size reduction of the hypothalamus, thalamus and striatum as well as a delay in brain development[24] (Fig. 1.6). Furthermore, Myelin basic protein (MBP) positive fibers were reduced in KO mice. Myelination alterations were also observed through lipid associated protein labeling; MBP was significantly reduced in KO P10 mice compared to wild-type mice (approximately 75%), while acid fibrillation protein, synapsin and neurofilaments did not show any expression differences.

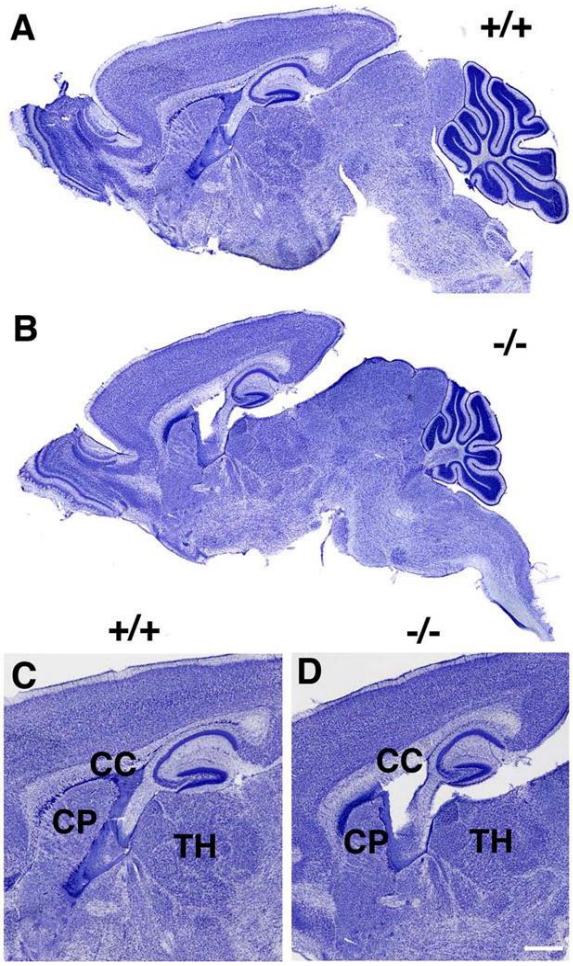

Figure 1.6: *SLC25A12 knockout pups have a smaller brain. P13 brain tissue section from a wild-type AGC1$^{+/+}$ (A, C) or knockout mouse, AGC1$^{-/-}$ (B, D). Brain regions are overall smaller in the knockout mouse brain. Corpus callosum (CC), caudate putamen (CP) and thalamus (TH).*

Alterations in Purkinje cells have been observed in AGC1 KO mouse cerebellum, confirming developmental delay. Purkinje cells were frequently misaligned and showed smaller dendritic spine extension, leading to thinning of the molecular layer. Immunohistochemical analysis performed on cortical sections of KO mice, by using an anti-SMI-31 antibody that recognizes the phosphorylated form of NF-M and NF-H neurofilament proteins (physiologically located in axons) showed an altered distribution of neurofilaments in the neocortex (Fig. 1.7). AGC1 KO mice showed neurofilament accumulation in the deeper layers of the cortex, while wild-type mice had more neural processes at layers IV and VI[24]. Moreover, a decrease in MAG expression (which encodes for a glycoprotein associated with myelin) was observed in the brain of adult heterozygous male mice, compared to WT mice.

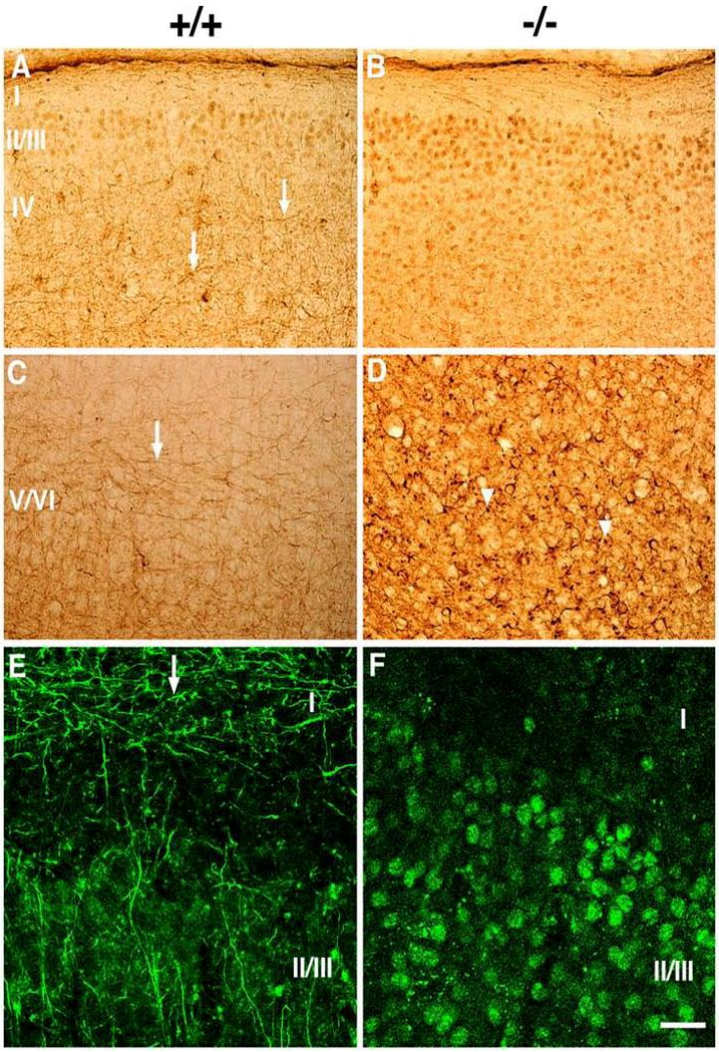

Figure 1.7: *Neurofilament alterations in SLC25A12 KO mice. Sagittal section of WT (A, C, E) and KO (B, D, F) 13-month old mouse cortex labeled with an anti-SMI-31 antibody, which recognizes phosphorylated NF-M and NF-H. Arrows in A, C, and E indicate some axonal processes in wild-type mice which are absent in KO mice. Arrows in D indicate neurofilament accumulation present in KO mice*[24].

Lastly, experiments conducted on coronal brain sections of SLC25A12 KO mice showed remarkable myelination defects compared to WT mice in the corpus callosum, anterior commissure, internal capsule, and the habenulo-interpeduncular tract[24] (Fig. 1.8). All these alterations highlight how the mouse model shows features very similar to AGC1 deficiency patients[2].

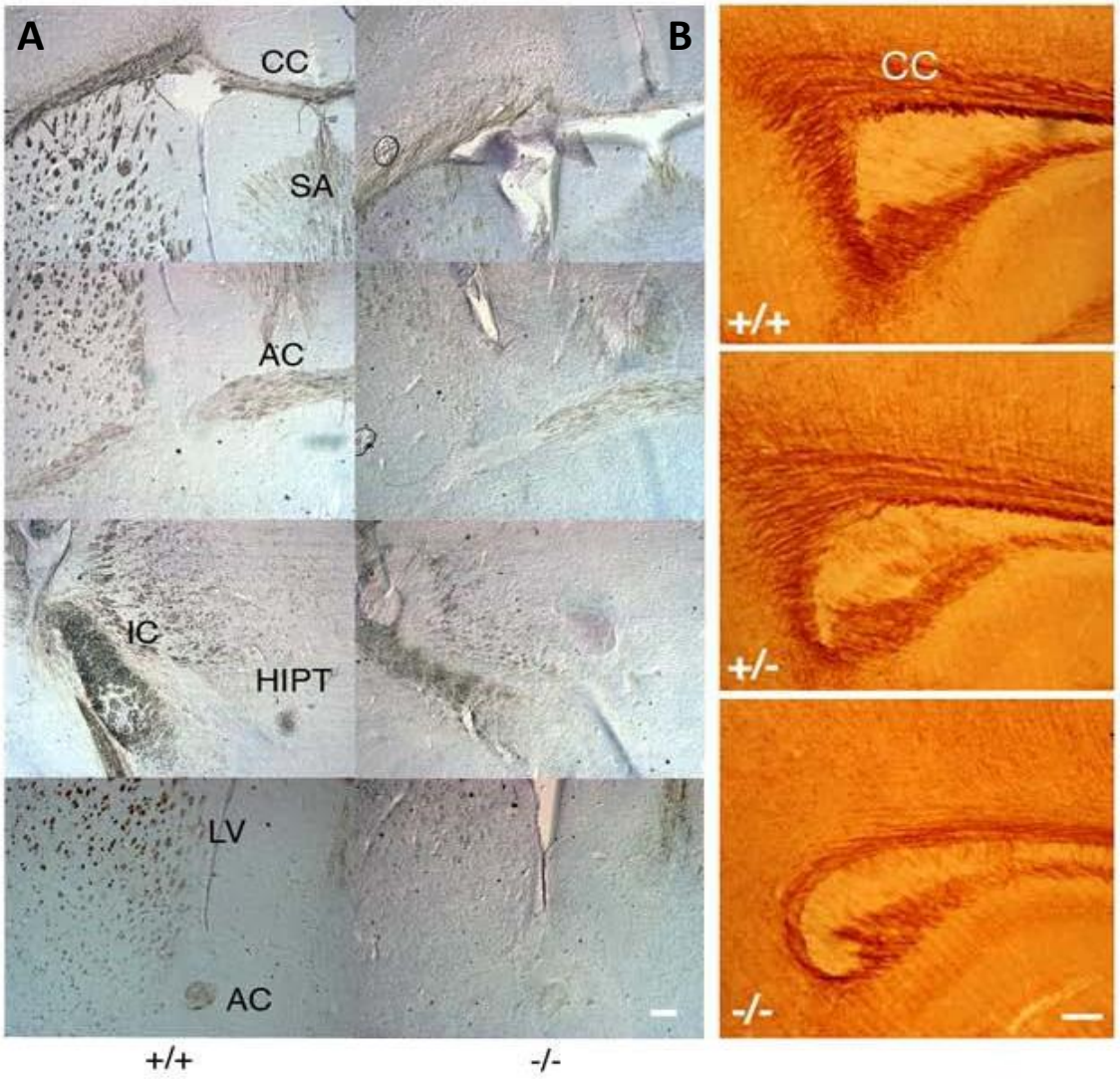

Figure 1.8*: Slc25a12-knockout mice show myelination defects. (A) crown coronal sections of WT and KO mice frontal cortex 14 days after birth. Sections were labeled with a primary anti-MBP antibody, an anti-HRP secondary antibody and stained with DAB. In KO mice there was a decrease in the number of axon fibers in the corpus callosum, anterior commissure, internal capsule and the habenulo-interpenducular tract. (B) Staining for Proteolipid Proteins (PLPs) on sagittal sections of WT and KO mice euthanized 13 days after birth. Scale bars, 200 µm. AC, front forward; CC, corpus callosum; DAB, 3,3'-Diaminobenzidine; HIPT, habenulo-interpenduclar tract; HRP, horseradish peroxidase; IC, internal capsule; LV, lateral ventricles; MBP, myelin basic protein; PLP, proteolipid protein; SA, septal area.*

Neuron-free oligodendrocyte cultures derived from Aralar$^{-/-}$ mice supplemented with fatty acids and metabolites were able to mature in a similar way to WT mice-derived cultures, supporting the idea that the defect found in AGC1$^{-/-}$ cells is due to the lack of NAA and neuronal lipids rather than being an oligodendrocyte-specific defect[36]. Therefore, the pathogenic mechanism at the base of AGC1 deficiency is considered to be represented by the inability of neurons to provide the lipid NAA precursor to oligodendrocytes, resulting in a reduced synthesis of galactocerebroside, the major component of myelin, leading to subsequent hypomyelination[35,37]. However, in none of these studies the effect of AGC1

deficiency in oligodendrocyte precursor cells and in neural stem cells has been addressed to clarify whether the lack of AGC1 activity could affect myelination and neuronal survival through an effect on precursor cell proliferation and differentiation.

1.5. Neural Stem Cells: proliferation and differentiation into neurons and glial cells during development and adulthood

Neurogenesis is the process by which new cells are formed from neural stem cells (NSCs), these are multipotent cells able to differentiate into different brain cell types (neurons or glia), or form progenitor cells (Fig. 1.9). It consists essentially of four main steps: cellular proliferation by asymmetric division, cellular fate specification, cell migration, and lastly differentiation, migration and integration into neuronal circuits[38]. Neurogenesis occurs mainly during prenatal development, allowing the expansion of neuronal cell number during embryonic life, and then remains active after birth only in specific brain areas.

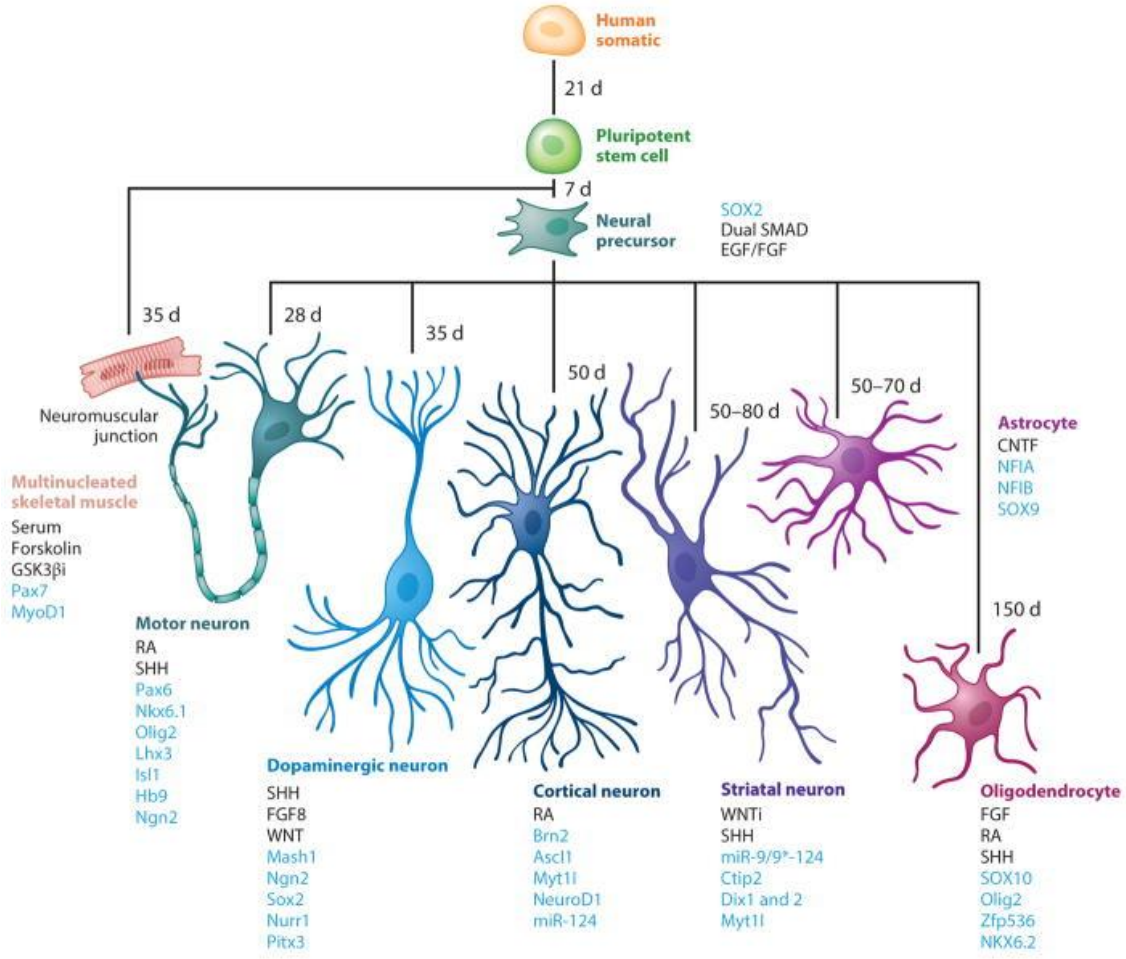

Figure 1.9: *Neuronal Lineage and Identification Markers*[39].

1.5.1. Embryonic neurogenesis

During the early stages of mammalian embryonic development, the newly formed neural tube is composed by a pseudostratified neuroepithelium of ectodermal origin that leads to the formation of all CNS cell types, producing firstly neurons and subsequently glial cells. Since neuroepithelial cells are formed through the inhibition of different signals inducing a non-neuronal fate, including BMPs (bone morphogenetic proteins) responsible for differentiation into epidermal cells at the beginning of the gastrication process[40], it is hypothesized that ectoderm cells tend to spontaneously differentiate into neuroeuroectoderm for the development of the central and peripheral nervous system in the absence of external stimuli. Prior and immediately after the neural tube closure, neuroepithelial cells are symmetrically divided to expand the cell population; with the onset of cortical neurogenesis (E9-10 in mice) they undergo morphological and structural changes accompanied by the acquisition of glial cell typical characteristics and form a homogeneous cell population called Radial Glia (RG cells). Radial glia cells are the precursors responsible for the formation of nearly all types of brain cells during CNS embryonic development except for microglia: neurons, oligodendrocytes, astrocytes, and ependymal cells. RG cells are anchored to each other by complexes of adherent junctions which are fundamental to maintain the integrity of the ventricular zone and cell specification[41]; they have an apical-basal polarity with a direct extension towards the surface of the ventricle and a radial process extending externally towards the pia mater. Staining studies with thymidine analogues have shown, however, that during the cell cycle, RG cells lose temporarily this bipolarity and the nucleus undergoes intracellular nuclear migration (INM), localizing in the apical part of the ventricular zone during the S phase and then migrating near the lumen of the neural tube during phase M (Fig. 1.10)[42,43].

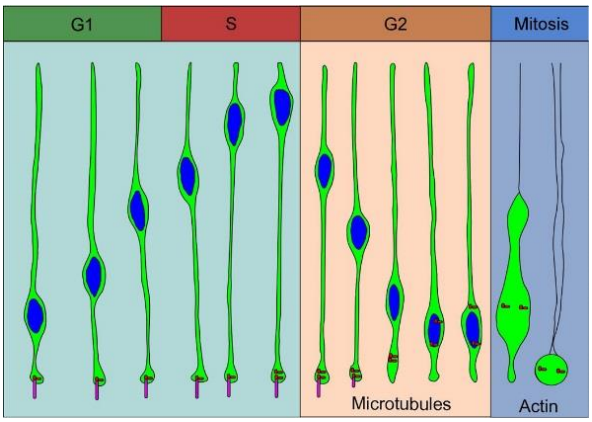

Figure 1.10: *Proposed model of INM. Nuclei migrate for short distances by contraction of actin microfilaments and along microtubules for greater distance movements through the involvement of dynein*[44].

1.5.2. Neuronal and glial differentiation

In the early stages of neurogenesis, BMPs at the dorsal pole and sonic hedgehog (SHH) at the ventral neural tube stimulate the expression of different bHLH (basic helix-loop- helix) genes, each associated with the production of specific types of neurons for the formation of the central nervous system[45]. In vertebrates, bHLH-proneural genes are classified in two families, Mash1 and NeuroD-like, based on homology with the bHLH genes necessary for neuronal differentiation in Drosophila[46], and act by inducing cell cycle arrest, epithelial delamination and the activation of gene expression necessary for general neuronal differentiation. Neuroepithelial and RG cells therefore, based on their localization along the neural tube, interpret these morphogenetic gradients and respond by activating certain gene expression programs able to produce the wide diversity of neuronal or glial cell types present in the CNS (Fig. 1.11). In addition to localization, regarding cell differentiation there is also a time control that determines which neurons or glial cells may derive from RG. For example, during cortical development, the first blasts that differentiate and migrate into the deeper layers of the cortex show the ability to give rise to all six-layer cells, and as development progresses, subsequent blasts and more external layers give rise to less cell types.

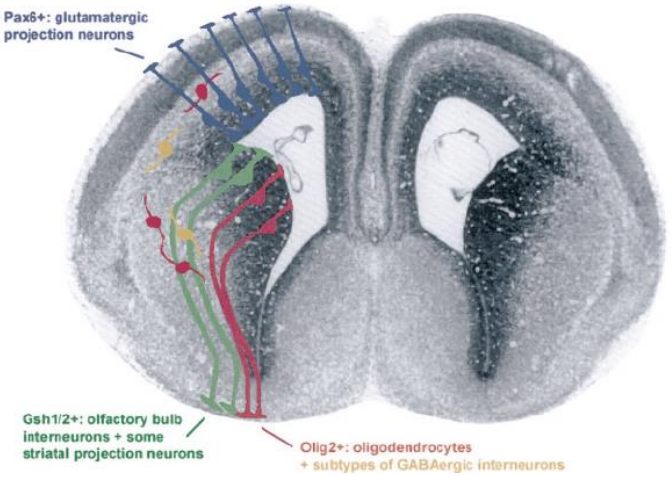

Figure 1.11: *Example of Radial Glia regional specification. Rostral section of the neurogenic embryonic telencephalus with different radial glia populations in the ventricular region. Based on the combination of transcription factor expression along the neural tube, Radial Glia generates different progeny along the dorsoventral axis of the telencephalus*[41].

At the time of cortical neurogenesis (E9-11), RG cells initiate a series of asymmetric cell divisions for neuronal differentiation in order to self-renew and at the same time generate a daughter, neuron or intermediate progenitor cell (nIPC or blast), which will be placed in the 6 layers of the cortex according to an inside-out mechanism. Therefore, for the formation of the cerebral cortex, as well as for the whole CNS, Radial Glia cells can produce neurons directly through the action of Neurogenin 1 and 2, or indirectly through the generation of nIPCs and subsequent division/amplification cycles through the action of FGF and Notch. In addition, immunostaining and electrophysiology analyses have shown that, in some cases, RG can reduce radial processes and move towards the cortical surface after division; these cells however, seem to mainly differentiate into astrocytes[47,48] (Figure 1.12).

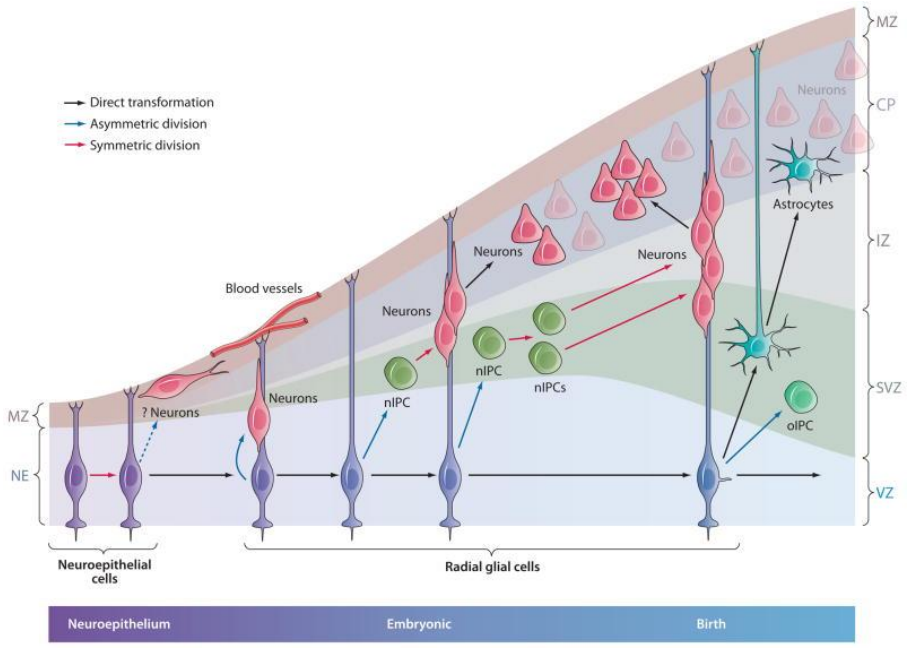

Figure 1.12: *Neurogenesis models during cortical development. Radial Glia cells can generate neurons in three ways: directly through asymmetric divisions; indirectly by generating nIPCs and an amplification cycle; indirectly with the formation of nIPCs but with two division cycles and future amplification, which is crucial for increasing the size of the cortex during development*[49].

At the end of neuronal differentiation there is the activation of a cascade leading to the expression of Nfia/GFAP and other factors that induce the transcription of astroglyogenic genes in proliferating RG cells. Cells lose contact with the neural tube ventricle, migrate through the cortical surface by somatic translocation and differentiate into astrocytes throughout the central nervous system. For oligodendrocyte differentiation, oligodendrocyte precursor cells (OPCs) originate in different brain regions after the expression of Olig1/2 and NKX2.2 factors, then localize in the white and gray matter where they may remain quiescent and proliferate symmetrically in response to local signals. The first precursors migrate into the dorsal cortex and hippocampus around E16 in the mouse brain, and derive from the medial ganglionic eminence (MGE) in the ventral part of the telencephalus[50-52]. The second wave of OPCs is generated more dorsally in the lateral and/or caudal (LGE/CGE) ganglionic eminence[53], while the last wave after E18 in the mouse brain, presumably from the dorsal cortex itself[53,54]. However, since many of the oligodendrocytes generated in the earliest stages disappear after birth, most oligodendrocytes present in the adult cortex derive from the last wave of oligodendrogenesis[53].

1.6. Adult Neurogenesis

For many years, mammalian neurogenesis was considered an exclusively embryonic process and of the very early stages of postnatal life. In the 60's, thanks to the use of 3H-thymidine incorporation into DNA during cell division, Altman reported the generation of new neurons in adult rat brain[55]. Although many postnatal CNS regions lose their ability to produce new brain cells, an NSC population persists in the adult able to generate neurons, astrocytes and oligodendrocytes in two brain regions: the subgranular zone (SGZ) of the dentate gyrus (DG), located at the interface between the granular cell layer and the elliptical junction, and the lateral ventricular subependymal area (V-SVZ). These regions, defined as neurogenic niches, are composed of different cell types, specific cell-cell contacts and particular extracellular environments[56].

1.6.1. Subventricolar zone (SVZ)

From an evolutionary point of view, the subventricular area is considered the continuation of the embryonic telencephalus ventricular area[57]. At the end of embryonic development, many Radial Glia cells differentiate into astrocytes and ependymal cells or may continue to function as NSCs in the newborn, while a small population known as type B cells, slows down proliferation. Type B cells show an astrocyte-like morphology, express several markers such as GFAP, Nestin, GLAST (glutamate aspartate transporter) and BLBP (brain lipid-binding protein) and, similarly to glial cells, exhibit an apical-basal polarity with a long process that contacts blood vessels and an apical region containing a process that contacts the ventricle[58] (Fig. 1.13).

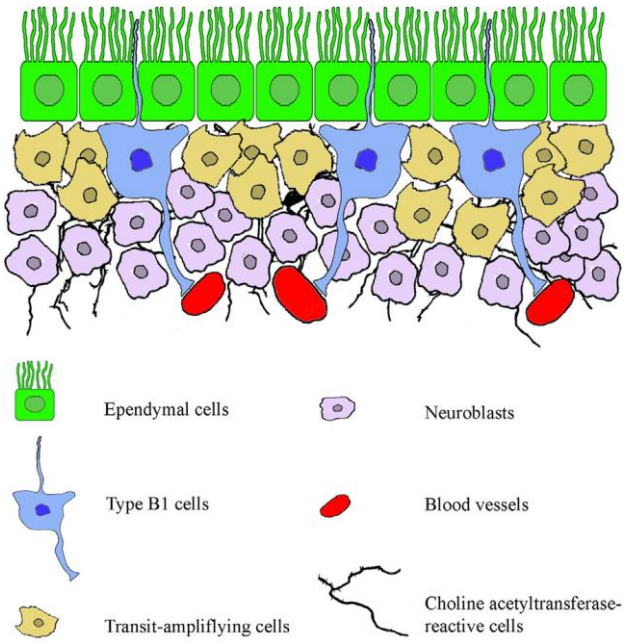

Figure 1.13: *V-SVZ architecture graphic representation. Type B cells with an apical process contact the ventricle and interact with multiciliated ependymal cells and blood vessels. Type B cells generate C-cells with high proliferative potency, which give rise to differentiated neuroblasts or type A cells*[59].

At the time of neurogenesis, type B cells increase their proliferation rate and become type C cells, important progenitors for amplification, which form small clusters within the SVZ before differentiating into neuroblasts. Neuroblasts, called Type A cells, continue proliferating, forming cell islands surrounded by type B cells and close to C cell clusters (Fig. 1.14) and then migrate from the front of the SVZ to the olfactory bulb where they differentiate in different types of interneurons depending on the origin area[60] (dorsal, medial or ventral SVZ).

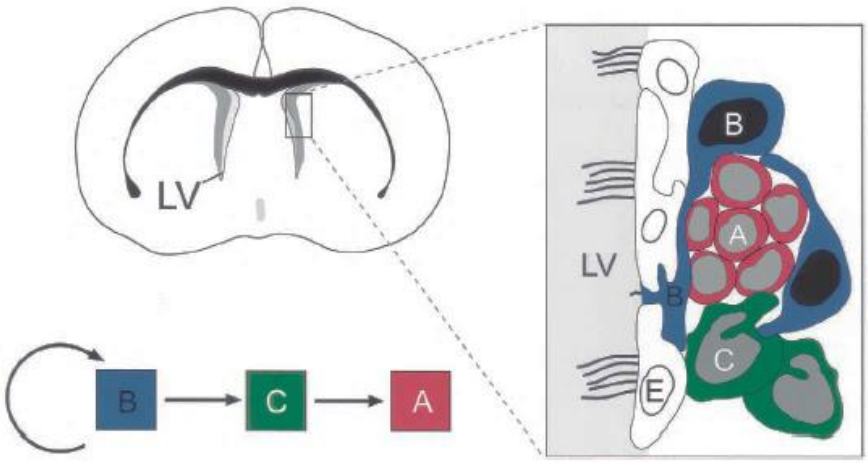

Figure 1.14: *Transversal section of adult rat brain (top left) and schematic illustration of SVZ composition and architecture (right). At the time of amplification, C cells give rise to neuroblasts (A cells) that proliferate to form clusters surrounded by B cells and close to C cell islands. On the bottom left the lineage of the olfactory bulb neurons is shown*[61].

1.6.2. Hippocampal dentate gyrus

The other major neurogenic niche that produces new neurons in the adult mammalian brain is the hippocampus[62], and alterations in the neurogenic process in this brain region are correlated with depression, neuroinflammation and epilepsy. During embryonic development, Radial Glia cells reach the hippocampus and differentiate into radial astrocytes at the subgranular zone, representing the first neuronal precursors of the DG (type I or B progenitors) characterized by a long process that crosses the granular cell layer and shorter processes horizontally aligned along the SGZ[63,64] (Fig. 1.15). Unlike astrocytes present in the DG that are GFAP positive, radial astrocytes express both GFAP and Nestin[64,65]. Similarly to what observed for the subventricular zone, these cells are localized near vascularized areas[66] suggesting that bloodstream factors may affect the behavior of NSCs in this area. Radial astrocytes do not give rise to neurons directly, but generate nIPCs called immature or progenitor type II cells[64,67,68] which, following cell division, mature in D2-D4 cells acquiring typical characteristics of neurons in different maturation states and then contributing to form the granular cell layer.

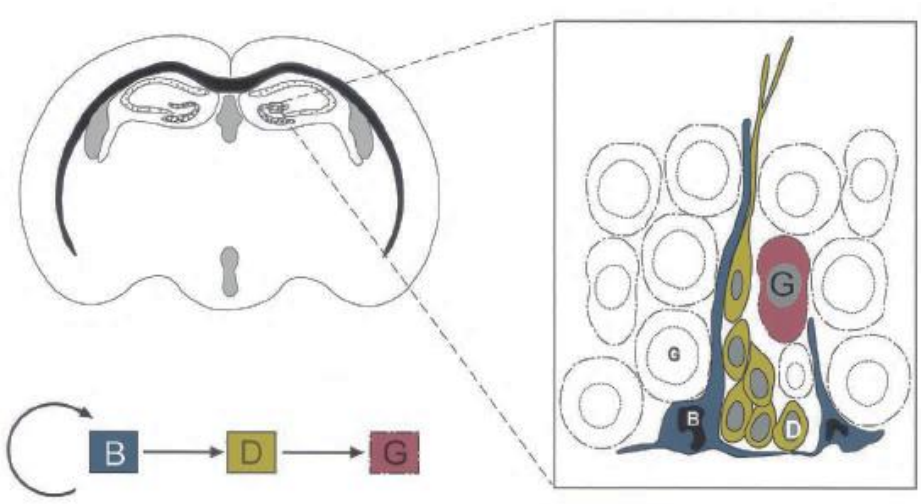

Figure 1.15: *Transversal section of adult mouse brain and hippocampus (top left) and schematic illustration of the subgranular layer composition and architecture (right). Astrocytes (B) have a long radial process that penetrates into the granular layer and short tangential processes parallel to the layer. The lineage of neurogenesis in the hippocampus is shown at the bottom left. Progenitors (B) give rise to immature cells (D) that divide into mature neurons (G)[61].*

Several Studies have shown that neurogenesis in the dentate gyrus, rather than in the SVZ, is influenced by multiple physiological and environmental signals including adrenal steroids[69,70], enrichment conditions[71] and antidepressants[72], which can directly and/or indirectly affect the behavior of radial astrocytes at the level of neuronal activity, subsequently causing changes in the proliferative rate of these cells and their progeny.

1.7. CNS myelination

1.7.1. Oligodendrogenesis regulation

Myelin is a lipidic and highly specialized laminar structure generated by glial cells that extend overlapping and compact membrane spirals around the axons of many neurons; in the central nervous system (CNS) it is formed by oligodendrocytes, while in the peripheral nervous system (PNS) the cells involved in myelin formation are Schwann cells. Histologically, myelin may be defined as a protein-like substance, very common in white matter, composed by 30% proteins and 70% lipids. Its importance lies in its high ability to increase the speed of nerve conduction and improve the passive flow of electric current reducing its ability to escape from the axon and thus prevent the dispersion of electric fields. Human diseases, such as multiple sclerosis, clearly demonstrate the importance of myelin in CNS functionality; in fact, in these diseases there is a loss of myelin sheath integrity around axons, making communication between the brain and spinal cord difficult, causing neurological symptoms to progress and leading to physical and cognitive disability. These observations were further supported by a study on mutant mice in which the myelination process was halted, showing a highly altered CNS phenotype[23,73]. Myelination can be defined as the nerve fiber maturation process in axons, essential for the good functionality of neural cells both in the CNS and PNS. Myelination is a very complex and dynamic mechanism that at birth has not reached completion in all brain areas (frontal lobe associated areas, for example, complete myelination only at the end of adolescence), showing substantial plasticity even during adult life. In non-pathological conditions, myelin is formed during the late fetal period, and develops for at least another 20 years (Fig. 1.16); during development, myelin axons which project to nerve structures away from cellular bodies and for which high conduction speed is essential, are substantially myelinated while axons from local circuit neurons are poor in myelin.

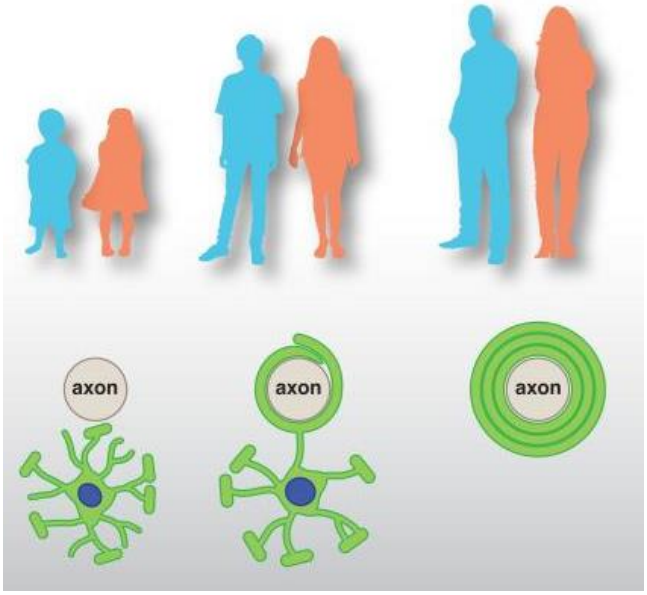

Figure 1.16: *Human myelination is mostly a postnatal process that peaks during childhood and can continue until early adulthood*[74].

From an evolutionary view, oligodendrogenesis in the brain and spinal cord is led by progenitor cells of the ventricular area, that is, the innermost cell layer surrounding the lumen of the neural tube constituting a region with an intense proliferative activity during gestation. It has been estimated that at the peak of cell proliferation in humans, 250,000 new neurons are generated every minute, and an even much higher number of glial cells. Progenitor cells of the ventricular zone, during the advancement of the mitotic cycle, give rise to oligodendrocyte progenitor cells (OPCs) which in turn divide and migrate throughout the CNS. OPCs are produced in successive waves; during the early stages of development, they predominantly derive from the ventral regions of the neural tube while during subsequent development phases they are largely replaced by OPCs from the more dorsal regions. Lastly, OPCs can differentiate into post-mitotic, pre-myelinating oligodendrocytes which, in the presence of appropriate environmental stimuli, may further mature and myelinate adjacent axons. OPCs migration from the source areas is a key process for the proper functionality of the CNS, however the molecular mechanisms that regulate this development phase are not clear yet, even though several molecules have been identified. Among these molecules, the family of calcium-dependent adhesion molecules, represented by cadherins, plays an important role. Cadherins have a modular structure that allows their interaction with other signal proteins, responsible for the correct sorting of OPCs[75-77]. During the OPCs migration process, the involvement of Platelet-Derived Growth Factors (PDGF) was also described. PDGFs consist of a homodimer or heterodimer of two A and B chains encoded by two different genes. In the

CNS, PDGF-A is released by neurons and astrocytes, while PDGF-B is derived from capillary endothelial cells. PDGFs bind and activate two membrane receptors PDGFRα and PDGFRβ; binding with these receptors mediates OPCs proliferation[78]. Moreover, PDGF-A exerts a mitogenic action on OPCs and plays a crucial role in embryogenesis. Recent studies have demonstrated that PDGF-A receptor activation in OPCs (PDGFRα) leads to the activation of numerous signaling pathways, including the ERK pathway, resulting in OPC migration[79,80].

1.7.2. Regulation of oligodendrocyte differentiation and myelination

Given the importance of myelination in CNS proper functionality, it is not surprising that oligodendrocyte development and axon myelination are processes highly regulated by extrinsic and intrinsic signaling mechanisms, and that this control involves the coordination of multiple intracellular pathways[73]. An example of extrinsic regulation is the involvement of some axonal ligands in the myelination process. Jagged, Lingo1 and PSA-NCAM inhibit oligodendrocyte differentiation and/or myelination[81-83]. Moreover, unlike the PNS where neuregulin axonal expression is the main permissive signal for myelination by Schwann cells, in CNS oligodendrocytes this signaling is largely superfluous, although it has been demonstrated that overexpression of neuregulin in the CNS induces hypermyelination[84]. On the other hand, the Wnt/β-catenin pathway also regulates oligodendrocyte development. Wnt is transiently activated in OPCs at the beginning of differentiation, while both the activity of β-catenin and expression of Tcf4/Tcf712 are down-regulated in mature oligodendrocytes[85,86]. Nevertheless, it is thought that Wnt signaling down-regulation may also be needed for differentiation; in this regard, it has been shown that in mutant mice displaying high Wnt/β-catenin signaling, oligodendrocyte differentiation is repressed and hypomyelination is present[85]. In addition to extracellular ligands, myelination is also partly driven by the electrical activity of axons themselves. In fact, neuronal activity may modulate the expression of ligands or cytokines and their localization on the axonal membrane[87]; may mediate the release of adenosine from active axons which can activate purinergic receptors on OPCs, promoting their differentiation and myelination; may mediate the release of axonal ATP thereby stimulating adjacent astrocytes to release the pro-myelinating factor LIF[88] (leukemia inhibitory factor) and lastly, the OPC surface can be well equipped to receive synaptic input directly from neurons and respond appropriately. A direct stimulation of OPCs by the release of glutamate from synaptic terminals was first documented in the hippocampus[89], as

documented for GABA in gray matter and white matter[90,91]. OPCs expressing glutamate ionotropic receptors and voltage-dependent ion channels, may respond to this direct stimulation with a depolarization event that is not different from a neuronal action potential[90,92,93]. Studies on knockout mice and chick embryo electroporation have led to the identification of a number of transcription factors necessary for oligodendrocyte specification or differentiation[73] (Fig 1.17).

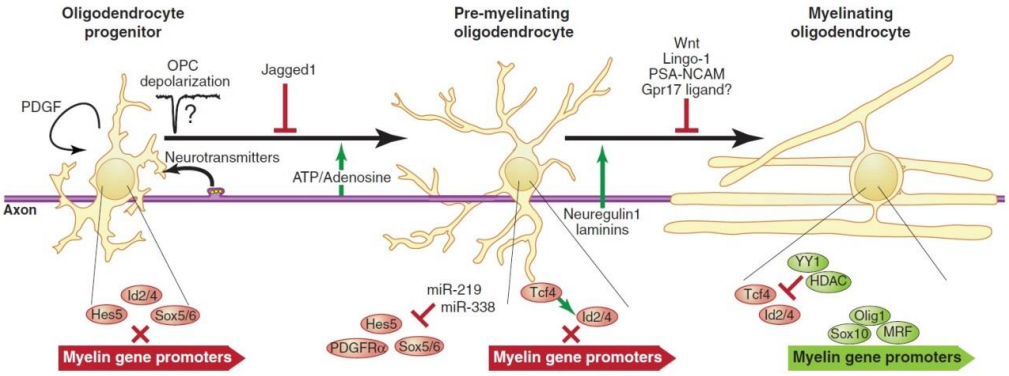

Figure 1.17: *Intrinsic and extrinsic factor mechanism of action on the differentiation and myelination of individual axons. Oligodendrocyte differentiation requires the integration of multiple extracellular signals through the coordination of multiple intrinsic pathways. Myelination is regulated both at the level of oligodendrocyte differentiation and more specifically of individual axons[73].*

Olig1, Ascl1, Nkx2.2, Sox10, YY1, and Tcf4 are required for the development of mature post-mitotic oligodendrocytes[94] and are all present in both OPCs and post-mitotic oligodendrocytes, with the exception of Tcf4 which is expressed only transiently during differentiation[85,95]. In addition, chromatin structure and protein factors that determine chromatin remodeling can also act as intrinsic control mechanisms; in fact, histone deacetylases (HDACs) may intervene in oligodendrocyte differentiation by suppressing the transcription of genes that normally block differentiation[96]. Lastly, molecules such as microRNAs that control post-transcriptional gene expression, can play a very important role in the regulation of CNS myelination. MicroRNA profiling studies led to the identification of miR219 and miR338, and revealed that the function of these miRNAs is activated during oligodendrocyte differentiation[97,98]. PDGFα, Sox6 and Hes5 are target genes of these miRNAs, which usually act by maintaining OPCs in an undifferentiated state, therefore miR219 and miR338, through a positive feedback loop, inhibit the genes that promote cell proliferation and promote differentiation[97,98]. Lastly, the microRNA cluster miR17-92, regulates OPC proliferation by PTEN regulation, and thus phosphorylation of Akt[99]. These

results clearly show an important role for microRNAs in CNS myelination control in different phases (Fig. 1.15). One of the best known and involved pathways in OPC maturation and CNS myelination is the transforming growth factor β pathway. TGFβ signaling is crucial to induce OPC cell cycle arrest during oligodendrogenesis, and postnatal CNS myelination. Increased oligodendrogenesis and subcortical white matter myelination (SCWM) is detected after inducing a TGFβ gain of function mutation, whereas TGFβ II receptor deletion in OPCs prevents their development into mature myelinating oligodendrocytes leading to hypomyelination of the SCWM in mice[100]. TGFβ1 binding to the TGFβ-RII membrane receptor on OPCs allows TGFβ-RII to phosphorylate the TGFβ-RI receptor leading to the activation of the signal transduction cascade resulting in the activation of the SMAD2/3 complex that interacts with SMAD4 and the transcription factors Sp1 and Fox01 which, following nuclear translocation, stimulate the expression of cycline-dependent kinase inhibitors, such as p15, p21 and p27. These inhibit c-myc pro-mitotic gene transcription and promote its cytoplasmic and non-nuclear localization[101] (Fig. 1.18).

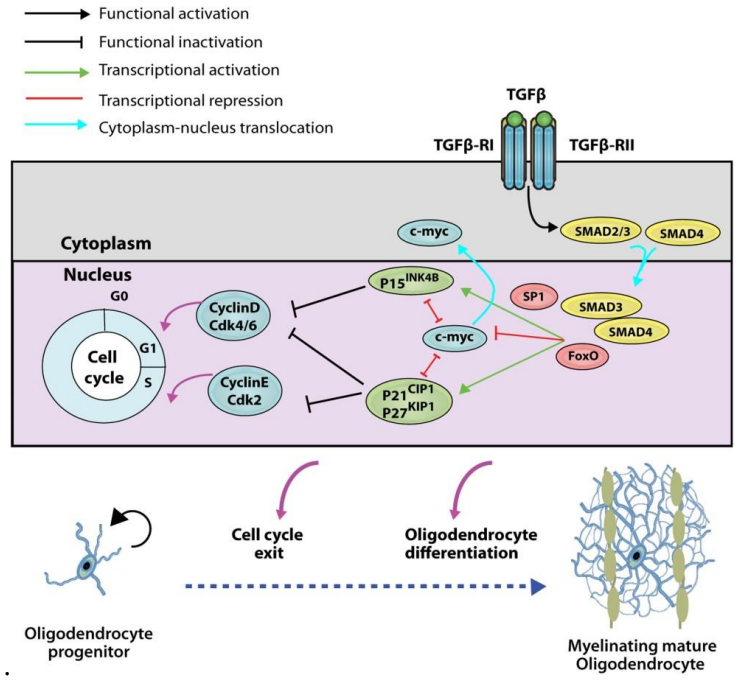

Figure 1.18: *Model scheme for the TGFβ pathway[100].*

This process leads to OPC cell cycle arrest and differentiation into mature oligodendrocytes able to synthesize myelin, as evidenced by reduced PDGFRα and Cdk2 protein levels and the resulting increase in Mbp, Cnp and Mog mRNAs, which occurs in the presence of TGFβ1[100].

1.8. *In vitro* cell models to study neurogenesis and OPCs: neurospheres and brain-cells derived from induced Pluripotent Stem (iPS) cells

1.8.1. Neurospheres

The neurosphere model[102] and the NSC monolayer culture systems are valid tools to determine the potential (proliferation and differentiation) of adult neural stem cells *in vitro*. These models can be used to compare the potential of neural precursors from genetically different or differently treated animals to determine the effects of exogenous factors or diseases on NSC proliferation and differentiation, or to generate cell lines that can be analyzed during successive steps. The "neurosphere assay" is mainly used for the identification of neural stem cells isolated from primary tissues and has the advantage to provide a rapid estimate of precursor number in brain tissue from animals with different genetic characteristics. On the other hand, NSC adherent monolayer cultures are not traditionally used to compare proliferation levels but they can be useful to monitor the differentiation processes of individual cells in culture, since they consist of a homogeneous precursor population.

In an attempt to isolate and expand adult rat neural stem cells for the first time, Reynolds and Weiss used a serum-free culture system then defined the "neurosphere assay" (NSA) in 1992[102]. With this system, they were able to demonstrate that single adult neural stem cells could proliferate to form a sphere of undifferentiated cellular composition called neurosphere, and how these neurospheres could subsequently be dissociated to generate numerous secondary neurospheres or induced to differentiate into the three major cell lineages of the CNS. Generally, neurospheres are floating cultures of NSCs and neural progenitors isolated from the adult or fetal central nervous system[103] and represent a nearly perfect system to provide a consistent and self-renewable source of CNS undifferentiated precursors for cell replacement therapies and *in vitro* studies for neural stem cell analysis/characterization. Defined as an "environmental adaptation", NSCs could be clustered to survive the non-physiological conditions of *in vitro* culture by optimizing their interactions and acquiring a thermodynamically favorable sphere shape[104]. Confocal and electron microscopy analysis conducted by Bez and colleagues in 2003 showed that neurospheres and neurosphere-derived cells present significant morphological and structural differences, despite being derived from NSCs plated at the same time and under the same culture conditions. During growth,

neurospheres may show a well-defined spherical shape or cluster of irregular cells, as well as occasionally present cytoplasmic processes that recall cilia or pseudopods (Fig. 1.19 A, B, C) occasionally. In addition, neurospheres able to proliferate more rapidly and of greater diameter are generally characterized by a darker central core corresponding to sites of necrotic cells due likely to reduced nutrient and oxygen availability in the central part, while smaller spheres appear more translucent and healthy, with no signs of suffering.

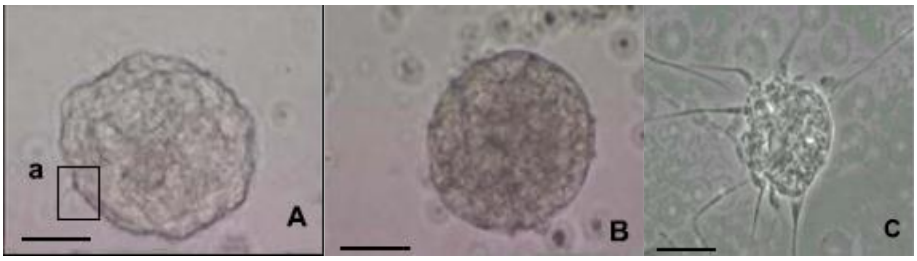

Figure 1.19: *Neurosphere phase contrast images (A-C). (A) Neurosphere with irregular edge and cilia-like cytoplasmic processes on the surface (a). (B) Neurosphere with regular edges and spherical shape well defined. (C) Neurosphere in low-adhesion dish with obvious cytoplasmic processes similar to pseudopods*[104].

In the case neurospheres are plated on matrices that allow plate adhesion for subsequent proliferation or differentiation analysis, they begin to flatten and spread becoming an adherent cell monolayer where cells from outer layers extend to form mitotically active cytoplasmic processes, similar to pseudopods. Bez and colleagues also documented the presence of apoptosis and apoptotic body phagocytosis, typically in the innermost regions, between the second and the third layers and the nucleus of the neurosphere, while BrdU incorporation experiments, showed intense transcriptional activity in the most peripheral cells, suggesting that the distribution of biological phenomena such as mitosis, transcription, or apoptosis is directly influenced by the position that the cells occupy in the neurosphere structure. Neurosphere vitality and the activity of the live cells present inside can therefore depend on the access of oxygen and nutrients present in the culture medium, and on the ability to quickly eliminate catabolites in the brain external environment[104]. This interpretation could justify the high transcriptional activity observed at the more peripheral cells where the exchange of nutrients, oxygen and catabolites is facilitated, while apoptosis, phagocytosis and necrosis are typical of the most internal layers where these exchanges are more difficult. Flow cytometry analysis has also shown that this morphological and functional heterogeneity characterizes not only neurospheres but also NSCs that derive from them. These cells have different size, metabolism and cytoplasmic content, and are as well in different phases of the cell cycle,

showing different morphological characteristics depending on the neurosphere layer they derived from[104].

The neurosphere assay (NSA) was the first *in vitro* cellular system to demonstrate unequivocally the presence of cells in the adult brain with true neural stem cell characteristics[102,105]. It remains currently an extremely useful tool to analyze proliferation, auto-regenerative capacity and multipotency of neural stem cells and cell progenitors. Analysis using serial clonal passages to determine the ability to form neurospheres (Figure 1.20 A) followed by *in vitro* differentiation to show the multipotency of individual spheres (Fig. 1.20 B, C) are very widespread and still represent the best functional assay to study NSCs[106-109].

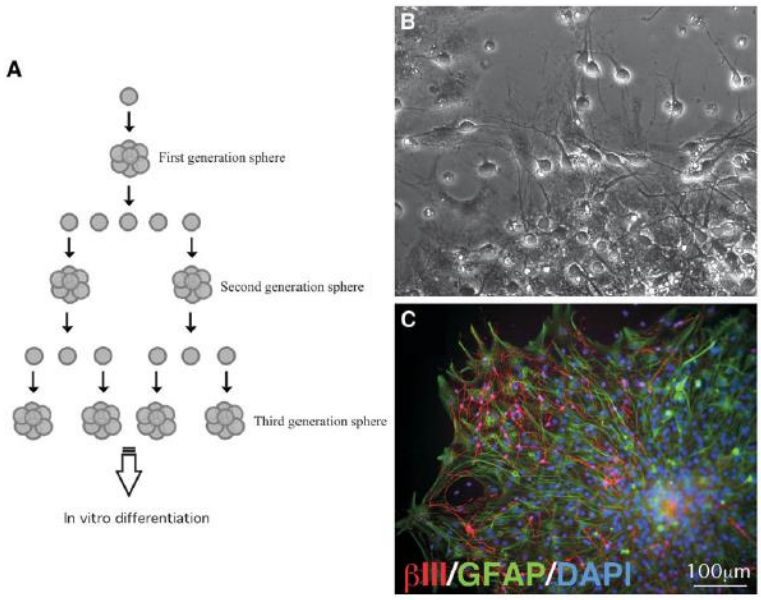

Figure 1.20: *Tests to determine the ability to form neurospheres followed by in vitro differentiation to analyze multipotency (A). During differentiation cells migrate from the core of the neurosphere (B) and express proteins such as GFAP (green) and BIII-tubulin (red), respectively typical astrocytic and neuronal markers[110].*

The major advantages of this method are its simplicity, reproducibility and ability to generate an indefinite number of cells, a small tissue section or a small group of cells in a chemically defined serum-free culture medium. However, to evaluate the results one should not consider the number of *in vitro* neurospheres as corresponding to the number of NSCs since these structures are extremely heterogeneous and characterized not only by a stem cell mix but also by progenitors and differentiated cells[102,111]. In this assay, the primary tissue is microdissected from a particular cerebral region (SVZ and/or hippocampus) and dissociated into single cells. During the first step, most differentiated cells die after 2-3 days while a small population of cells respond to proliferation-inducing growth factors, generating after 6-8 days

undifferentiated colonies ready to be sub-reactivated to expand the NSC pool or induce differentiation into the three major cell lines of the CNS: neurons, astrocytes and oligodendrocytes[112].

Although the two main neurogenic regions of the adult mouse brain contain both neural precursors, it has been shown that SVZ-derived cells proliferate more rapidly forming larger neurospheres than those derived from the dentate gyrus.

Neurospheres are also a valid *in vitro* model for neurogenesis and neural development, enabling the study of precursor-specific intrinsic processes during the different phases of development, or the potential of these cells once removed from their physiological growth conditions[110]. In general, neurospheres are a very effective study system because they can be maintained in culture under well-defined serum free conditions, and their expansion or differentiation phase can be manipulated by simply adding factors of interest in the growth medium[113,114]. In addition, comparative studies of fetal murine brains and neurosphere cultures have shown how cells derived from neurospheres have a temporally and spatially similar behavior to their *in vivo* counterparts while retaining the ability to differentiate into the neuronal type characteristic of the brain origin region[107,115].

1.8.2. Brain-cells derived from human iPS cells

Embryonic Stem Cells (ESCs) are cells derived from the inner cell mass of the mammal blastocyst and have the ability to grow indefinitely to maintain pluripotency and the ability to differentiate into cells of the three germinal layers[116,117]. Human ESCs can be used to treat diseases such as Parkinson's disease, spinal cord injuries or diabetes, though there are a number of ethical issues regarding the use of human embryos as a cell source, as well as the possibility of rejection following transplantation. Over the years, a possible solution has been the generation of pluripotent cells directly from differentiated patient cells then identified by the name of iPS cells (induced pluripotent stem cells). Takahashi and Yamanaka in 2006 were able to obtain iPS from adult and embryonic mouse fibroblasts by ectopic co-expression of 4 genes, Oct3/4, Sox2, c-Myc and Kfl4 under cultured conditions typical of embryonic stem cells. Specifically, Oct3/4 and Sox2 act to maintain pluripotency both in ESCs and in early embryos, while c-myc and Kfl4 contribute to the long-term maintenance of the embryonic stem cell phenotype and rapid proliferation in culture. The iPS cells obtained by Takahashi and Yamanaka, showed the same morphology, proliferation properties, and typical ES cell markers. In addition, subcutaneous transplantation of iPS into mice resulted in the

development of tumors formed from tissues derived by all three germinal layers whereas through blastocyst injection contributed to the development of mouse embryos which demonstrates their potency[118]. However, mouse and human iPS cells show different morphological characteristics that resemble those of embryonic stem cells in different stages of development. Mouse iPS cell colonies appear dome-shaped, are refractory, exist in a pre-inactivation state of the X chromosome and are phenotypically similar to inner mass cells at E5.5-7.5 of mouse embryonic development. Human iPS colonies are smoother, tend to inactivate one of the two X chromosomes and are similar to stem cells observed in the epiblast phase (Fig. 1.21).

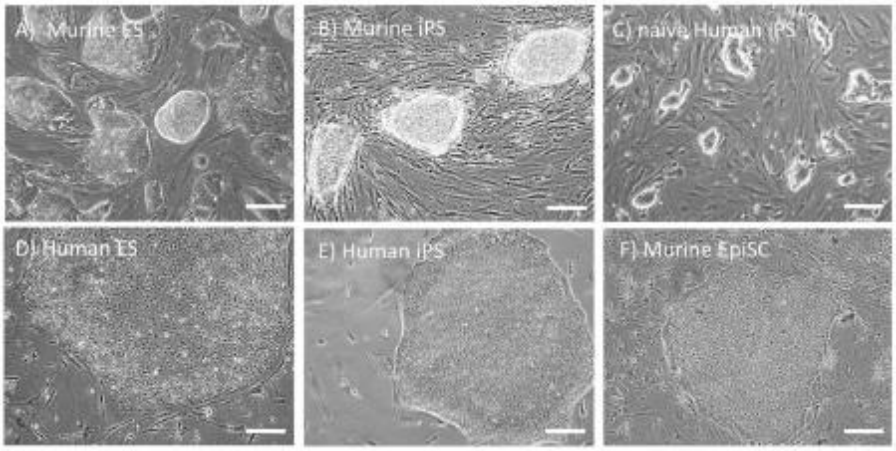

Figure 1.21: *Pluripotent Stem Cell morphology. Mouse ESCs (A) and iPS cells (B) form dome-shaped refractile colonies. Human ESCs (D) and iPS cells (E) exhibit a more crushed morphology, recalling mouse stem cells derived from the epiblast*[119].

Irrespective of their derivation, iPS cells maintain the main characteristics of embryonic stem cells, including the ability to propagate indefinitely in culture and the ability to generate cells from each of the three germinal layers, commonly seen as compact colonies with well-defined edges, composed of cells with a large nucleus, large nucleoli and little cytoplasm. To distinguish accurately iPS cells completely reprogrammed from those where reprogramming has been only partially performed, markers such as Oct4, Sox2, and Nanog which should be expressed at levels comparable to ESCs are used; methylation status of gene promoters responsible of the maintenance of pluripotency or differentiation beyond the reactivation of the silenced chromosome X can also be evaluated. If iPS cells acquire all these features, they are expected to be reprogrammed successfully. For functional ability characterization, cells may be induced to differentiate into embryoid bodies (spheres of undifferentiated cells that, morphologically, resemble a gastrula), or plated on Petri dishes and then tested with specific markers for each germinal layer. To evaluate hiPS cell potential, the most widely used test

involves the formation of a teratoma following subcutaneous or intramuscular injection into immunodeficient mice. If the cells are really pluripotent, they will be able to form tumors containing elements from each layer: ectoderm, mesoderm or endoderm. Given the high ability to differentiate into any cellular line (neuronal, muscular, epithelial, cardiac, etc.), the generation of patient-specific stem cells is a valuable tool for the study and treatment of diseases. In fact, iPS cells can be used to understand disease mechanisms, perform pharmacological tests and evaluate their therapeutic potential, as well as study the efficacy of the genetic remedy associated with cellular replacement therapy. In a study conducted by Wernig and colleagues in 2008, iPS-derived dopaminergic neurons obtained from reprogrammed fibroblasts, when implanted in the brain showed to be functionally integrated into neuronal circuits improving the symptoms of a Parkinson's disease rat model[120]. Implantation and functional recovery in this *in vivo* model is representative of the therapeutic value of iPS cells in cell replacement therapy in the central nervous system. After appropriate stimulation these stem cells can generate all major brain cells. For these purposes, somatic cell types have been derived from pluripotent stem cells, embryonic stem cell (ESC) - or induced pluripotent stem cell (iPSC)-derived neural stem cells (NSCs)[121]. Neural stem cells (NSCs) are self-renewing multipotent stem cells that can differentiate into neurons, astrocytes and oligodendrocytes. Oligodendrocyte Precursor cells (OPCs) can be obtained from NSCs (Fig. 1.22) as a useful therapeutic approach for the treatment of demyelinating diseases. Remyelination restores the physiological interaction between oligodendrocyte and axons and the structural support needed for axonal maintenance and efficient pulse conduction[122].

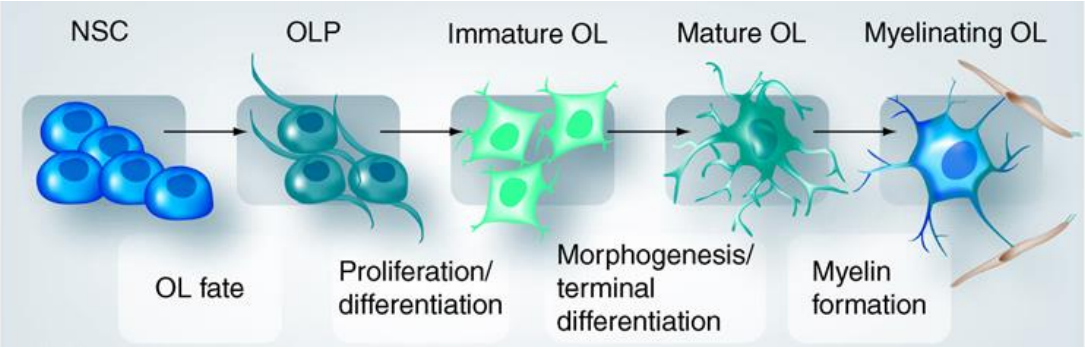

Figure 1.22: *Representation of oligodendrocytes lineage development*[123].

Therefore, NSCs can potentially assist in the study of neural development/differentiation and various neurodegenerative disorders and developing appropriate protocols to differentiate pluripotent stem cells into specific cell types is a key step in the study of developmental biology and for the advancement in the clinical phase.

1.9. Role of mitochondrial dysfunction in demyelinating diseases

AGC1 deficiency belongs to the group of rare diseases that affect 6-8% of the world population, for which 70% of cases are pediatric pathologies. Among these rare diseases, including "orphan" diseases, whose cause has not yet been identified, many are demyelinating and extremely disabling. A common feature of these pathologies is mitochondrial dysfunction, present not only in AGC1 deficiency, but also in other neurodegenerative and demyelinating diseases, of which some are rare while others are very widespread, such as multiple sclerosis[4-6]. Moreover, all these pathologies are characterized by alteration of the myelin sheath development, neurodegeneration and neuroinflammation, permanent and diffuse neurological deficits not only at the motor level, but also at the cognitive level. In proliferating neurons, AGC1 activity supports mitochondrial pyruvate oxidation with acetyl-CoA production that enters the TCA cycle but is also required for biosynthetic purposes, such as lipid and NAA synthesis. AGC1 is also a source of essential cytosolic aspartate for protein, nucleotide and NAA synthesis. In a neuronal cell model of AGC1 deficiency[124], higher glutaminolysis can counteract reduced mitochondrial aspartate output due to AGC1 deficiency and allow normal cell proliferation. However, glutamine oxidation cannot restore NAA synthesis, potentially being still compromised by acetylCoA reduction caused by MAS inhibition after AGC1 deficiency. A recent article reported that treatment of AGC1 deficiency patient with a ketogenic diet has led to psychomotor improvement restoring myelination[125]. A ketogenic diet is often used in the treatment of epilepsy with positive effects also against neurodegeneration probably because it provides ketone bodies and fatty acids. However, the biochemical, molecular, and cellular mechanisms underlying this nutritional approach have not been clarified[126]. In AGC1 deficiency patients, a ketogenic diet could provide sufficient levels of ketone bodies as an alternative source of mitochondrial acetyl groups, overcoming NAA deficit in undifferentiated neurons and favoring myelination in patients. The contribution of oligodendrocyte loss in other demyelinating and neurodegenerative diseases, such as multiple sclerosis, is relatively easy to predict; immuno-mediated damage to the myelin sheath and mature oligodendrocytes results in localized demyelination exhibiting myelinated axons in a toxic environment and consequently neuronal death. In other neurodegenerative diseases such as ALS (amyotrophic lateral sclerosis) and AD (Alzheimer's disease), the contribution of the oligodendrocyte lineage is less defined. Several studies support that myelin sheaths provide physical protection to axons; the oligodendrocyte lineage

provides metabolic support for adjacent axons[127] and, in ALS animal models, recent molecular studies implicate changes in lactate carrier expression in oligodendrocytes (MCT1) as a contributor to neuronal loss. A more widespread mechanism of oligodendrocyte/OPC influence on neurodegenerative diseases may be associated with maintaining iron levels in the central nervous system. In fact, oligodendrocytes are the main source of iron in the CNS and express high levels of ferritin[128,129]. Damaged oligodendrocytes can release iron into the surrounding environment that can be absorbed by macrophages stimulating their cytotoxicity. Alternatively, high levels of iron have been implicated in elevating oxygen-reactive species and intracellular iron is capable of triggering a new type of cell death called ferroptosis[130,131] distinct from apoptosis or necrosis. Specifically in AD, iron released by oligodendrocytes may promote Aβ oligomer formation enhancing Aβ peptide toxicity[132,133]. Aβ oligomers cause damage to the white substance including oligodendrocyte death and reduction in myelin proteins leaving axons and neurons vulnerable. Amyotrophic lateral sclerosis (ALS) is characterized by metabolic decoupling and transport of lactate interrupted between oligodendrocytes and neurons in the CNS, resulting in oligodendrocyte loss and neuronal death. Demyelination in multiple sclerosis (MS) is caused by acute inflammation in which oligodendrocytes and myelinated sheaths are damaged generating myelin debris that inhibits OPC differentiation. The absence of an appropriate signaling environment further prevents OPC differentiation into mature oligodendrocytes with consequent failure of remyelination. These advances have generated new potential therapeutic targets for myelin repair in the CNS[134,135]. Two general approaches are the use of direct pharmacological intervention to stimulate the development or function of existing oligodendrocyte lineage cells to promote recovery or the generation of oligodendrocytes selectively designed for transplantation to replace defective host cells[136]. Moreover, since there are no pharmacological therapies available to cure these devastating demyelinating and neurodegenerative diseases, it is particularly important to find new approaches to counteract these pathological conditions. In order to find new therapeutic approaches, it is crucial to clarify biochemical and molecular mechanisms that are the basis of these pathologies in order to identify new potential therapeutic target to try to counteract deficits derived from demyelination. Each result can be useful and potentially translate to humans to understand disease mechanisms, as well as give hope for the treatment of many demyelinating pathologies.

2. AIM OF THE THESIS

AGC1 deficiency is a rare genetic neurodegenerative disease caused by defects in the SLC25A12 gene encoding for Aralar/AGC1, a mitochondrial aspartate-glutamate carrier, important in the metabolism of brain amino acids and myelin synthesis. In patients, AGC1 mutations lead to drastic reduction of carrier activity, which results in severe hypotonia, developmental delay, intractable epilepsy and cortical atrophy with altered myelin formation in the CNS, most likely due to a dramatic reduction of N-acetyl aspartate (NAA) levels in the brain[1,2]. AGC1 deficiency mechanisms are not yet clear and currently there is no therapeutic treatment. It was recently demonstrated that reduced AGC1 expression and activity alter proliferation and differentiation of neuronal precursors through a biochemical effect at the mitochondrial level[124]. In fact, AGC1 is a key component of the malate-aspartate shuttle (MAS) that transfers the reducing equivalents of $NADH^+$ from the cytosol to mitochondria, representing a crucial pathway to support mitochondrial oxidative phosphorylation[137]. However, although the role of AGC1 in this biochemical pathway is well known, it is not clear how this carrier could play a direct role in NAA synthesis and myelin formation in the CNS. Above all, it is still unknown how this carrier could affect cerebral precursor proliferation, especially oligodendrocytes, whose role in myelin synthesis is crucial.

Therefore, the aim of this PhD thesis was to study the molecular mechanisms underlying AGC1 deficiency in appropriate *in vitro* and *in vivo* disease models, in particular by focusing on oligodendrocyte precursor alterations to better define pathogenetic mechanisms that could potentially lead to identify new therapeutic targets, potentially interesting for nutritional and/or pharmacological strategies useful in AGC1 deficiency patients.

To this aim, the first studies were conducted on immortalized mouse oligodendrocyte precursor cells, Oli-Neu cells (kind gift from Dr. Trotter), where we partially silenced AGC1 expression in order to obtain a reduction of carrier activity down to about 30-40% compared to control cells, as observed in mitochondria from human patients. Then, the obtained results were validated in an AGC1 deficiency *in vivo* model represented by SLC25A12 heterozygous knockout mice ($AGC1^{+/-}$ C57BL6/N background). $AGC1^{+/-}$ mice represent a good model for the study of AGC1 deficiency, since patients with this disease are characterized by reduced carrier activity rather than total loss of carrier activity.

In both *in vitro* and *in vivo* models, expression of AGC1 and its homolog, AGC2, was analyzed as well as cell proliferation, expression of growth factors and receptors known to be

involved in OPC proliferation/differentiation, such as the PDGFα and TGFβ pathways. In collaboration with Dr. Massimo Lasorsa (Institute of Biomembranes, Bioenergetics and Molecular Biotechnologies, IBIOM, CNR, Bari, Italy) and Prof. Paolo Pinton (University of Ferrara, Italy), biochemical analyses were conducted to understand the effect of AGC1 silencing on Oli-Neu cells at the mitochondrial bioenergetics level. This part of research was supported by the grant GGP11139 from the Comitato Telethon Fondazione Onlus to the project *"Mitochondrial Aspartate/Glutamate Carrier 1 Deficiency: Pathogenetic Mechanisms and Mutational Analysis"* (2011-2014; national scientific coordinator, Prof. Ferdinando Palmieri, University of Bari).

Furthermore, our study focused first on the evaluation of NSC proliferation and differentiation in $AGC1^{+/+}$ and $AGC1^{+/-}$ neurospheres derived from the subventricular zone (SVZ) of our mouse AGC1 deficiency model. Our study also focused on parallel, but preliminary studies on NSCs derived from AGC1 deficiency iPS cells, in order to further validate our data in human cells and to reduce the number of animals to be used for experimental purposes in the future. Studies on brain cells derived from human iPS cells are in the framework of the research project *"Biochemical changes in the rare genetic demyelinating and neurodegenerative disease AGC1 deficiency: a study on the different brain cells derived from human iPS"* from the Italian Ministry for Foreign Affairs and International Cooperation (MAECI) Italy-USA 2016-2018 in collaboration with Prof. SA Anderson (Children's Hospital of Philadelphia - Department of Psychiatry at Upenn, USA).

The importance of this study lies also on the fact that mitochondrial dysfunction is at the basis not only of AGC1 deficiency, but also of other neurodegenerative and demyelinating diseases, some of which are rare while others are widely spread such as multiple sclerosis[4-6]. Thus, the obtained results could be useful to understand disease mechanisms and give hope for the treatment of many human demyelinating diseases.

3. MATERIALS AND METHODS

3.1. Cell cultures

Immortalized mouse oligodendrocyte precursor cells (Oli-Neu, kind gift from Dr. Jacqueline Trotter, University of Mainz, Germany) were used for this study. These cell lines were grown on poly-L-lysine (Sigma-Aldrich, St Louis, MO, USA) coated Petri dishes at 37ºC in a humidified atmosphere with 5% CO_2 in SATO medium (DMEM medium, 2 mM glutamine, 10 ug/ml insulin, 5.5 ug/ml transferrin, 38.72 nM sodium selenite, 100 uM putrescine, 520 nM, L-thyroxine, 500 nM triiodo-L-thyronine (T3), 200 nM progesterone, 25 ug/ml gentamycin) supplemented with 1% heat-inactivated Horse Serum (HS) and 1 µg/ml puromycin (Trotter J., *et al*., 1989). Cell culture media and all chemicals were from Sigma-Aldrich, except for insulin-transferrin-sodium selenite 100X supplement (Thermo Fisher Scientific, Waltham, Massachusetts, USA). When cells reached confluence, they were washed once with PBS and detached with 0.01% trypsin - 0.02% EDTA-HBSS (Sigma-Aldrich) for 5 minutes at 37ºC and the same volume of medium with serum was added to block the reaction; lastly cells were centrifugated at 300g for 5 minutes and resuspended in fresh medium. Growing density for Oli-Neu cells was $1x10^6$ cells/100mm diameter Petri dish, $3x10^5$ cells/60-mm diameter Petri dish, 10^5/35 mm diameter Petri dish and 10^4 cells/well in 96 multiwell plates (Corning). We generated stable cellular models by partially silencing the SLC25A12 gene with RNAi in Oli-Neu cells (A36 for control cells and siAGC1 for silenced cells). To obtain Oli-Neu stable cell clones $3x10^5$ cells were plated on 60-mm diameter poly-L-lysine coated Petri dishes. After 24h of incubation, cells were transfected using Lipofectamine 2000 reagent (Thermo Fisher). Following the manufacturer's instructions, 10 µl of Lipofectamine 2000 reagent and 5 µg of pLKO1-pure DNA plasmid (Sigma-Aldrich) containing a scrambled control sequence or an AGC1 targeting sequence were diluted in 250 µl of Opti-MEM medium (Thermo Fisher). Silencing and scrambled sequences were digested with AgeI/EcoRI and cloned into the pLKO.1 vector, as previously published[138]. The sequences were respectively:

scrambled control sequence:

5'-CCGGTACAACCAACGCACGCTAATCTCGAGATTAGCGTGCGTTGGTTGTTTTTTG-3'

AGC1 targeting sequence:

5'-CCGGTGCTTGCAGACCTATATAATGCctcgagGCATTATATAGGTCTGCAAGCTTTTT-3'

Both solutions were then gently mixed together. After 5 minutes of incubation, the plasmid DNA-lipofectamine solution was added directly into each Petri dish. 24 hours after transfection, the cell medium was replaced with fresh medium containing 1 µg/ml puromycin (Sigma-Aldrich) to select stably transfected cells. The cell medium was replaced every day. When puromycin resistant cells reached confluence, they were passaged. For each plasmid transfection, 500 cells were plated on a 60-mm diameter poly-L-lysine coated Petri dish and allowed to grow until visible colonies appeared. Then, isolated colonies were gently aspirated with a micropipette by using a microscope under sterile conditions and transferred into 48-well tissue culture plates. Isolated colonies were allowed to grow. AGC1 expression was tested by western blotting in at least ten different clones per plasmid transfection.

3.2. *In vitro* cell count

10^6 Oli-Neu cells/well were plated in 6-well plates. After 24 hours, cells were detached with a solution containing 0.01% trypsin - 0.02% EDTA-HBSS (Sigma-Aldrich). Cells were then diluted with an equal amount of DMEM - 10% HS and centrifuged for 5 minutes at 400g. The cell pellet was resuspended in 1ml of SATO-1% HS medium and cell number was determined by using a Neubauer chamber. Three experiments were conducted in duplicate on control and silenced Oli-Neu cells.

3.3. Measurement of cell process length

Cell morphology characterization was performed by microscopy analysis which highlights the number and length of cell processes from photographs obtained with an Eclipse TS100 (Nikon) optical microscope. 10^6 control and silenced Oli-Neu cells were plated per 35-mm diameter Petri dish. After 24 hours, images from five randomly selected fields for each Petri dish were acquired. Process length was measured by using Fiji (ImageJ2, developed by the National Institutes of Health, NIH, USA) software using the reference scale bar and using first the SET SCALE function (Analyze menu) by setting the scale bar distance in pixels and the actual distance in micrometers and then the MEASURE function (Analyze menu) after tracing each cell process with the segmented line function.

3.4. Evaluation of cell proliferation by BrdU incorporation

BrdU (5'-bromo-2'-deoxy-uridine) is a thymidine analog. Following incubation with BrdU, cells that undergo DNA replication (phase S of the cell cycle) incorporate BrdU instead of thymidine in their DNA. These cells can be identified by using an anti-BrdU antibody, which specifically recognizes BrdU, but not thymidine. To estimate cell proliferation by BrdU incorporation in control and silenced Oli-Neu cells, a colorimetric ELISA kit (Roche S.P.A., Milan, Italy) was used. 10^4 control and silenced Oli-Neu cells were plated in 96-well plates. After 4 hours, in order to allow cell adhesion, BrdU was added at a final concentration of 10 µM to each well and cells were incubated for 24 h at 37°C. Subsequently, the medium was removed and cells left to air dry. To quantify the BrdU incorporation, cells were fixed according to the manufacturer's instructions and after 30 minutes cells were incubated for 90 minutes with an anti-BrdU antibody conjugated with horseradish peroxidase (POD; 1: 100). After three washes with PBS, the substrate was added and absorbance was detected with a plate reader (Microplate Reader, Benchmark BIO-RAD); parameters were set at 405 nm for reading and 492 nm as reference wavelength.

3.5. Cell cycle analysis by flow cytometry

Flow cytometry allows a fast and quantitative analysis of suspended cell populations, measuring their physical and biochemical characteristics (volume, granularity, fluorescence). With this tool, multiple parameters for each cell can be stored at the same time without the photobleanching phenomenon. A disadvantage of flow cytometry is the inability to describe cell shape and structure. In flow cytofluotimetry, the suspended cell population is pushed through a flow chamber where single cells are set in a row and, after being struck by a light beam, they reflect light and emit fluorescence. Thus, the generated signals are collected and transformed into digital signals and sent to a computer. The first application of flow cytometry is cell cycle analysis, and therefore the cell distribution in the various phases, through the quantification of DNA. DNA is labeled with propidium iodide which has an absorption wavelength at 488 nm and an emission wavelength at 625 nm. Propidium iodide cannot pass through the cell membrane of healthy cells and therefore enters only into dead or permeable cells. Flow cytometry analysis was performed by using an Epics-XL Beckman Coulter flow cytometer equipped with a 15 mW Argon ion laser source and analyzed with

ModFit (Verity Software House, USA) software in collaboration with Dr. Capri Miriam and Dr. Rita Ostan (University of Bologna, Bologna, Italy).

3.5.1. Sample preparation for the flow cytometry

Cell cycle analysis was performed according to Nüsse[139].10^6 Oli-Neu cells were collected in a tube and centrifuged at 400g for 10 minutes. 1 ml of buffer, composed by 1 g/l of sodium citrate (to preserve the integrity of isolated nuclei), 10 mg/ l of RNase (to degrade RNA that may interfere) and 1 ml/l of Triton X-100 (a detergent that solubilizes cell membranes), was added to the obtained pellet. Propidium iodide (50mg/l) was added to the cell suspension (all reagents were from Sigma-Aldrich) and cells were incubated for at least 30 minutes at 37 ° C, or left overnight at 4 °C to allow RNAase to degrade remaining RNA. Cells could also be prepared in advance by fixing them in 90% ethanol and maintained at -20 ° C until used. In this case, 2 x 10^6 cells were collected and centrifuged at 400g for 10 minutes. After two washes with 5 ml of PBS, 1 ml of cold ethanol was added dropwise to the pellet while vortexing. Cells were stored at -20 °C. When needed, fixed cells washed twice with PBS and resuspended in the propidium iodide staining solution.

3.6. Subcellular fractionation

Cell fractionation consists in the isolation of subcellular structures in order to study their morphology, composition, and subcellular localization. In order to extract separately nucleic, mitochondrial and cytosolic proteins from Oli-Neu cells, modified protocol from Grove BD and Bruckey was used[140]; cells were scraped, resuspended in 300 µl of isotonic buffer (10 mM Hepes, 200 mM mannitol, 70 mM sucrose, 1 mM EDTA pH 7.6, 10µl/ml protease and phosphatase inhibitor cocktails) per 10 cm diameter Petri dish and left on ice for 30 minutes (all reagents were from Sigma-Aldrich). Cells were then lysed with a Potter homogenizer (B.Braun, Melsungen AG) at 1000rpm/30 strokes. Nuclei were pelleted by centrifugation at 800g for 10 min at 4°C. The cytoplasmic supernatant fraction (CF) was transferred into another Eppendorf tube. Nuclei were washed with 300 µl of isotonic buffer (10 mM Hepes, 200 mM mannitol, 70 mM sucrose, 1 mM EDTA pH 7.6, 10 µl/ml protease and phosphatase inhibitor cocktails) and centrifuged at 800g for 10 min at 4°C. The supernatant was discarded and the nuclei pellet was resuspended in 300 µl of buffer A (20 mM Hepes, pH 7.9, 10 mM NaCl, 3 m M $MgCl_2$, 0.1% NP40, 10% glycerol, 0.2 mM EDTA, 1 mM DTT, 10 µl/ml

protease and phosphatase inhibitor cocktails), left on ice for 10 min and centrifuged at 800g for 10 min at 4°C. Pelleted nuclei were then washed with buffer B to remove NP-40 (20 mM Hepes, pH 7.9, 0.2 mM EDTA, 200 mM glycerol, 1 mM DTT, 10 µl/ml protease and phosphatase inhibitor cocktails) and centrifuged at 800g for 10 minutes at 4°C. Nuclei were then resuspended in 60 µl of extraction buffer with salt (20 mM Hepes, pH 7.9, 400 mM NaCl, 2% SDS, 0.2 mM EDTA, 200 mM glycerol, 1 mM DTT, 10 µl/ml protease and phosphatase inhibitor cocktails) and left on ice for 45 minutes. The cytoplasmic supernatant fraction (CF) was centrifuged at 800x for 10 min at 4°C; then the supernatant was transferred into another eppendorf tube and centrifuged at 14,000g for 20 min. While the cytoplasmic supernatant fraction was transferred to another eppendorf tube, the mitochondrial pellet was resuspended in 500 µl of isotonic buffer (10 mM Hepes, 200 mM mannitol, 70 mM sucrose, 1 mM EDTA pH 7.6, 10 µl/ml protease and phosphatase inhibitor cocktails) and centrifuged at 14,000g for 20min. The mitochondrial pellet was resuspended in 100µl of mitochondrial lysis buffer (50 mM Tris, 1% SDS, 1 mM EDTA, pH 7.4) and left on ice for 30 min. All samples were sonicated with with a Branson 250 digital sonifier for 3 pulses of 2 seconds each (waiting for 5 seconds between each pulse) at 10% power output and stored at -80°C until used. Total protein sample content was determined by using the Lowry quantification method (Lowry *et al*., 1951).

3.7. Lactate measurement in extracellular medium

Lactic acid was quantified in the laboratory of Dr. Massimo Lasorsa (IBIOM, CNR, Bari, Italy) in conditioned complete DMEM medium in the presence of high glucose concentration, (4,5 g/l), harvested from Oli-Neu cell cultures after 24 h and 48 h respectively[138]. This assay was performed on both control and AGC1 silenced cells, untreated or treated with db-cAMP. The medium was collected and centrifuged at 700g for 5 min to remove cell debris. Lactate in the supernatant was assayed as per Gutmann and Wahlefeld, using the following reaction:

L(+)Lactate + ß-NAD + Hydrazine $\xrightarrow{\text{LDH}}$ Pyruvate Hydrazone + ß-NADH

ß-NAD = ß-Nicotinamide Adenine Dinucleotide, Oxidized Form;
ß-NADH = ß-Nicotinamide Adenine Dinucleotide, Reduced Form;
LDH = L-Lactic Dehydrogenase.

The reagents were pipetted into suitable cuvettes as in the following table:

	Sample	***Blank***
Deionized water	0.35 ml	1.35 ml
600 mM Hydrazine buffer (Sigma), 1 M glycine, 5.6 mM EDTA, pH 9.5	1.4 ml	1.4ml
Dilutions of extracellular medium	1 ml	---
50 mM ß-NAD (Sigma)	0.15 ml	0.15 ml

The reaction solution was mixed well by inversion and equilibrated to 25°C. The absorbance at 340 nm (A_{340nm}) was monitored until it became constant, using a suitably thermostated spectrophotometer. The initial absorbance of the sample and blank were recorded. Then 0.1 ml of L-Lactic Dehydrogenase (5000 units/ml, Fluka) were added to the sample and blank and the two cuvettes were immediately mixed by inversion. The increase in absorbance at A_{340nm} was recorded until the reaction was complete (approximately 30 minutes). The final absorbances were recorded. To determine the concentration of L(+)Lactic acid in our samples, the following formula was applied:

Micromoles Lactic Acid/weighed sample =
$\Delta A = Af - Ai$;
Ai = Initial Absorbance;
Af = Final Absorbance;
df = Dilution factor of sample solution;
3 = Final volume (in milliliters) of assay;
6.22 = Millimolar extinction coefficient of ß-NADH at 340 nm.

3.8. Aequorin and luciferase luminescence measurements

Oli-Neu cells were transiently transfected with plasmids carrying the coding sequence of recombinant aequorins selectively targeted to the cytosol (cytAEQ) or mitochondria (mtAEQmut), and recombinant luciferase targeted to mitochondria (mtLuc)[141]. Transfected cells were incubated for 1h at 37°C with Krebs–Ringer modified buffer (KRB; 125 mM NaCl, 5 mM KCl, 1 mM Na3PO4, 1 mM MgSO4, 5.5 mM glucose, and 20 mM 4-(2-hydroxyethyl)-1-piperazineethanesulfonic acid [HEPES], pH 7.4, at 37° C) supplemented with 1 mM CaCl2 and 1 g/l glucose (+ 5 µM coelenterazine for aequorin reconstitution). Cells were subsequently perfused in the same buffer (+ 20 mM luciferin for luciferase assay) in a

purpose-built luminometer where they were stimulated with 500 μM Carbachol (Cch). Aequorin experiments were terminated by lysing the cells in a hypotonic solution with 0.1 mM digitonin and 10 mM CaCl2, and light output was collected and calibrated in [Ca2+]. In luciferase assays, data were expressed as mtLuc light output of cells. These experiments were performed in the laboratory of Dr. Massimo Lasorsa (IBIOM, CNR, Bari, Italy).

3.9. Cell fluorescence analysis

Measurements of intracellular reactive oxygen species were performed in the laboratory of Prof. Paolo Pinton (University of Ferrara, Ferrara, Italy) by loading cells with 5 μM 5-(and-6)-chloromethyl-2′,7′-dichlorodihydrofluorescein diacetate, acetyl ester (CM-H2DCFDA; Life Technologies, C-6827) for 20 min at 37°C, and green fluorescence of cells was analyzed with a Tali® Image-Based Cytometer. Mitochondrial hydrogen peroxide levels were measured in Oli-Neu cells cultured on 24x24 mm glass coverslips and transfected with the ratiometric fluorescent probe with mitochondrial localization pHyPer-dMito (mt-HyPer). After 24 h of expression, cells were maintained in KRB supplemented with 1 mM $CaCl_2$ and carbon sources (1 g/l glucose, 1 mM pyruvate and 2 mM glutamine), and placed in an open Leyden chamber on a 37°C thermostated stage. 494/406 nm excitation filters and a 500-nm long-pass beam splitter were used, and an image pair was obtained every 200 ms with a 40x objective. For a ratiometric measurement, at the end of each measurement, probe efficiency was ascertained by adding H_2O_2 as reference. Fluorescence data were expressed as emission ratios. The experiments were performed on a Cell^R Olympus multiple wavelength high-resolution epi-fluorescence microscope. Mitochondrial inner membrane potential (Ψm) and mitochondrial morphology were measured by loading the cells with 20 nM tetramethyl rhodamine methyl ester (TMRM; Life Technologies, T-668) for 30 min at 37°C. Images were taken on an inverted Nikon LiveScan Swept Field Confocal Microscope (*SFC*) Eclipse Ti equipped with NIS-Elements microscope imaging software (Nikon Instruments). TMRM fluorescence intensities (exc. 560 nm; emis. 590-650 nm) were imaged every 5 s with a fixed 20 ms exposure time. At the end of the experiments, 10 μM FCCP was added after 240 acquisitions to completely collapse the Ψm and subtract the non-mitochondrial TMRM fluorescence, as previously described. For mitochondrial morphology experiments, 51-plane z-stacks where acquired with a voxel dimension of 133 × 133 × 200 nm (X × Y × Z). The mitochondrial network, described in number and volume, and 3D renders were obtained with Imaris 4.0 (Bitplane).

3.10. *In vivo* model

For *in vivo* AGC1-deficiency studies, a mouse model represented by C57BL/6N heterozygous SLC25A12 mice (*Mus musculus*) was obtained by using the gene trapping technique by the Texas A & M Institute for Genomic Medicine (Houston, Texas, USA). A 6.5 kb VICTR 76 construct designed to be inserted into the intronic region between exons 2 and 3 of the SLC25A12 gene was used. Through homologous recombination, the vector determined an insertion of a premature stop codon between exon 2 and 3 of AGC1 mRNA, which resulted in a truncated protein with no catalytic sites able to bind the carrier substrates and therefore inactive. The targeting vector was linearized and electroporated into C57BL/6N mouse totipotent stem cells and labeled cell clones were identified and blastocysts were implanted in pseudopregnant female C57BL/6N to obtain a mouse F1 generation; Fi mice were the paired with females of the same C57BL/6N background. Crossing was made either between an $AGC1^{+/-}$ parent and an $AGC1^{+/+}$ wild type, or both heterozygous parents and the colony obtained was used for experiments. Animals were bred with ad libitum access to food and water, maintained in a 12/12 hour light-dark cycle at 20 °C ± 2 °C and controlled humidity. In order to guarantee their well-being, appropriate environmental enrichment was introduced to stimulate spontaneous motor activity, curiosity and play. The health and physical state of mice was periodically controlled by veterinarians at the University of Bologna and experiments were conducted in accordance with European Community laws and Italian legislation and were also approved by an Ethical committee for Animal Experimentation at the University of Bologna (Protocol No 17-72-1212).

3.11. Mice genotyping

Genotyping was performed at 14 days after birth by extracting DNA from mouse tail tips by using the Extract-N-Amp tissue extraction kit (Sigma-Aldrich) and performing a PCR assay. The following set of PCR primers (Sigma-Genosys, Texas, USA) were used to identify wild-type (WT), heterozygous (HET) and KO mice:

IST11936G6-Forward. 5 'GGAGACTGACAGTCAACAAG 3' (all animals). Tm = 52.76 °C
IST11936G6-Reverse. 5 'GGCATTTGCACACCGTGGA 3' (WT, HET animals). Tm = 58.26 °C
Downstream Reverse. 5 'CCAATAAACCCTCTTGCAGTTGC 3' (HET, KO animals). Tm = 58.30 °C.

Two separate PCR reactions were performed for each animal according to Table 1 and 2 and amplification reactions were resolved in a 2% agarose/TBE gel.

Reaction Components	***Volume (µL)***
LongAmpTaq 2x Master Mix (Biolabs)	10.00
Reverse Primer 10µM	1.00
Forward Primer 10µM	1.00
MilliQ H2O	4.00
Tail lysate 1:20 dilution; boil 5 min	4.00
Total reaction volume	20.00

Table 1: *reaction components and corresponding volumes to assemble the PCR reactions.*

Step	*Temp*	*Time*	*Note*
1	95° C	30"	
2	95° C	10"	
3	60-65°C	30"	
4	65°C	1'	Go to 2, for 35 cycles
5	65°C	5'	
6	4°C	∞	

Table 2: *amplification cycle.*

Reactions were carried out using the IST1193G6-F and IST1193G6-R primers which allow to detect wild-type or heterozygous animals and primers IST1193G6-F and Downstream Rev, which, on the contrary, show heterozygous or knock-out mice. Expected PCR product lengths were for WT animals one 369bp band, for heterozygous animals both a 369 and a 342 bp band, whereas for KO animals only one 342bp band was expected.

3.12. Measurement of AGC1 aspartate/glutamate and glutamate/glutamate exchange activity in brain mitochondria

Brain mitochondria were isolated by using a kit (Pierce Biotechnology, Rockford, USA) with the Halt Protease Inhibitor Mixture (Pierce Biotechnology, Rockford, USA) according to the manufacturer's instructions. In the laboratory of Dr. Massimo Lasorsa (IBIOM, CNR, Bari, Italy), mitochondria were then solubilized (0.6 mg protein/ml) in solubilization buffer (3% Triton X-114, 10 mM Pipes pH 7.0, 1 mM EDTA, 4mg/ml DPG). After 1 h of incubation on ice, extracts were centrifuged (12500 × g, 10 min at 4°C) to remove membranes and other unsolubilized impurities. An aliquot of the supernatant was reconstituted into liposomes. 30 µg of solubilized mitochondria were added to a mixture consisting of 70 µL 10% Triton X-114, 100 µL preformed liposomes previously sonicated [10% (WT/vol) from egg yolk

phospholipids in 2 mM Pipes-NaOH, pH 7.0] + 20 mg/ml DPG, 70 µL 200 mM Pipes pH 7.0, 70 µL 200 mM substrate (Aspartate, Glutamate, or ATP) pH 7,0 and water to a final volume of 700 µL. This mixture was recycled 13 times through an Amberlite column XAD-2 (Bio-Rad Laboratories, Srl, Segrate (MI), Italy) (4.0 × 0.5 cm). All operations were carried out at 4°C, except for the passage through the Amberlite column conducted at room temperature. Subsequently, the external substrate was removed from proteoliposomes by gel filtration chromatography on Sephadex G-75 columns (15 x 0.7 cm) pre-equilibrated with a buffer containing 10 mM PIPES pH 7, 50 mM NaCl and 1 mM EDTA. Proteoliposomes eluted from the chromatography column, about 650 µl, were aliquoted into reaction tubes and used to perform transport measurements. Each test was performed in duplicate. Transport activity was determined at 25°C by measuring the incoming flow of radiolabeled substrate. Transport was started by adding L-[^{14}C] aspartate, [^{14}C] ATP, L-[^{14}C] glutamate and terminated by addition of 8 mM Pyridoxal5'-phosphate and 6 mM bathophenanthroline according to the "inhibitor-stop" method[17]. In control samples, inhibitors were added from the beginning together with the labeled substrate. Lastly, the external substrate was removed by passing samples through a Sephadex G-75 column (8 x 0.6 cm) and the eluted proteoliposomes were collected into appropriate vials to which 4 ml of Ultima-Flo M (Packard BioScience Company, Meriden, USA) scintillating mixture were added, vials were then shaken and placed in a liquid phase scintillator (Beckman LS 6000 IC) to measure radioactivity counts per minute (cpm). Experimental values were corrected by subtracting control values. The initial transport rate was calculated from the radioactivity taken up by proteoliposomes after 1 min (during the initial linear range of substrate uptake).

3.13. CNPase activity measurement

CNPase (2 ', 3' cyclic nucleotide, 3 'phosphohydrolase) hydrolyses 2', 3' nucleotides opening their phosphatidic ring and transforming them into the corresponding 2'-phosphate nucleotides. This enzyme accounts for about 4% of total myelin proteins in the central nervous system and immunocytochemical studies showed that it is predominantly localized in the myelin-axon interface[142]. CNPase specific physiological functions are not yet clear, jowever its distribution seems to be exactly the same as that of myelin, the main oligodendroglial product. In this regard, it has been observed that the corpus callosum, a structure containing axons originating from neurons in both cerebral hemispheres that contact the nerve cells of the opposite hemisphere, contains CNPase levels ten times greater than in

the cortex. This enzyme is evaluated as a marker for oligodendrocytes and myelination. This assay[143] is based on a colorimetric reaction resulting the formation of a ferrous salt reduced complex between molybdate and inorganic phosphate. Initially, samples were prepared by adding 5 µl of AGC1 $^{+/+}$ and AGC1 $^{+/-}$ mouse brain homogenate and 195 µl of substrate (2 '3' cyclic-AMP, 7.7 mM Tris/50 mM Maleate pH 6,2); and then samples were shortly vortexed. Samples were then incubated at 30°C for 20 min, and then the CNPase enzyme reaction was blocked by transferring the tubes at 100°C for 1 minute; the temperature was afterwards brought back to 30°C and 100 µl of Tris HCl $MgCl_2$ solution (Tris HCl 300mM - $MgCl_2$ 2 1 mM, pH 9.0) were added, in which alkaline phosphatase (0.7 mg/ml) was dissolved, allowing adenosine monophosphate hydrolysis. The reaction was then blocked after 45 min by adding 900 µl of 10% acetic trichloroacetic acid (TCA) to each sample and then samples were shortly vortexed. Samples were centrifuged at 3500 rpm for 10 minutes to precipitate the proteins. Subsequently, 700 µl of supernatant were transferred into an eppendorf in which 500 µl of reagent [$FeSO_4$ * 7 H_2O + molybdate reagent (Ammonium heptamolybdate in H_2SO_4 10 N) + H_2O] were added and then samples were shortly vortexed. The colorimetric reaction was expected to develop after 2/3 minutes at 30°C. At the same time, the standard calibration curve was set up with a 1mM Na_2HPO_4 solution. Each measurement of the calibration curve and samples was performed in duplicate and the reaction was quantitatively measured reading the absorbance with a spectrophotometer at a wavelength of 660 nm. It was thus possible to calculate the relationship between the concentration of Na_2HPO_4 and its absorbance values and analyze the obtained data through linear regression to determine CNPase activity.

3.14. Intracardiac perfusion

Intracardiac perfusion is the best technique to fix tissues by replacing circulating blood with a fixative, allowing rapid and uniform fixation of the sample and maintaining cellular constituents in a nearly physiological state. Intracardiac perfusion was performed on AGC1 $^{+/+}$ and AGC1 $^{+/-}$ mice both at 21 days after birth and in adult mice previously anesthetized by intraperitoneal injection with xylor (2%) and zoletyl (100mg/kg). A 23 ¾ butterfly needle was inserted into the left ventricle while connected to a peristaltic pump set at a flow rate of 20-25 ml/min and first a PBS solution and then a 4.0% paraformaldehyde (PFA)- phosphate buffer (0.194 M Na_2HPO_4, 0.026 M NaH_2PO_4) solution were injected into the heart. In order to allow blood and PFA outward flow, a small opening in the right atrium was performed. PBS was used to remove red blood cell residues in the blood vessels and avoid the formation of

blood clots due to fixative-hemoglobin interactions. To minimize the risk of cerebral ischemia, perfusion was started quickly avoiding the formation of air bubbles in the capillary; correct fixation was verified by monitoring the color of the liver and stiffness of the mouse body. The mouse brain was then isolated, post-fixed for 24 hours at 4°C in PFA and left in 18% sucrose-phosphate buffer (0.194 M Na_2HPO_4, 0.026 M NaH_2PO_4) for 24 hours at 4°C. After 3 washes in PBS in order to remove PFA and sucrose residues, the tissue was cut into the two hemispheres and stored at -80°C until needed for cryostat sectioning.

3.15. NSCs *in vitro* models

In order to study the effect of AGC1-deficiency on proliferation and differentiation *in vitro*, two different cellular models of Neural Stem Cells (NSC) were prepared: neurospheres and NSCs derived from iPS cells (induced Pluripotent Stem cells).

3.15.1. Neurospheres

Neurospheres are cluster of neural stem cells in suspension, a valuable instrument to determine the potential (proliferation or differentiation) of neuronal stem cells *in vitro*[144]. Sub-ventricular zone (SVZ) microdissection were performed in adult male mice (8-month old) (3 $AGC1^{+/+}$ and 3 $AGC1^{+/-}$ mice respectively). The brain was cut transversely near the optic chiasm and the olfactory bulbs and cerebellum were removed. The rostral part of the brainstem containing the lateral ventricles and their respective periventricular regions was then used for sub-ventricular (SVZ) withdrawal. The caudal part of the brain was separated at the level of the *corpus callosum*, the diencephalus was removed and the dentate gyrus was dissected from the hippocampus (Fig.3.1).

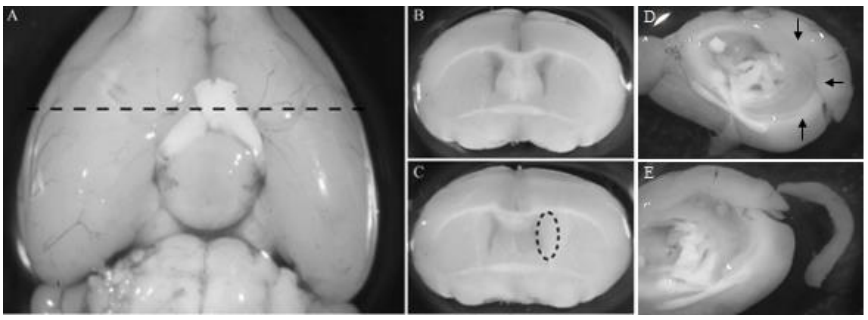

Figure 3.1: *Brain microdissection. (A) Ventral view of an adult rat brain. The dotted line indicates the cutting site in the rostro-caudal direction for the subsequent isolation of the SVZ. (B) Coronal section obtained by cutting along the dotted line in A. The rostral periventricular region of the lateral ventricle can be observed. (C) Sub-ventricular area visible after removal of striated tissue. (D) Dentate gyrus and hippocampus visible after the separation of the two hemispheres at the level of the corpus callosum. (E) Dissection and isolation of the dentate gyrus from the hippocampus*[145].

Dissected tissues were mechanically disaggregated by chopping with a sterile blade in Hank's Balanced Salt Solution (HBSS; HEPES 3.9 mg/ml, NaHCO 0.5 mg/ml, Glucose 0.9 mg/ml, penicillin/streptomycin 0.5%) under a sterile cell culture hood and centrifuged at 300g for 5 min. The pellet was resuspended in papain solution (0.2 mg/ml EDTA + 0.66 mg/ml Papain + 0.2 mg/ml cysteine in HBSS) to facilitate stem cell release and placed in a centrifuge tube at 37 °C for 20 minutes in a water bath, shaking every 5 min. The pellet was then resuspended in HBSS and left in a water bath at 37 °C for another 10 min. Papain was inhibited by the addition of DMEM-F12 (Gibco Life Technologies, Waltham, MA, USA) supplemented with insulin from bovine pancreas (Sigma-Aldrich) (10 µg/ml) and the sample was centrifuged at 300g for 5 min. The pellet was resuspended in HBSS and centrifuged at 400g for 5 min, the supernatant was discarded and the pellet was resuspended in DMEM-F12 (Gibco) supplemented with 2 mM glutamine, insulin (10 µg/ml), 20 ng/ml Epidermal Growth Factor (EGF; PeproTech EC, London, UK) 20 ng/ml Fibroblast Growth Factor-2, (FGF2; Peprotech), 1% N2 (Thermo Fisher), 1% B27 (Thermo Fisher) and 10 units/ml penicillin and 10 µg streptomycin/ml (Sigma-Aldrich). In order to induce neurosphere growth, EGF and FGF growth factors were added every other day (FGF concentration was halved by the third passage onwards (10 ng/µl); neurospheres were passaged every week (5/7 days of growth) by mechanical procedures. For this purpose, neurospheres were collected in a centrifuge tube with 5 ml of DMEM-F12 medium, centrifuged at 300g for 5 minutes and the pellet was resuspended in sterile PBS (4-5 times). Neurospheres were then centrifuged at 300g for 5 minutes, the supernatant was removed and 1 ml of Acutase (Aurogene Srl, Roma, Italy) was added to the pellet by gently resuspending 2 times and incubated at 37 °C for 5 minutes. 4 ml of DMEM:F12 were then added to the neurosphere suspension and then centrifuged at 1000 rpm for 5 minutes. Single cells were counted and plated in complete DMEM;F12 supplemented with insulin (10 µg/ml), 1% N2, 1% B27, 20 ng/ml EGF, 20 ng/ml FGF, 2 mM glutamine and 10 units/ml penicillin and 10ug streptomycin/ml (Sigma-Aldrich).

3.15.2. Neurospheres proliferation assay

To evaluate the proliferation and growth rate of SVZ-derived NSCs from $AGC1^{+/+}$ and $AGC1^{+/-}$ mice, neurospheres were plated as single stem cells in 96 multiwell plates ($5x10^3$ cells/well). Neurosphere proliferation experiments were set up after passage 3; cells were allowed to grow at 37˚C and 5% CO_2 in an incubator for 4 days. After 4 days in culture, 5

different image fields per well were acquired by using an eclipse TE 2000-s microscope (Nikon) in bright field mode using a 10x objective. Acquired images were then analyzed with Fiji ImageJ2 using the publicly available cell colony edge macro[146] and only neurospheres with an area bigger than 400 μm^2 were considered; results were expressed as average neurosphere number and average neurosphere size and analyzed using the two-tailed t-test Student to determine statistically significant variations.

3.15.3. Neurospheres BrdU proliferation assay

AGC1 $^{+/+}$ and AGC1 $^{+/-}$ mouse neurospheres were passaged as single cells (1.43 x 10^5 single cells/6-cm diameter Petri dish) in complete DMEM-F12 medium supplemented with 10 μm BrdU (Sigma-Aldrich). BrdU was added every day for 4 days and then 30 neurospheres were plated in poly-L-lysine (10 μg/ml) and fibronectin (1 μg/ml) treated 13-mm diameter glass coverslips in complete DMEM-F12 medium and BrdU was added again. After 24 hours, neurospheres were fixed with 4% PFA for 30 minutes, washed with PBS and stored at 4°C in PBS until used. Experiments were conducted in duplicate with 3 replicates per condition.

3.15.4. Neurospheres differentiation

To study neurosphere differentiation, AGC1 $^{+/+}$ and AGC1 $^{+/-}$ SVZ-derived neurospheres were counted and plated on 13-mm coverslips (30 neurospheres/well) previously treated with poly-L-lysine (10 μg/ml) and then incubated at 37°C for at least 3 hours with fibronectin (1 μg/ml) in order to allow stem cell adhesion and subsequent differentiation. Cells were then plated in complete DMEM-F12 medium and allowed to differentiate for 1 or 7 days in an incubator at 37°C. After differentiation, neurospheres were fixed with 4% PFA for 30 minutes, washed with PBS and stored at 4°C in PBS until used for immunofluorescence analysis.

3.16. hiPS (human induced Pluripotent Stem cells)

Human induced pluripotent stem cells (hiPSCs) were generated through human adult somatic cell reprogramming by using four transcription factors: Oct4, Sox2, Klf4 and c-Myc[118]. iPS cells are a great advantage for the study of neurodegenerative diseases since they can be used to reproduce *in vitro* the various types of specialized cells in the body, enabling the ability to study multiple levels of disease cellular effects. For the study of AGC1, control iPS cells were obtained from human fibroblasts of healthy patients, kindly donated by Dr. Massimo Lasorsa

(IBIOM CNR Bari) whereas iPS cells derived from AGC1-deficient fibroblasts (from a pair of Indian twins affected by AGC1-deficiency), AGC1 M1-01 (male) and AGC1 F1-03 (female), were kindly provided by Professor Stewart Anderson (Children's Hospital of Philadelphia, Upenn School of Medicine). Petri dishes were prepared adding diluted matrigel (consulting the Certificate of Analysis supplied with the Matrigel, add the recommended aliquot size"Dilution Factor"to make up 24 mL of diluted matrix) in cold DMEM-F12 and incubated at 37°C for 1-3 hours before use. Control and AGC1-deficiency patient iPS cells were thawed in a water bath at 37°C, taking care to leave a pea-sized liquid fraction in order not to over-stress the cells, and were then resuspended in DMEM F12 medium at room temperature. After a centrifugation at 300g for 5 minutes, the iPS pellet was resuspended in an appropriate volume of mTeSR1 (Basal Medium + 5X Supplement, STEMCELL Technologies, Cambridge, UK) with 10 μM Y-27632 dihydrochloride (RHO/ROCK pathway inhibitor, STEMCELL Technologies) and penicillin-streptomycin (10 units/ml penicillin and 10 μg streptomycin/ml Sigma-Aldrich). Every day, half the volume of the culture medium was replaced and Y-27632 added only on the day cells were either plated or passaged. Two different protocols were used for iPS passaging depending on the reagent used: Accutase (Innovative Cell Technologies, Farmington Hills, MI, USA) or ReleSR (STEMCELL Technologies). When passaging with Accutase, cells were incubated with the reagent for different times (5-10 minutes) depending on cell sensitivity. After verifying cellular detachment through optical microscopy, Accutase was inhibited adding an equal volume of mTeSR1 medium (STEMCELL Technologies) and cells were centrifuged at 300g for 5 min. The supernatant was then discarded, the pellet was resuspended in mTeSR1 medium + 10 μM Y-27632 (STEMCELL Technologies) and cells were plated into matrigel-treated dishes (STEMCELL Technologies). The passaging protocol with ReleSR reagent is faster, and was used to remove differentiated cells within iPS cultures; in fact, ReleSR allows differentiated cells to remain attached to cell culture plates. After removing the growth medium and washing the cells with sterile PBS, iPS cells were incubated with ReleSR for 1 min. Then ReleSR was almost completely aspirated by leaving a thin liquid layer in the Petri dish and iPS cells were incubated at 37°C for 5-7 minutes. The reaction was inhibited by adding equal volume of mTesR1 medium. Lastly, cells were collected, resuspended in mTeSR1 medium + 10 μM Y-27632 and plated.

3.16.1. iPS cell differentiation into NSCs

Control and male patient-derived iPS cells were expanded and then differentiated to generate Neural Stem Cells (NSCs). In order to obtain NSCs, two different protocols were tested. The first protocol[121] was performed by forming Embryoid Bodies (EBs, spheres of undifferentiated cells that, morphologically, resemble a gastrula) from suspended iPS cell aggregates. To obtain EBs, iPS cells were passaged as single cells and plated for 3/4 days in ultra-low adeshion (Corning) culture plates without matrigel and maintained in N2-B27 medium (Table 3) (10 μM Y-27632 was added during the first passage).

N2-B27 MEDIUM

DMEM F-12 (StemCell) + Neurobasal (Invitrogen)	1 : 1
Basic fibroblast growth factor (bFGF; Peprotech)	10 ng/ml
Epidermal growth factor (EGF; Peprotech)	10 ng/ml
N2 supplement (Thermo Fisher)	1%
B27 supplement (Thermo Fisher)	2%
Penicillin-Streptomycin (Sigma-Aldrich)	1%
L-Glutamine (Sigma-Aldrich)	2 mM

Table 3: *N2B27 Medium composition.*

EBs were passaged as single cells after 3/4 days and plated on poly-L-lysine (10 mg/ml) and fibronectin (1μg/ml) treated culture plates in DMEM-F12 differentiation medium (Table 4) to allow cell adhesion and differentiation into NSCs (10 μM Y-27632 was added during the first passage).

DMEM F-12 DIFFERENTIATION MEDIUM

DMEM F-12 (StemCell)	
Basic fibroblast growth factor (bFGF; Peprotech)	10 ng/ml
Epidermal growth factor (EGF; Peprotech)	10 ng/ml
B27 supplement (Thermo Fisher)	1%
N2 supplement (Thermo Fisher)	1%
Bovine serum albumin (BSA, Sigma-Aldrich)	50 µg/ml
Penicillin-Streptomycin (Sigma-Aldrich)	1%
L-Glutamine (Sigma-Aldrich)	2 mM

Table 4: *DMEM F-12 differentiation medium composition.*

For the second iPS differentiation protocol[147], iPS cells were passaged as single cells in ultra-low adhesion (Corning Incorporated, NY, USA) culture plates with Neurobasal Medium + supplements (Table 5) (10 µM Y-27632 was added during the first passage).

Neurobasal MEDIUM

Neurobasal 1X (Gibco)	
Insulin-transferrin-selenium (ITS; Sigma)	1%
N2 supplement (Thermo Fisher)	1%
B27 supplement (Thermo Fisher)	2%
Penicillin-Streptomicyn (Sigma-Aldrich)	1%
L-Glutamine (2mM, Sigma-Aldrich)	2 mM
Noggin (Peprotech)	200 ng/ml

Table 5: *Neurobasal Medium composition.*

After 10 days, the cells were plated on poly-L-lysine (10 mg/ml) and fibronectin (1 µg/ml) treated culture plates with complete Neurobasal Medium without Noggin (PeproTech), and allowed to grow for 6-11 days. For NSC maintenance, culture medium was changed every 2/3 days and cells passaged into poly-L-lysine (10 mg/ml) and fibronectin (1 µg/ml) treated culture plates once a week.

3.17. Cell and tissue lysate preparation

Oli-Neu cell lysate samples were obtained by washing cell cultures with PBS and resuspending cell cultures in an appropriate volume of lysis buffer (50 mM Tris pH 7.4, 1 mM EDTA, 1% SDS, 10 µl/ml protease inhibitors). Mouse brain tissues were lysed in lysis buffer (10mM Hepes, 200mM mannitol, 70mM sucrose, 1% NP40, 1 mM EDTA pH 7.6, 10 µl/ml protease and phosphatase inhibitor cocktails, (all chemicals were from Sigma-Aldrich) with a Potter homogenizer at 1000rpm/30 strokes and then sonicated with a Branson 250 digital sonifier for 3 pulses of 2 seconds each (waiting for 5 seconds between each pulse) at 10% power output. All samples were stored at -80°C until used. Total protein sample content was determined by using the Lowry quantification method[148].

3.18. Lowry quantification method

Through the Lowry assay[148] it is possible to quantify the total protein content in a sample. For quantification, bovine serum albumin (BSA, 1.5 mg/ml) was used to obtain a calibration curve. Each sample and each point of the curve were measured in duplicate: to 5µl of sample double-distilled water (ddw) was added up to 200 µl. Subsequently, 1 ml of solution I (98% solution A; 2% Na_2CO_3 in 0.1 N NaOH; 1% solution B: 0.5% $CuSO_4$; 1% solution C; 1% Na-K tartrate) was added to each sample and after a 10-minute incubation at room temperature, 100 µl of solution II (50% Folin reagent and 50% bd H_2O, all reagents were from Sigma-Aldrich) were added and the samples were vortexed and allowed to incubate for 30 minutes at room temperature. Absorbance was then read at 700 nm and the relationship between BSA concentration and absorbance values was analyzed through linear regression in order to determine protein concentration of all samples.

3.19. Western blot

Sonicated samples were resolved in SDS-PAGE (Sodium Dodecyl Sulphate - PolyAcrylamide Gel Electrophoresis). Equal protein amounts (30 µg) from each sample were resuspended in 4X Loading buffer (1M Tris-HCl pH 6.8; 20% sodium dodecyl sulfate; 0.4 µl/ml glycerol; 2 g/l bromophenol blue and 2M dithiothreitol; all from Sigma-Aldrich), loaded onto sodium dodecyl sulfate–polyacrylamide gels, subject to electrophoresis and transfer onto a nitrocellulose membrane (GE Healthcare Life Sciences, Little Chalfont, UK). After blocking aspecific sites with PBS containing 0.1% Tween 20 (Sigma) and 5% nonfat dried milk (Bio-Rad) for 1 hour at room temperature, membranes were incubated with a primary antibody overnight at 4 °C. The next day, after 3x10 min washes with 0.1% Tween-20/PBS, membranes were incubated with a specific secondary antibody conjugated to horseradish peroxidase for 90 minutes at room temperature in 0.1% Tween-20/PBS. Labeled proteins were visualized by using Clarity™ Western ECL Substrate (Bio-Rad) and detected using the software Image Lab with a ChemiDoc™ MP imaging system. Densitometric analysis was performed using Image Lab software (BioRad).

Table 6 shows the antibodies used for Western Blot analysis.

Primary antibody	*Dilution*	*Secondary antibody*	*Dilution*
AGC1/Aralar1 mouse monoclonal IgG (Santa Cruz)	1: 1000	Goat anti-mouse IgG HRP (Santa Cruz)	1:2000
MAG rabbit polyclonal IgG (Santa Cruz)	1: 1000	Goat anti-rabbit IgG HRP (Santa Cruz)	1:2000
Histone H3 rabbit polyclonal IgG (Santa Cruz)	1: 1000	Goat anti-rabbit IgG HRP (Santa Cruz)	1:2000
HSP60 rabbit polyclonal IgG (Santa Cruz)	1: 1000	Goat anti-rabbit IgG HRP (Santa Cruz)	1:2000
TGFβ 1 rabbit polyclonal IgG (Santa Cruz)	1: 1000	Goat anti-rabbit IgG HRP (Santa Cruz)	1:2000
TGFβ 2 rabbit polyclonal IgG (Santa Cruz)	1: 1000	Goat anti-rabbit IgG HRP (Santa Cruz)	1:2000
TGFβ 3 rabbit polyclonal IgG (Santa Cruz)	1: 1000	Goat anti-rabbit IgG HRP (Santa Cruz)	1:2000
TGFβ R1 rabbit polyclonal IgG (Santa Cruz)	1: 1000	Goat anti-rabbit IgG HRP (Santa Cruz)	1:2000
TGFβ R2 mouse monoclonal IgG (Santa Cruz)	1: 1000	Goat anti-mouse IgG HRP (Santa Cruz)	1:2000
PDGFα rabbit polyclonal IgG (Santa Cruz)	1: 1000	Goat anti-rabbit IgG HRP (Santa Cruz)	1:2000
PDGFRα rabbit polyclonal IgG (Santa Cruz)	1: 1000	Goat anti-rabbit IgG HRP (Santa Cruz)	1:2000
GAPDH mouse monoclonal IgG (Santa Cruz)	1: 20000	Goat anti-mouse IgG HRP (Santa Cruz)	1:2000

Table 6: *Primary and secondary antibodies used for Western Blot analysis.*

3.20. Immunohistochemistry

Immunohistochemistry (IHC) is a technique used to localize antigens or proteins in tissue sections or cells. IHC was performed on brain sections from AGC1 $^{+/+}$ and AGC1 $^{+/-}$ 21-day old and adult mice, previously fixed with 4.0% PFA. Brain tissue dissection was performed by using a cryostat at a cutting temperature of -30 /-40 °C and sections of 40 µm were obtained. For protein detection, an indirect immunoperoxidase technique was used. This technique involves the use of a secondary antibody conjugated to horseradish peroxidase (HRP) able to recognize the primary antibody directed against a specific antigen of interest;

HRP thus, reacting with the chromogenic substrate DAB (3,3'-diaminobenzidine), forms an insoluble colored precipitate visible through optical microscopy. Various antibodies were used for immunohistochemical analysis of the different brain cell types and proliferation levels. The main advantages of this method compared to the direct method are the greater sensitivity and lower amount of primary antibody required. Brain slices were washed in PBS and incubated for 30 minutes in 0.3% H_2O_2 in methanol to inactivate endogenous peroxidases. After 3 x 10 minutes washes with PBS and additional 3 x 10 minutes washes with PBS-0.1% Triton (Sigma-Aldrich), aspecific sites were blocked by incubating brain slices for 1 hour in blocking buffer (PBS-0.1% Triton + 2% normal goat serum [Sigma-Aldrich]). Brain slices were incubated overnight at 4^{o}C with primary antibodies diluted in blocking buffer. Then brain slices were washed 3 x 10 minutes in PBS-0.1% Triton and incubated for 2 hours with secondary antibodies in blocking buffer. After incubation with secondary antibodies, the sections were washed 2 x 10 minutes in PBS-0.1% Triton and 1 x 10 minutes in 50 mM Tris, pH 7.6. Brain slices were then incubated with diaminobenzydine (DAB) following the manufacturer's instructions (Vector Laboratories, Burlingame, Ca, USA) for 30-300 seconds depending on the antibody used and then washed in H_2O. Slices were mounted on gelatin coated glass slides, air-dried overnight, dehydrated 1 x 1 minute in 90% ethanol and 2 x 1 minute in 100% ethanol, then incubated for 1 minute in xylene and mounted with Permount (Sigma-Aldrich). Glass slides were allowed to dry overnight and observed with an Eclipse Hoechst staining TE 2000-S microscope (Nikon) equipped with an AxioCam MRm (Zeiss, Oberkochen, Germany) digital camera. Table 7 shows the antibodies used for immunohistochemistry analysis.

Primary antibody	*Dilution*	*Secondary antibody*	*Dilution*
MBP mouse monoclonal (ABCAM)	1: 500	Goat anti-mouse IgG HRP (Santa Cruz)	1:500
OLIG 2 rabbit polyclonal IgG (Santa Cruz)	1: 500	Goat anti-rabbit IgG HRP (Santa Cruz)	1:500
CNPase rabbit monoclonal (Cell signaling)	1: 500	Goat anti-rabbit IgG HRP (Santa Cruz)	1:500
pHistone H3 (Ser10) rabbit polyclonal IgG (Santa Cruz)	1: 500	Goat anti-rabbit IgG HRP (Santa Cruz)	1:500
Ki67 rabbit polyclonal (ABCAM)	1:500	Goat anti-rabbit IgG HRP (Santa Cruz)	1:500
DCX rabbit polyclonal (ABCAM)	1:1000	Goat anti-rabbit IgG HRP (Santa Cruz)	1:500
GFAP rabbit immunoglobulins (Dakopatts, Missouri, California, USA)	1:2000	Goat anti-rabbit IgG HRP (Santa Cruz)	1:500

Table 7: *Primary and secondary antibodies used for immunohistochemistry analysis.*

3.21. Immunofluorescence

Immunofluorescence is a direct or indirect antigenic detection technique based on the use of antibodies labeled with fluorescent probes. Unlike IHC, immunofluorescence has the advantage of labeling at the same time two or more proteins using different fluorochromes with different emission wavelengths; double labeling was performed both on cells and tissue samples. After 3 x 10 minutes washes with PBST (PBS + 0.1% Triton) 4% PFA fixed cells, pre-fixed brain sections or neurospheres were incubated for 1h with Blocking Buffer (PBS-0.1% Triton + 5% normal goat serum) to block non-specific antigenic sites and then incubated with primary antibodies overnight at 4ºC in Blocking Buffer (PBST + 2% normal goat serum). After 3 x 10 minutes washes in PBST, samples were incubated with secondary antibodies diluted with Blocking Buffer (PBST + 2% normal goat serum) for 2 hours at room temperature in the dark. After secondary antibody incubation, samples were washed 3 x 10 minutes with PBST, 1 x 10 min with PBS and then samples were incubated for 5 minutes with Hoechst 33258 (2 µg/ml, Sigma-Aldrich) to label nuclei. Samples were then washed in PBS for 5 min and brain slices and cells were then mounted using Ultracruz Aqueous Mounting Medium with DAPI and stored at 4ºC in the dark until needed for Nikon EZ-C1 confocal microscopy. Table 8 shows the antibodies used for immunofluorescence analysis.

Primary antibody	*Dilution*	*Secondary antibody*	*Dilution*
AGC1/Aralar1 mouse monoclonal IgG (Santa Cruz)	1: 250	Goat anti-rabbit IgG **Alexafluor 488** (ABCAM)	1:1000
HSP60 rabbit polyclonal IgG (Santa Cruz)	1: 500	Anti-mouse IgG **Alexafluor 555** (ABCAM)	1:1000
Olig2 rabbit polyclonal IgG (Santa Cruz)	1:500	Goat anti-rabbit IgG **Alexafluor 488** (ABCAM)	1:1000
MAG rabbit polyclonal IgG (Santa Cruz)	1: 500	Goat anti-rabbit IgG **Alexafluor 488** (ABCAM)	1:1000
TGFβ R1 rabbit polyclonal IgG (Santa Cruz)	1: 500	Goat anti-rabbit IgG **Alexafluor 488** (ABCAM)	1:1000
DCX rabbit polyclonal (ABCAM)	1:500	Goat anti-rabbit IgG **Alexafluor 488** (ABCAM)	1:1000
GFAP rabbit immunoglobulins (Dakopatts)	1:500	Goat anti-rabbit IgG **Alexafluor 488** (ABCAM)	1:1000
Nestin mouse monoclonal (ABCAM)	1:500	Anti-mouse IgG **Alexafluor 555** (ABCAM)	1:1000
Ki67 rabbit polyclonal (ABCAM)	1:500	Goat anti-rabbit IgG **Alexafluor 488** (ABCAM)	1:1000
CNPase rabbit monoclonal (Cell Signalling)	1:500	Goat anti-rabbit IgG **Alexafluor 488** (ABCAM)	1:1000
SSEA4-4 mouse monoclonal (Santa Cruz)	1:500	Anti-mouse IgG **Alexafluor 555** (ABCAM)	1:1000
BrdU rat anti- monoclonal antibody (ABCAM)	1:100	Goat anti-rat IgG **Alexafluor 488** (ABCAM)	1:1000

Table 7: *Primary and secondary antibodies used for immunofluorescence analysis.*

3.21.1. Oli-Neu BrdU immunofluorescence

For Oli-Neu BrdU immunofluorescence, 10^5 cells/well were plated in 6-well plates previously treated with poly-L-lysine (10 µg/ml) coated glass coverslips. After 3-4h, BrdU (10 µM) was added to the medium. 24 hours later, cells were fixed for 30 minutes at room temperature with 4% PFA and stored in PBS at 4°C until used. Coverslips were incubated with 2N HCl for 30 minutes at room temperature, washed 4 x 10 minutes with PBS and then 3 x 5 min with PBS-0.1% Triton (PBS-T). In order to block aspecific sites, cells were incubated at room temperature for 1 h in blocking buffer (PBS-T + 2% bovine serum albumin, BSA) and incubated overnight at 4°C in a humidifed chamber with a rat anti-BrdU antibody (1:500 dilution in blocking buffer, Abcam). After 3 x 10 min washes with PBS-T, cells were

incubated for 2 hours with goat anti-rat Alexa 488-conjugated antibody (1:1000 in blocking buffer, Abcam) and washed in PBS for 5 minutes. Lastly, coverslips were mounted on glass slides with UltraCruz Mounting medium with DAPI (Santa Cruz, cat. no. sc-24941) and stored at 4°C until used. 5 randomly selected fields for each coverslip were acquired and total nuclei stained with DAPI and BrdU positive nuclei counted. Labeling index was expressed as the *ratio* of BrdU positive/DAPI stained cells.

3.21.2. Neurosphere BrdU immunofluorescence

For BrdU immunofluorescence, previously fixed neurospheres were washed 3 x 5 minutes with PBS and then incubated for 1 hour in 2N HCl in order to denature DNA. After 6 x 10 min washes with PBS and then 3 x 5 minutes permeabilization washes with PBS-0.1% Triton, neurospheres were incubated for 1 hour in blocking buffer (PBS-0.1% Triton + 5% normal goat serum [Sigma-Aldrich]) to block aspecific sites. Neurospheres were then incubated overnight at 4ºC with a rat anti-BrdU antibody (1:500; Abcam) in blocking buffer. The next daym neurospheres were washed 3 x 5 minutes in PBS-0.1% Triton and incubated for 2 hours in the dark with a secondary anti-rat antibody (anti-rat Alexa 488, 1:1000; Abcam) in blocking buffer. Neurospheres were then washed 3 x 5 minutes in PBS-0.1% Triton, 1 x 5 minutes in PBS, then incubated for 5 minutes with Hoechst 33258 (2 µg/ml, Sigma-Aldrich) and after a 5-minute wash in PBS, glass slides were mounted with Ultra Cruz mounting medium (Santa Cruz, cat. no. sc-24941). 5 randomly selected fields for each coverslip were acquired and total nuclei stained with DAPI and BrdU positive nuclei counted. Labeling index was expressed as the *ratio* of BrdU positive/DAPI stained cells.

3.22. Cell counting after immunofluorescence and immunohistochemistry

Positive cell number quantification after immunohistochemical and immunofluorescence analysis was performed with Image J software provided by the National Institutes of Health (NIH). Tissue section images, previously obtained with the Eclipse TS100 (Nikon) optical microscope or Nikon EZ-C1 confocal microscope, were analyzed considering always the same area of corpus callosum (CC) and subventricular zone (SVZ). Considering the area of interest and the slice thickness (40 µm), obtained data were compared with the total volume of the section and subject to statistical processing and evaluation. For immunofluorescence surveys, 3D images for each slice of tissue were obtained by z-stack acquisition of 1 µm

thickness layers (40 stacks), then 3D image reconstruction was performed by using Fiji ImageJ2 software with the z-project plugin. All cell count values were subject to Student's test.

3.23. Statistical analysis

All results were subject to statistical analysis by using one-way ANOVA followed by Bonferroni *post-hoc* comparison test or Student′s t-test, depending on the experiment considered, in order to evaluate difference significance. Statistical analysis was performed by using the Graph Pad Prism 4 software and p values less than 0.05 were considered statistically significant.

4. RESULTS

As previously described, the aim of this thesis was to study the molecular mechanisms underlying AGC1 deficiency in appropriate *in vitro* and *in vivo* disease models, in particular by focusing on oligodendrocyte precursor alterations in order to clarify whether a deficit in these cells, so important for myelin formation, could play a role in the demyelination and consequent neurodegeneration observed in patients.

To this aim, we carried on experiments by using three different models of the disease:

1) First, we developed an *in vitro* model by using the Oli-Neu cell line, which are immortalized mouse oligodendrocytes precursor cells (kind gift from Dr. Trotter); in these cells we partially silenced AGC1 expression, in order to obtain a reduction in the carrier activity down to about 30-40% of control cells, as in mitochondria from human patients.
2) Then, we confirmed the results obtained in the cellular model by using the animal model of the disease, i.e. heterozygous mice for the AGC1 knock-out ($AGC1^{+/-}$ C57BL6/N background), as well as in neurospheres derived from the subventricular zone of the same animal model.
3) Lastly, we performed preliminary experiments to further confirm the results obtained in mouse *in vitro* and *in vivo* models by using neural stem cells from iPS derived from AGC1-deficiency patients.

In all these models, we studied the expression of AGC1, cell proliferation, as well as the expression of growth factors and receptors known to be involved in proliferation/differentiation of OPCs, mainly the PDGFα and TGFβ pathways. In addition, in collaboration with Dr. Massimo Lasorsa (IBIOM, CNR Bari) and Prof. Paolo Pinton (University of Ferrara), the mitochondrial effect of AGC1 silencing was evaluated in Oli-Neu cells.

4.1. Study of AGC1-silencing in Oli-Neu cells

4.1.1. AGC1 expression in control and AGC1-silenced Oli-Neu cells

Stably-silenced AGC1 and controls Oli-Neu cells were prepared as described at paragraph 3.1. In order to quantify AGC1 reduction, its expression was analyzed in control and AGC1 stably-silenced Oli-Neu cells by Western blot. Densitometric analysis confirmed statistically significant reduced AGC1 expression in silenced Oli-Neu cells compared to control cells (fig 4.1 A, B). To evaluate whether Oli-Neu cell differentiation could be altered or not after AGC1 silencing, control and AGC1-silenced cells were stimulated for 1 to 3 days *in vitro* (DIV) with 1 mM db-cAMP, which induced differentiation[149]. As shown in figure 4.1 C, obtained by optical microscopy, AGC1 silencing did not cause macroscopic morphological alterations and AGC1 silencing was maintained during cell differentiation, namely for 3 days, as shown by Western blot analysis (fig. 4.1 D). Moreover, undifferentiated and differentiated Oli-Neu cells expressed AGC1 and myelin associated glycoprotein (MAG) as observed in figure 4.1 D.

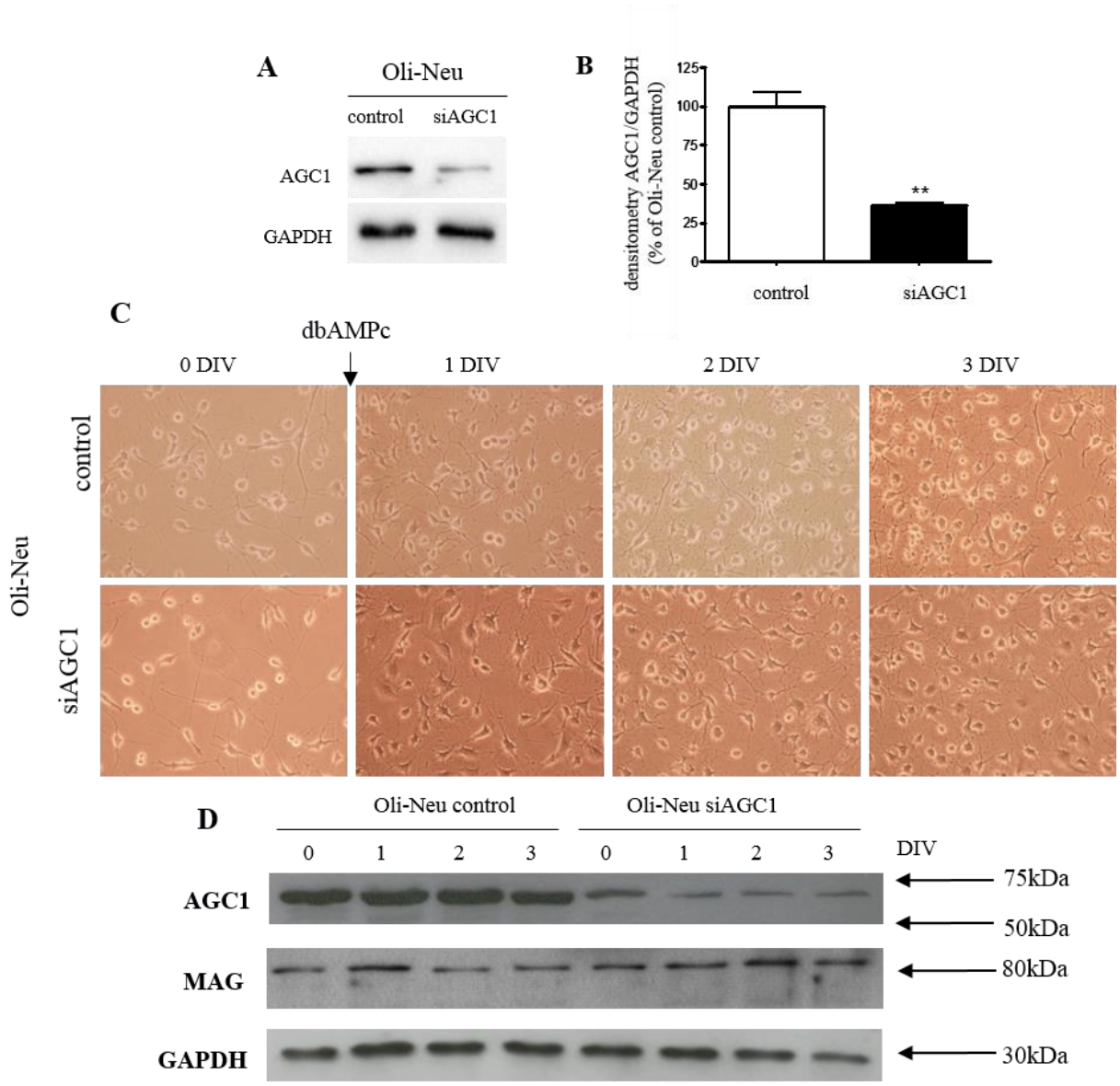

Figure 4.1: ***(A)*** *AGC1 expression was evaluated by Western blot;* ***(B)****: Densitometric analysis showed that AGC1 reduced expression in AGC1 silenced Oli-Neu cells was statistically significant; GAPDH was used as an endogenous control to normalize data. Values are the mean ± SD from 3 independent experiments performed in triplicate, * P <0.05, ** P <0.01, *** P <0.001 compared to wild-type, t-test Student.* ***(C)*** *Optical microscopy images of control and siAGC1 Oli-Neu cells during differentiation with 1 mM db-cAMP.* ***(D)*** *AGC1 expression analysis by Western blot during differentiation; AGC1 silencing was maintained during the cell differentiation, namely for 3 days; moreover, undifferentiated and differentiated Oli-Neu cells express AGC1 and myelin associated glycoprotein (MAG) during differentiation.*

4.1.2. Analysis of AGC1 subcellular localization

To evaluate AGC1 subcellular localization, cytosol, mitochondria and nuclei were isolated by subcellular fractionation of control Oli-Neu cells and analyzed by Western blot. GAPDH (glyceraldehyde 3-phosphate dehydrogenase) was used as a control for cytosol, HSP60 (a mitochondrial chaperonine present on the internal mitochondrial membrane) for mitochondria, whereas histone H3 was used as a nuclear control to demonstrate the purity of subcellular fraction. Western blot results showed that the AGC1 carrier was as expected, present in mitochondria (fig 4.2A). A further confirmation of AGC1 mitochondrial localization was obtained by confocal microscopy analysis carried out on control Oli-Neu cells (fig 4.2 B), where mitochondria were labeled with HSP60 (red). Moreover, Western blot analysis showed that the AGC1 carrier was unexpectedly present also in the nucleus (Figure 4.2A); no role for nuclear localization of a mitochondrial carrier has been already described in the literature. A further confirmation of AGC1 nuclear presence was obtained by confocal microscopy analysis carried out on control Oli-Neu cells (fig 4.2C), where nuclei were labeled with histone H3 (green) and AGC1 (red) was also present in nuclei.

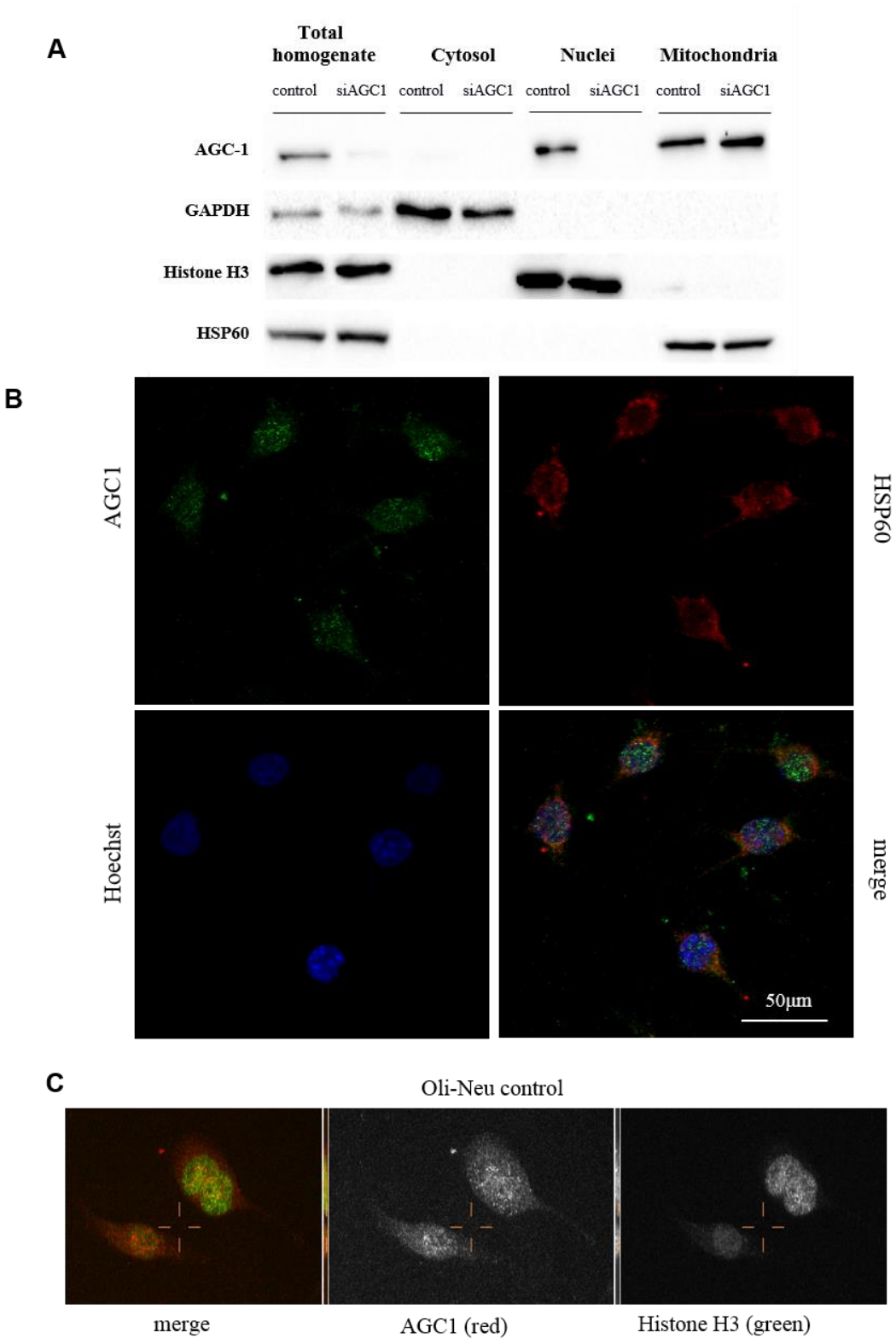

Figure 4.2: (A) *Subcellular fractionation Western blot analysis on control and AGC1-silenced Oli-Neu cells. GAPDH was used as a control for the cytosol, while HSP60 for mitochondria and histone H3 for nuclei.* ***(B-C)*** *Confocal microscopy analysis of AGC1 localization in control cells:* ***(B)*** *AGC1 mitochondrial localization obtained by confocal microscopy analysis carried out on control Oli-Neu cells where mitochondria were labeled with HSP60 (red) and AGC1 (green);* ***(C)*** *AGC1 nuclear presence obtained by confocal microscopy analysis carried out on control Oli-Neu cells; nuclei were labeled with histone H3 (green) and AGC1 (red).*

4.1.3. Effect of AGC1-silencing on Oli-Neu cell proliferation

To study the possible role of AGC1 silencing in Oli-Neu cells proliferation, cell counting with a Neubauer chamber was performed 24 hours after plating cells. Cell count analysis (fig 4.3) showed that siAGC1 Oli-Neu cell number was statistically lower than control cells, suggesting that silenced cells proliferated less compared to controls.

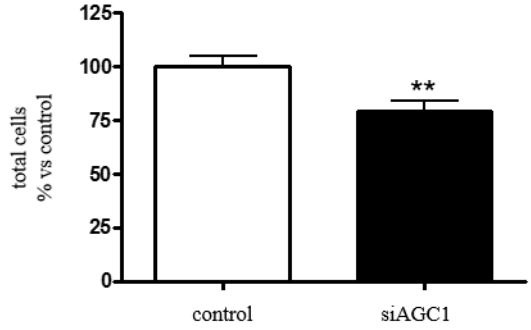

Figure 4.3: *Cell count analysis; siAGC1 Oli-Neu cell number was decreased compared to control cells 24 hours after plating. Values are the mean ± SD of 3 independent experiments performed in triplicate, * P <0.05, ** P <0.01, *** P <0.001 compared to control, t-test Student.*

To confirm the observed possible proliferation defect, BrdU incorporation was performed on control and silenced Oli-Neu cells both through immunofluorescence and ELISA assay. Immunofluorescent analysis showed decreased BrdU incorporation in silenced cells compared to control cells (expressed as labelling index; fig. 4.3.2B); the ELISA quantification was made after 6h (fig. 4.3 C) and 24h (fig. 4.3 D) BrdU incubation and results confirmed again reduced BrdU incorporation in AGC1-silenced cells, suggesting lower proliferation rates in siAGC1 Oli-Neu cells. All these differences were statistically significant.

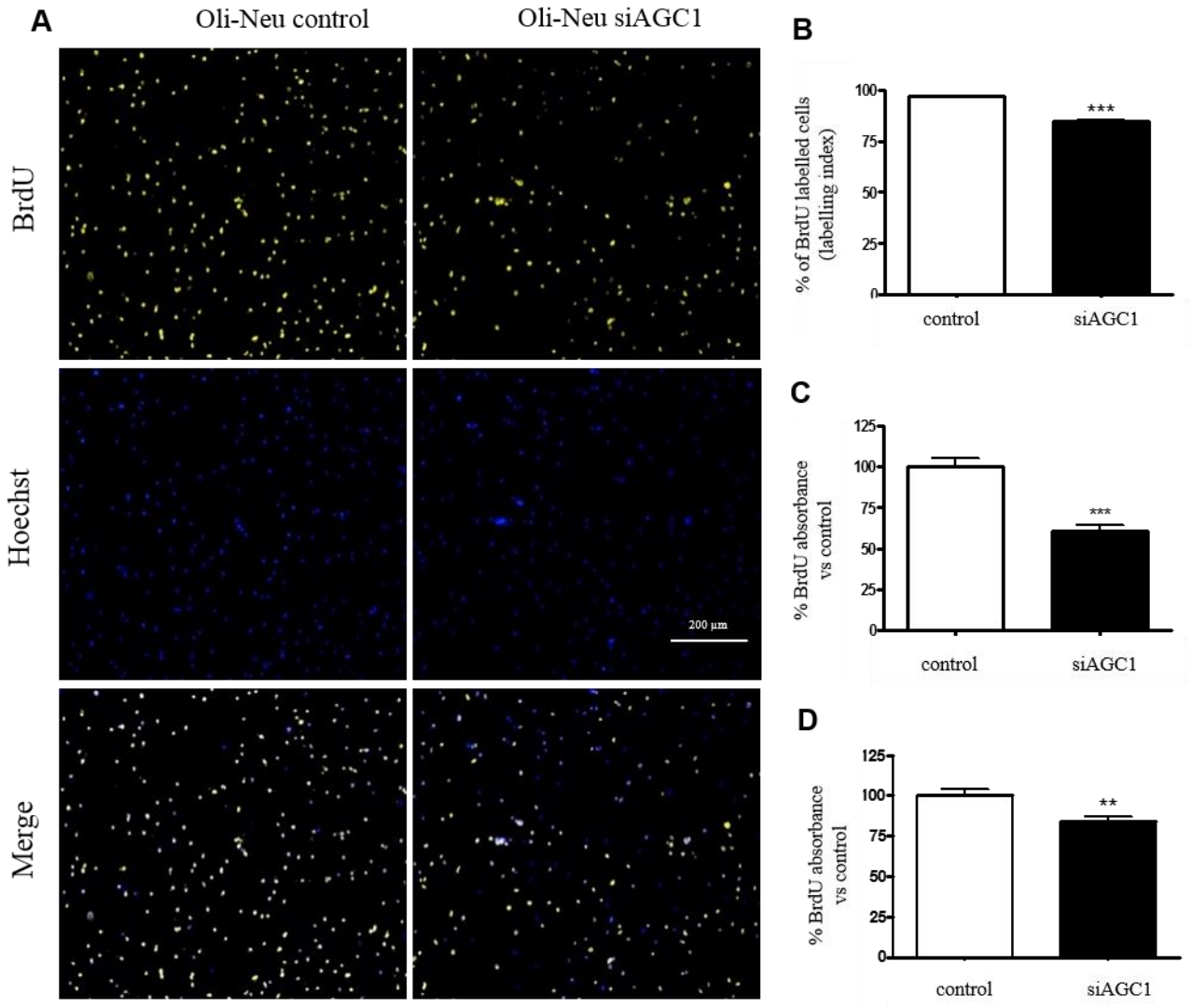

Figure 4.3: ***(A)*** *BrdU immunofluorescence of control and AGC1-silenced Oli-Neu cells. Actively proliferating cells incorporated BrdU (yellow), while nuclei were stained with Hoechst (blue).* ***(B)*** *BrdU positive-cell count analysis expressed as labelling index.* ***(C, D)*** *BrdU incorporation by ELISA assay in control and siAGC1 Oli-Neu cells after 6* ***(C)*** *and 24-hour* ***(D)*** *BrdU incubation. Values are the mean ± SD of 3 independent experiments performed in triplicate. * P <0.05, ** P <0.01, P < 0.001 compared to control cells, t-test Student.*

In collaboration with Dr. Miriam Capri and Dr. Rita Ostan (University of Bologna), to further confirm proliferation studies, flow cytometry was used to detect the percentage of cells in the various cell cycle phases (M, G1, S, G2). DNA content was measured using propidium iodide, which dyes DNA, entering only into dead and permeable cells. Flow cytometry analysis (fig 4.4) showed that wild-type cells were predominantly in G0/G1 phase (58.56%) and in quiescence phase G2, while S phase cells were 15.37%; on the other hand, silenced cells in G0/G1 phase were 64.06% and 13.87% in S phase. Flow cytometry analysis

confirmed that AGC1-silenced Oli-Neu cell number in S phase was lower than wild-type cells suggesting a reduction in proliferation.

Oli-Neu control

Oli-Neu siAGC1

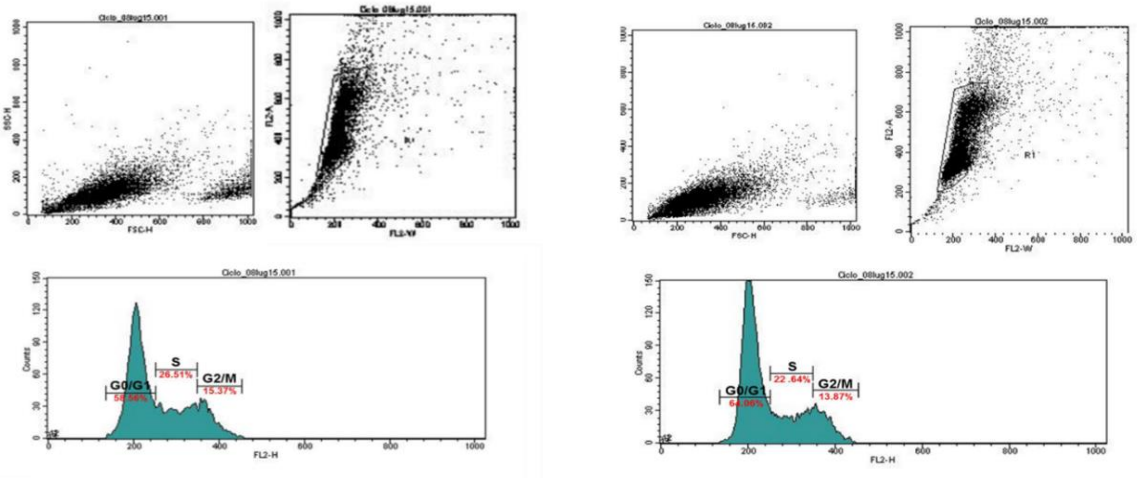

	OLI NEU control	OLI NEU siAGC1
G0-G1	58.56%	64.06%
S	26.51%	22.64%
G2/M	15.37%	13.87%

In collaboration with Dr. Capri M and Dr. Ostan R

Figure 4.4: *Flow cytometry analysis on control and AGC1-silenced Oli-Neu cells in order to evaluate the percentage of cells in the various cell cycle phases (G0-G1, G2-M and S).*

4.1.4. Effect of AGC1-silencing on Oli-Neu cell morphology

Considering that AGC1-silencing does not affect cAMP-induced Oli-Neu differentiation (fig 4.5), while it reduces their proliferation, we decided to evaluate whether it could induce by itself the differentiation of these cells. Therefore, the effect of AGC1 silencing on cell morphology, including its effect of filament length and number, which are index of differentiation, was evaluated in control and AGC1-silenced Oli-Neu cells. Silenced cells showed a more elongated and branched morphology compared to control cells. In fact, AGC1-silenced Oli-Neu cells showed a decrease in cell and process number (fig 4.5 B and fig 4.5 C respectively) and an increase in average process length (fig 4.5 D). These differences were all statistically significant.

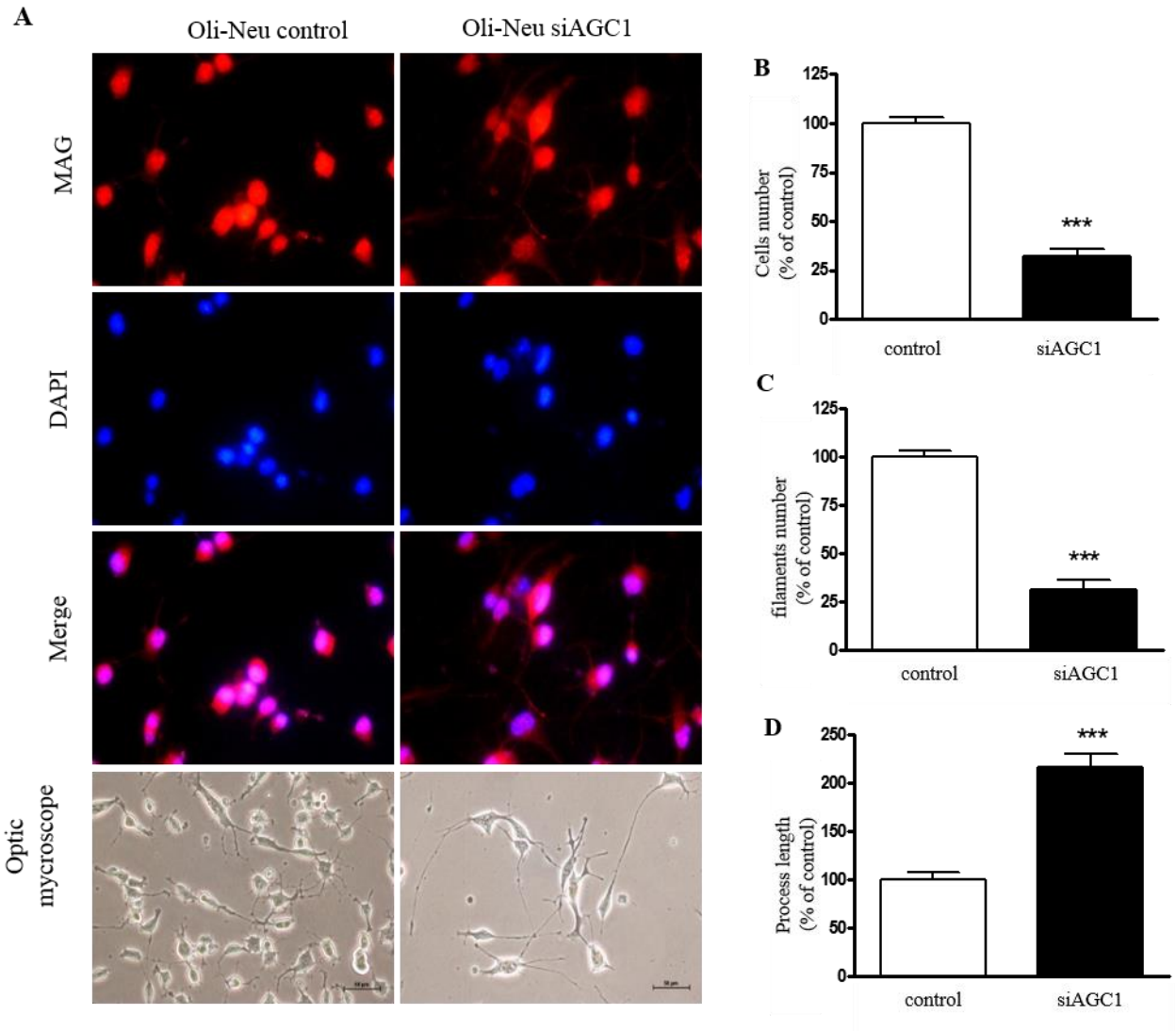

Figure 4.5*: (A) Immunofluorescence staining and optical microscopy images of control and AGC1-silenced Oli-Neu cells. For immunofluorescence analysis nuclei were labeled with DAPI while MAG, a myelin associated glycoprotein was used as a specific marker for Oli-Neu cells. (B, C, D) Analyses for cell number, filament number and length calculated with ImageJ software. Values are the mean ± SD of 3 independent experiments performed in triplicate, * P <0.05, ** P <0.01, *** P <0.001 compared to wild type, t-test Student.*

4.1.5. Biochemical measurements

In collaboration with Dr. Massimo Lasorsa (IBIOM, CNR Bari) and Prof. Paolo Pinton (University of Ferrara), biochemical analyses were conducted to understand the effect of AGC1 silencing on Oli-Neu cells at the mitochondrial level.

4.1.5.1. Lactate production in AGC1-silenced Oli-Neu cells

Since AGC1 down-regulation inhibits mitochondrial pyruvate oxidation in undifferentiated Neuro2A cells leading to increased production of lactic acid[124], whether a similar effect could occur in AGC1-silenced Oli-Neu cells was hypothesized. After 48-hour incubation, lactic acid release levels in conditioned high-glucose medium from both undifferentiated and differentiated siAGC1 Oli-Neu cells was similar to levels measured in conditioned media from control cells (fig. 4.6). These data suggest that AGC1 down-regulation in Oli-Neu cells did not reduce the rate of glucose oxidation, probably due to the parallel expression of AGC2 in Oli-Neu cells.

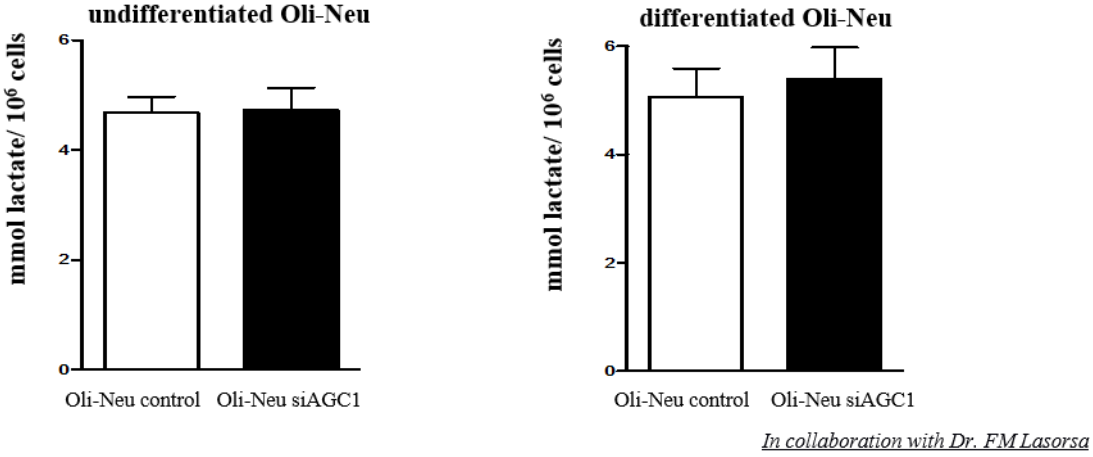

Figure 4.6: *Lactic acid was quantified in conditioned complete Oli-Neu cell medium harvested from control Oli-Neu (white bars) or AGC1-silenced Oli-Neu cells (black bars). Conditioned media from undifferentiated cells were harvested after 48 h of incubation; conditioned media from differentiated cells were harvested 48 h after addition of 1 mM dibutyryl-cAMP. Values are the mean ± SD of 3 independent experiments performed in triplicate.*

4.1.5.2. Oli-Neu Mitochondrial Membrane Potetial (Ψm)

Mitochondrial Ψm was measured by loading cells with 20 nM tetramethyl rhodamine methyl ester (TMRM; Life Technologies, T-668) for 30 minutes at 37°C. Images were taken on an inverted microscope (Nikon LiveScan Swept Field Confocal Microscope (SFC) Eclipse Ti equipped with NIS-Elements microscope imaging software, Nikon Instruments). TMRM

excitation was performed at 560 nm and emission was collected through a 590 to 650 nm band-pass filter. Images were taken every 5 seconds with a fixed 20 ms exposure time. FCCP (carbonyl cyanide p-trifluoromethoxyphenylhydrazone, 10 µM), an uncoupler of oxidative phosphorylation, was added after 12 acquisitions to completely collapse the electrical gradient established by the respiratory chain. As imaged by fluorescence microscopy, TMRM-stained mitochondria from AGC1-silenced cells did not appear remarkably different from mitochondria from control cells, in terms of morphology and membrane potential (fig. 4.7), suggesting that AGC1 silencing in Oli-Neu cells did not affect the mitochondrial network and OXPHOS activity.

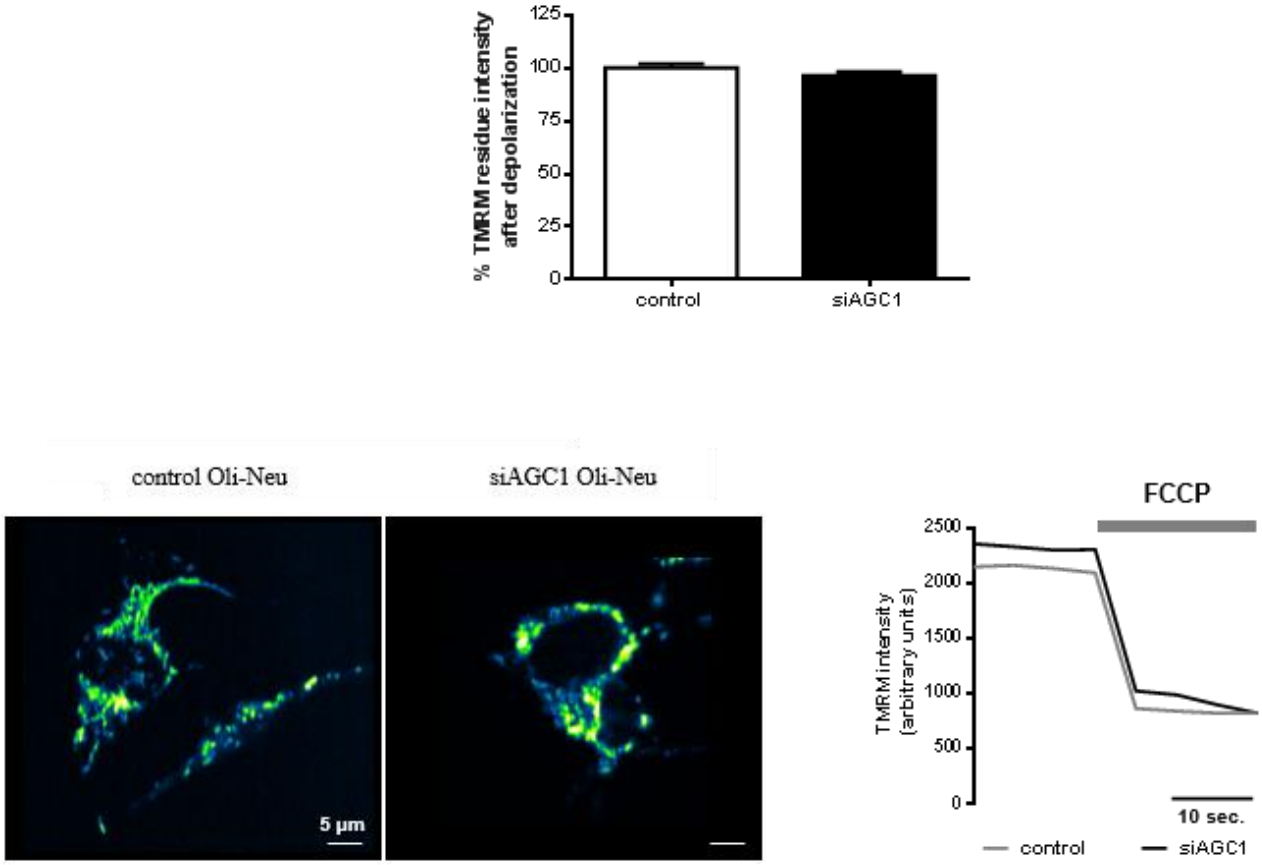

In collaboration with Dr. FM Lasorsa and Prof. P. Pinton

Figure 4.7: *Oli-Neu Mitochondrial Membrane Potential (Ψm). Images were taken on an inverted microscope (Nikon LiveScan Swept Field Confocal Microscope (SFC) Eclipse Ti equipped with NIS-Elements microscope imaging software, Nikon Instruments). Images were taken every 5 seconds with a fixed 20 ms exposure time. FCCP (carbonyl cyanide p-trifluoromethoxyphenylhydrazone, 10 µM), an uncoupler of oxidative phosphorylation, was added after 12 acquisitions to completely collapse the electrical gradient established by the respiratory chain. Data are the mean ± SD of TMRM percentage intensities normalized to values before agonist stimulation in three independent experiments.*

4.1.5.3. Measurement of intracellular ROS

Although AGC1-silenced cells showed a slight but significant increase of ROS production in the cytosol, as compared to control cells (fig. 4.8 A), no difference in mitochondrial ROS production were imaged with the ratiometric mt-Hyper (fig. 4.8 B), used as a ROS sensitive probe directly targeted to mitochondria.

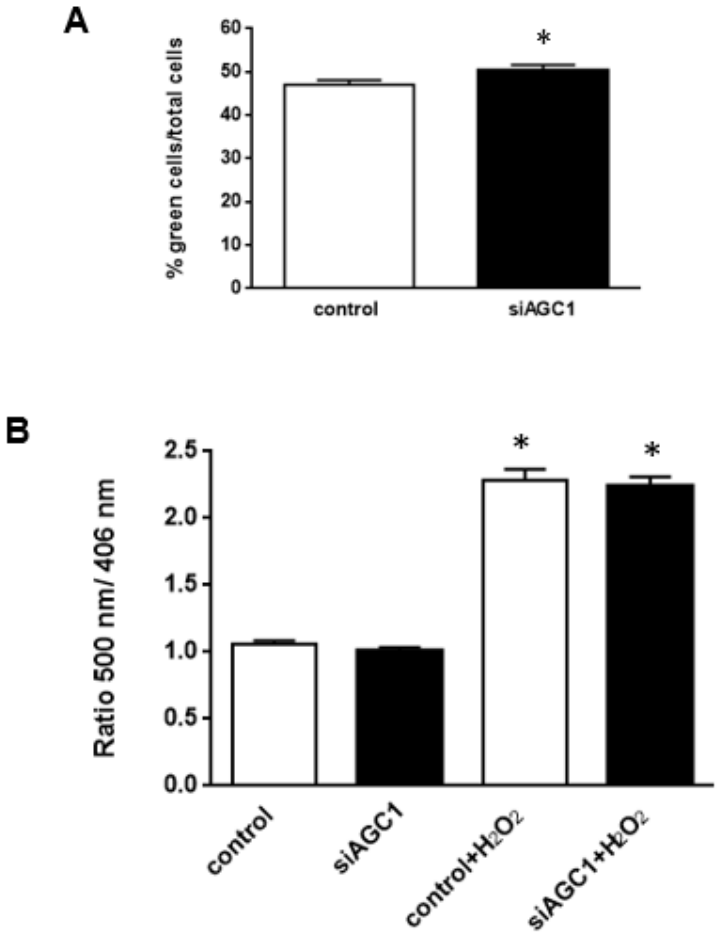

In collaboration with Dr. FM Lasorsa and Prof. P. Pinton

***Figure 4.8**: **(A) Measurement of cytosolic hydrogen peroxide concentration (DCFDA):** Mitochondrial and cytosolic hydrogen peroxide concentration was measured by loading cells with 5 µM 5-(and-6)-chloromethyl-2',7'-dichlorodihydrofluorescein diacetate, acetyl ester (CM-H2DCFDA; Life Technologies, C-6827) for 20 minutes at 37°C. The measurement was performed with a Tali® Image-Based Cytometer. **(B) Measurement of mitochondrial hydrogen peroxide concentration (mtHYPER):** Mitochondrial hydrogen peroxide concentration was measured by transfecting cells with a chimeric protein with mitochondrial localization pHyPer-dMito (mtHYPER). Images were taken on an epi-fluorescence microscope (Cell^R Olympus, multiple wavelength high resolution fluorescence microscopy system). For a ratiometric measurement, H2O2 (hydrogen peroxyde) was added. * P <0.05.*

4.1.5.4. Mitochondrial morphology measurement

The mitochondrial morphology of Oli-Neu cells was detected by loading cells with 100 nM tetramethyl rhodamine methyl ester (TMRM; Life Technologies, T-668) for 30 minutes at 37°C; control Oli-Neu cells are represented in the left panel and white columns while silenced Oli-Neu cells in the right panel and blue columns (fig. 4.9). Images were taken with a Nikon Swept Field confocal microscope equipped with a CFI Plan Apo VC60XH objective (n.a. 1.4) (Nikon Instruments) and an Andor DU885 EM-CCD camera (Andor Technology Ltd.) with NIS-Elements microscope imaging software (Nikon Instruments). TMRM excitation was performed at 560 nm, emission was collected through a 590 to 650 nm band-pass filter and 51 planes z-stacks where acquired with a voxel dimension of 133 × 133 × 200 nm (X × Y × Z). No significant differences between control and silenced Oli-Neu cells were observed for number of objects, total mitochondrial network (μm^3) and single object volume (μm^3).

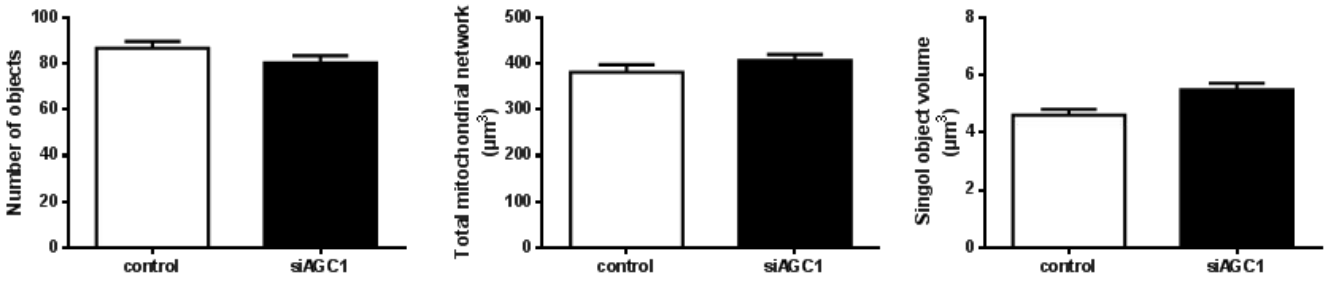

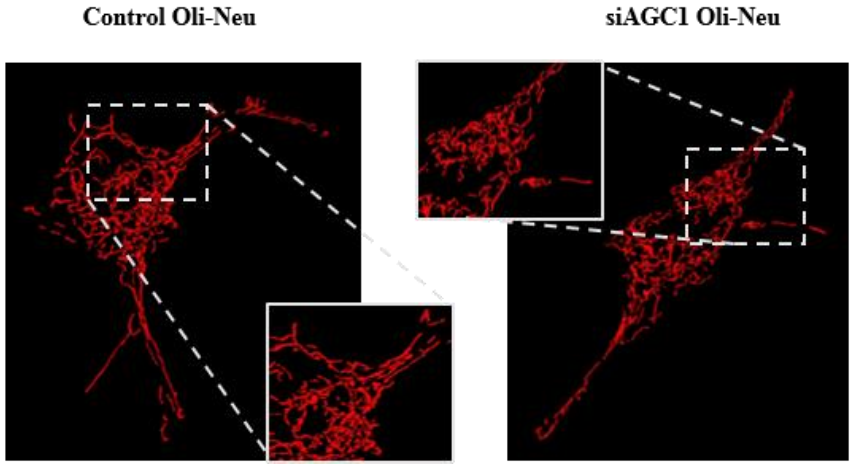

In collaboration with Dr. FM Lasorsa and Prof. P. Pinton

Figure 4.9: *Mitochondrial morphology of control Oli-Neu (left panel and white columns) or AGC1-silenced Oli-Neu (right panel and red columns) cells was analyzed by loading cells with 100 nM tetramethyl rhodamine methyl ester (TMRM) for 30 min at 37°C. Images were taken through confocal microscopy. Mitochondrial networks, described in number and volume, and 3D renders were obtained with Imaris 4.0 (Bitplane). Representative images and quantitative data illustrating the number of TMRM+ 3D objects per cell (means ± SEM, n = 80).*

4.1.5.5. Measurement of mitochondrial and cytosolic Ca^{2+} and mitochondrial ATP concentration

Since AGC1 is a Ca^{2+}-stimulated transporter and its down-regulation in undifferentiated Neuro2A cells induced an increased mitochondrial response to Ca^{2+} stimulation[124], whether a similar effect could occur in AGC1 down-regulated Oli-Neu cells challenged with Ca^{2+}-releasing agonists was tested. In stimulated AGC1-silenced Oli-Neu cells expressing the recombinant Ca^{2+}-sensitive aequorin probe, cytosolic $[Ca^{2+}]$ ($[Ca^{2+}]_c$) was slightly, but significantly increased when compared to controls (fig 4.10 A), but no difference in mitochondrial $[Ca^{2+}]$ ($[Ca^{2+}]_m$) was measured (Fig 4.10 B). As a consequence, the similar mitochondrial Ca^{2+} uptake in both types of cells resulted in unvaried increase of Ca^{2+}-induced mitochondrial ATP synthesis in stimulated cells (Fig. 4.10 C).

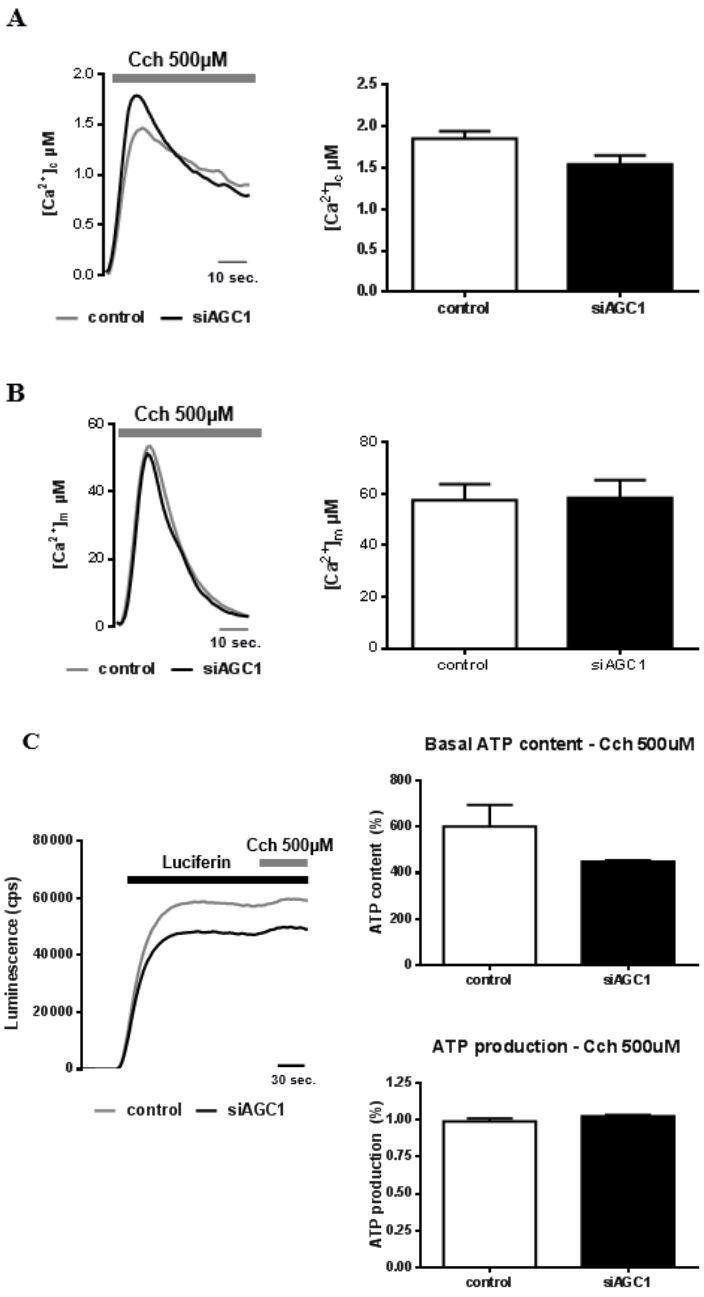

Figure 4.10: (A, B) Cytoplasmic and mitochondrial Ca^{2+}: *Oli-neu control and AGC1-silenced cells (10^5 cells/well) were seeded on poly-L-lysine coated (10 µg/ml) 13-mm glass coverslips. Cells were transfected with 1.5 µg of chimeric aequorins targeted to the cytosol (cytAEQ) or mitochondria (mtAEQmut) using Lipofectamine 2000 (Invitrogen-Life Technologies). All measurements were performed 24h after transfection. For aequorin measurements, 500 µM carbachol was used as an agonist. Shown traces are representative of the following measurements: for LVshMM-OliNeu cells, [Ca2+]c peak values, 1.54 ± 0.14 µM, n = 20; [Ca2+]m peak values, 58,4 ± 6.2 µM, n = 20; for LVshAGC1-OliNeu cells, [Ca2+]c peak values, 1.85 ± 0.09 µM, n = 20; [Ca2+]m peak values, 57,6 ± 4.1 µM, n = 20.* ***(C) Mitochondrial ATP concentration****: Oli-Neu control and AGC1-silenced cells (10^5 cells/well) were seeded on poly-L-lysine coated (10 µg/ml) 13-mm glass coverslips. Cells were transfected with 1.5µg of mitochondrial luciferase (mtLUC) using Lipofectamine 2000 (Invitrogen-Life Technologies). All measurements were performed 24 hours after transfection. For mitochondrial ATP concentration, 500µM carbachol was used as an agonist. Data are expressed as percentage of mtLuc light output increase from cells normalized to the prestimulatory values. Shown traces are representative of the following results: for LVshMM-OliNeu cells, 101 ± 8%, n = 20 of the prestimulatory value; for LVshAGC1-OliNeu cells: 103 ± 9%, n=20.*

4.1.6. AGC1 silencing effect on PDGFα and TGFβ pathways in Oli-Neu cells

Previous results showed that AGC1 silencing does not alter cAMP-induced Oli-Neu differentiation, but it significantly reduced their proliferation and by itself induced a partial differentiation of the cells. However, this does not seem to be due to the bioenergetics function of this carrier, since biochemical data produced do not demonstrate any significant change in mitochondrial parameters. Therefore, we decided to evaluate the expression of PDGFα, TGFβ and respective receptors, as these are known to influence OPCs proliferation and differentiation[78,100]. As shown by Western blot analysis, AGC1-silenced Oli-Neu cells expressed significantly less PDGFα, which is the most important factor to stimulate OPC proliferation in an autocrine and paracrine manner, compared to control Oli-Neu cells (fig 4.11 A), whereas PDGFRα expression did not change in AGC1-silenced cells compared to control cells (fig 4.11 B).

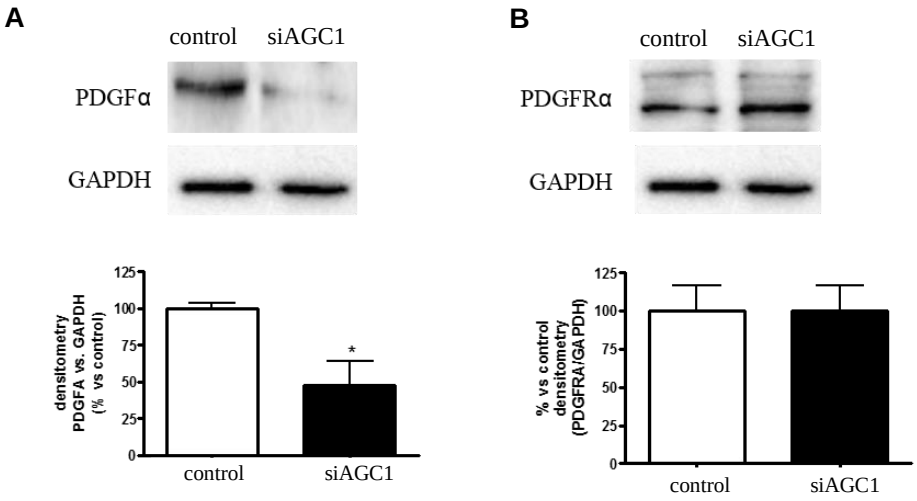

Figure 4.11: *PDGFα* ***(A)*** *and PDGFRα* ***(B)*** *expression was evaluated by Western blot analysis. Densitometric analysis showed that PDGFα expression was significantly reduced in siAGC1 Oli-Neu cells compared to control cells, while PDGFRα expression did not change; GAPDH was used as an endogenous control to normalize data. Values are the mean ± SD of 3 independent experiments performed in triplicate, * P <0.05, compared to control, t-test Student.*

Considering the analysis of TGFβ factors, which regulate OPCs differentiation in mature oligodendrocytes, only immature (precursor) TGFβ1, 2 and 3 forms were expressed, whereas no mature (cleaved) forms were detected (fig 4.12). Pre-TGFβ1 expression was increased in siAGC1 Oli-Neu cells (fig 4.12 A), while pre-TGFβ2 expression was decreased in the same cells, when compared to control Oli-Neu cells (fig 4.12 B). While these differences were statistically significant, no difference was observed for pre-TGFβ3 expression (fig 4.12 C).

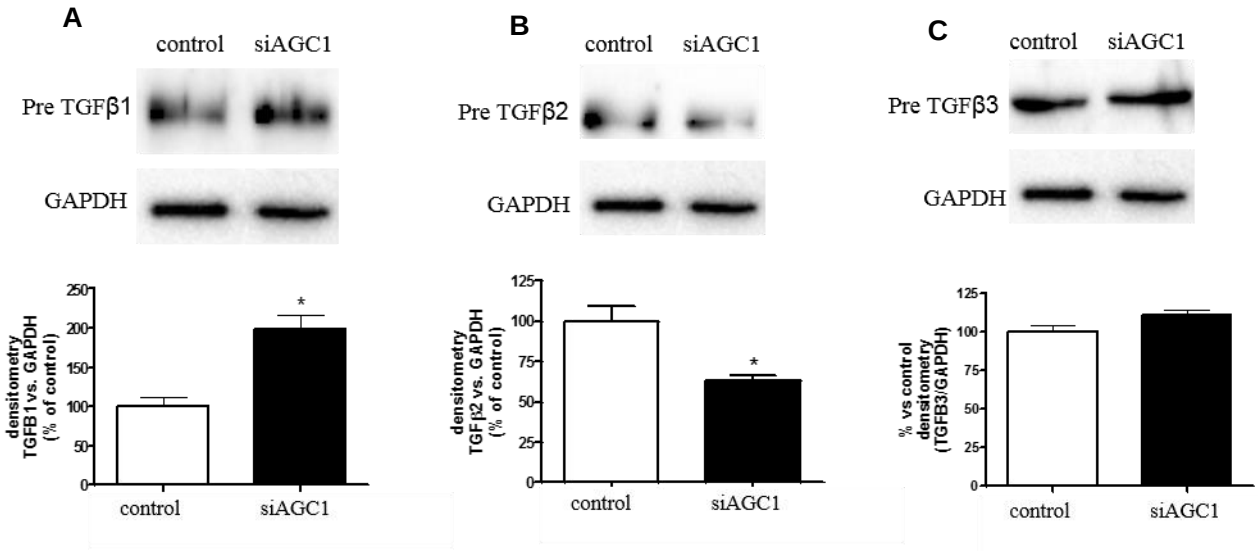

Figure 4.12: *Western blot and respective densitometric analyses of pre-TGFβ1* ***(A),*** *pre-TGFβ2* ***(B)*** *and pre-TGFβ3* ***(C)*** *expression performed on wild-type and AGC1-silenced Oli-Neu cells; while pre-TGFβ1 expression was increased in silenced cells and pre-TGFβ2 was decreased in silenced cells, no difference was observed in pre-TGFβ3 expression. GAPDH was used as an endogenous control to normalize data. Values are the mean ± SD of 3 independent experiments performed in triplicate.*

TGFβ receptor 1 and TGFβ receptor 2 expression was also analyzed in the same samples. Expression of both TGFβR1 and TGFβR2 was significantly increased in AGC1-silenced Oli-Neu cells compared to control Oli-Neu cells (fig 4.13 A and B). To further confirm these data, immunofluorescence analysis showed stronger labeling against TGFβR1 in AGC1-silenced Oli-Neu cells compared to control cells (fig 4.13 C).

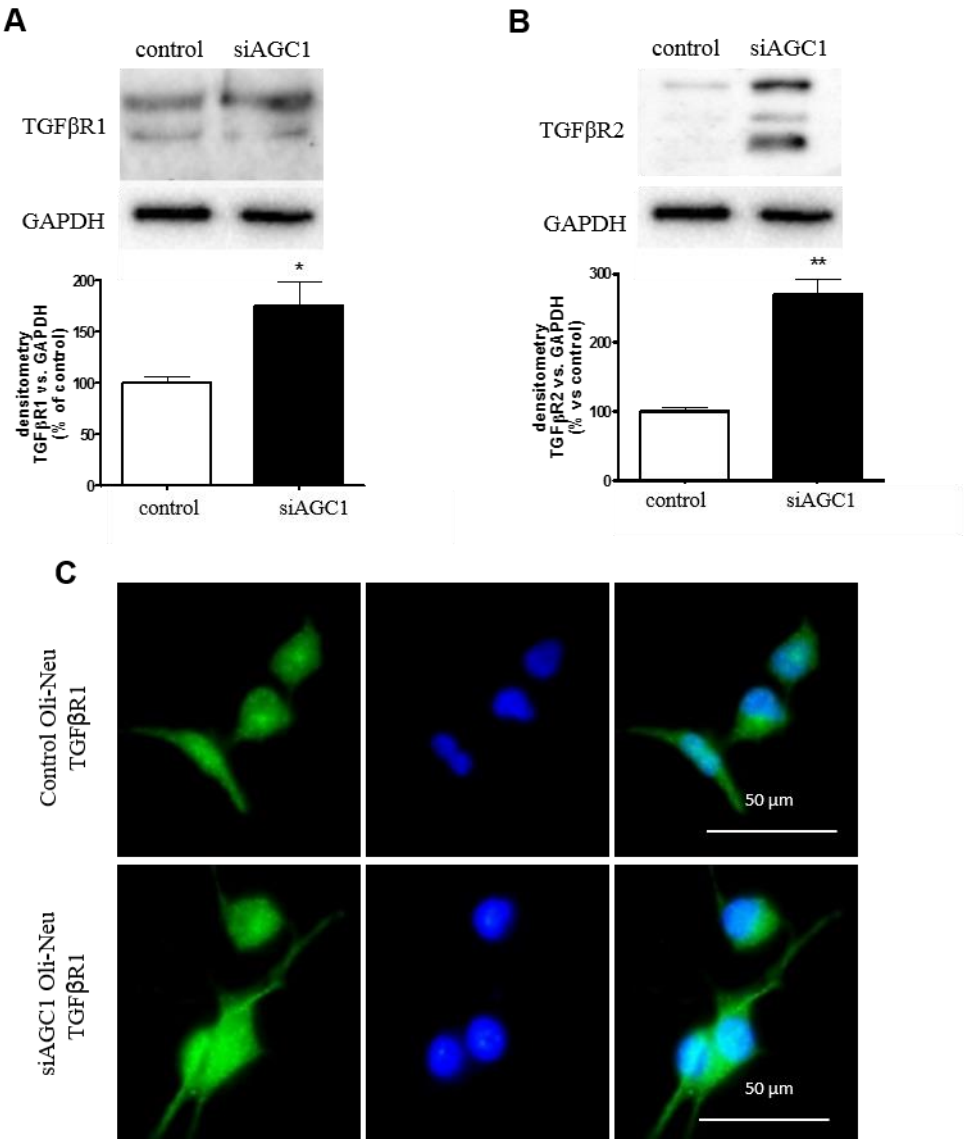

Figure 4.13: *Western blot and respective densitometric analysis of TGFβR1* ***(A)*** *and TGFβR2* ***(B)*** *expression performed on-wild type and AGC1-silenced Oli-Neu cells; the expression of both receptors was significantly increased in AGC1-silenced Oli-Neu cells compared to control cells. GAPDH was used as an endogenous control to normalize data. Values are the mean ± SD from 3 independent experiments performed in triplicate.* ***(C)*** *Immunofluorescence staining of TGFβR1 (green) showed stronger labeling in AGC1-silenced Oli-Neu cells compared to control cells.*

4.2. Study of AGC1-silencing in the mouse animal model

4.2.1. *In vivo* analysis of AGC1 expression in AGC1 $^{+/+}$ and AGC1 $^{+/-}$ mice

To study whether the effect of decreased AGC1 expression and, therefore, also decreased AGC1 activity could affect OPCs proliferation *in vivo*, we focused on AGC1 $^{+/+}$ and AGC1 $^{+/-}$ mice. Firstly, AGC1 expression was analyzed in 21 day-old (fig 4.14 A) and adult (fig 4.14 B) AGC1 $^{+/+}$ and AGC1 $^{+/-}$ mice, since no AGC1 $^{-/-}$ mice were born. We chose 21 day old-mice, since this is the postnatal day in which OPCs reach a peak in proliferation; as previously done by Jalil and collaborators who studied 18-21day old AGC1-deficiency mice[35]. As shown in figure 4.14, while in AGC1 $^{+/+}$ and AGC1 $^{+/-}$ adult mice several brain regions (cortex, hippocampus, cerebellum and spinal cord) were isolated, only whole brain and the cerebellum were analyzed in pups since they were too small and the different brain areas were difficult to dissect. In all analyzed areas, a statistically significant decrease in AGC1 expression was observed in AGC1 $^{+/-}$ mice.

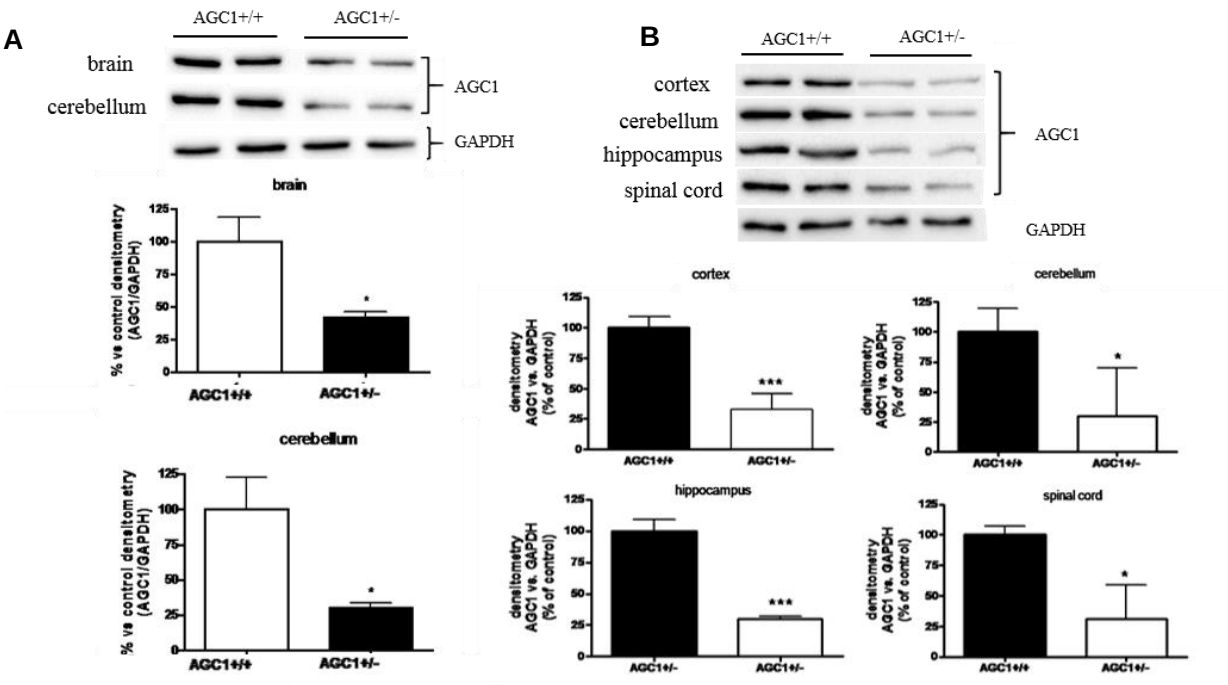

Figure 4.14: *AGC1 expression analysis by Western Blot in wild-type (AGC1$^{+/+}$ n = 8) and heterozygous (AGC1$^{+/-}$ n = 8) in 21-day old* ***(A)*** *and adult mice* ***(B).*** *To normalize data with respect to the amount of protein loaded, GAPDH was used as endogenous control. Respective densitometric analyses are shown below. Bars represent the mean ± SD of 3 independent experiments performed in triplicate, * P <0.05, ** P <0.01, *** P <0.001 compared to wild type, t-test of Student.*

As shown in figure 4.15, a significant decrease in AGC2 expression was also observed in 21-day old (fig 4.15 A) and adult (fig 4.15 B) AGC1 $^{+/+}$ and AGC1 $^{+/-}$ mice.

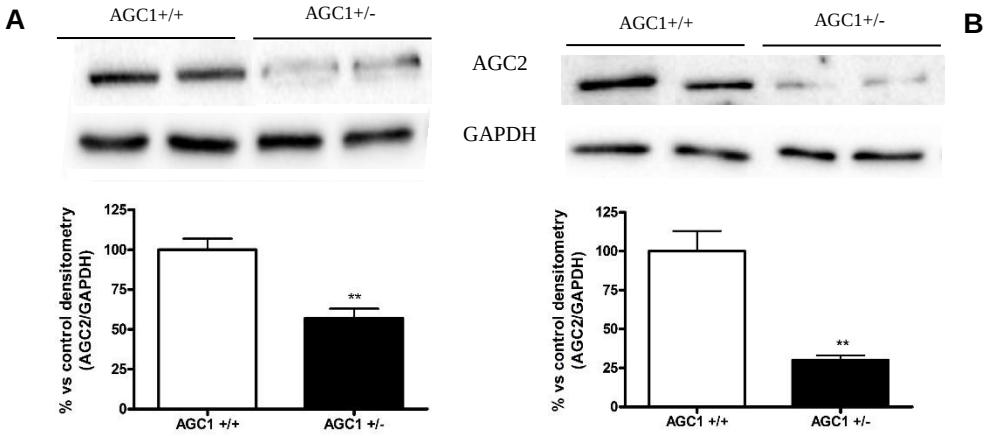

Figure 4.15: *AGC2 expression analysis by Western Blot in wild-type (AGC1$^{+/+}$ n = 4) and heterozygous (AGC1$^{+/-}$ n = 4) in 21-day old* ***(A)*** *and adult mice* ***(B).*** *To normalize data with respect to the amount of protein loaded, GAPDH was used as endogenous control. Respective densitometric analyses are shown below. Bars represent the mean ± SD of 3 independent experiments performed in triplicate, * P <0.05, ** P <0.01, *** P <0.001 compared to wild type, t-test of Student.*

4.2.2. Aspartate/glutamate and glutamate/glutamate exchange activity in mouse brain mitochondria

In order to confirm that the reduction in expression causes also a reduction in activity of AGC1, in collaboration with Dr. Massimo Lasorsa (IBIOM, CNR Bari) we assayed its activity in liposomes reconstituted with mitochondrial extracts and we observed that AGC1 reduced expression in the brain of AGC1 $^{+/-}$ mice significantly inhibits both the aspartate/glutamate and glutamate/glutamate exchange of about 40 % and 25 % respectively, when compared to AGC1 $^{+/+}$ mice. By contrast no difference in ATP/ATP exchange activity was measured (Fig. 4.16). These data suggested that also in the presence of one functional AGC1 allele, AGC activity is impaired even in the presence of unaffected AGC2 expression.

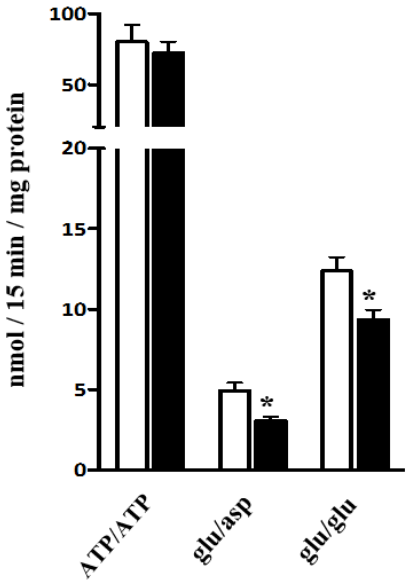

Figure 4.16: Aspartate/glutamate and glutamate/glutamate exchange activities in brain mitochondria from AGC1$^{+/-}$ mice. *[^{14}C]ATP$_{ext}$/ATP$_{int}$ (0.1 mM ext/20 mM ext), [^{14}C]aspartate$_{ext}$/glutamate$_{int}$ (0.05 mM ext/20 mM ext) and [^{14}C]glutamate$_{ext}$ /glutamate$_{int}$ (0.1 mM ext / 20 mM ext) were assayed in liposomes reconstituted with mitochondrial protein extracts isolated from brain of AGC1$^{+/+}$ (white column) and AGC1$^{+/-}$ mice (black column). Transport activities were measured 30 minutes after the addition of radiolabeled substrates. Data are the mean ± SD, n=6, *p< 0.01 compared to liposomes reconstituted with AGC1$^{+/+}$ mitochondrial extracts, one-way analysis with Bonferroni's post-test.*

In collaboration with Dr. FM Lasorsa

4.2.3. Effect of AGC1 deficiency on cell proliferation and differentiation in 21-day old AGC1 $^{+/+}$ and AGC1 $^{+/-}$ mice

In order to confirm *in vivo* the effect of AGC1 deficiency on cell proliferation and differentiation in the central nervous system, immunohistochemical and immunofluorescence analyses on 40 μm thick mouse brain sections were performed. Analyses were conducted both in 21 day-old and in adult AGC1 $^{+/+}$ and AGC1 $^{+/-}$ mice, however since the most significant results were obtained in 21 day-old mice, at which also OPCs reach a proliferation peak, only these data are shown.

4.2.3.1. Cell proliferation

To evaluate proliferation differences, two different cell proliferation markers, pH3 and Ki67 were considered. Phosphorylated histone H3 (pH3) represents a mitotic and cell proliferation marker[150] because phosphorylation of Ser 10 on the N-term tail of histone H3 by Aurora A and B kinases[151,152] (Aurora/AIK family), is fundamental for the beginning of mitosis. Ki67 is expressed during active phases of the cell cycle (in particular in G2 and mitosis), but is absent in the quiescent phase (G0)[153]. A quantification of pH3 and Ki67 positive cell number was conducted in the corpus callosum, an OPC rich region[154] and subventricular zone (SVZ), the main source of neural precursor cells (NPCs)[155]. Cell count showed a lower number of pH3$^+$ (fig. 4.17 A) and Ki67$^+$ (fig. 4.17 B) cells in the corpus callosum and SVZ of AGC1 $^{+/-}$ mice

compared to AGC1 $^{+/+}$ mice. Only pH3 data were statistically significant (fig. 4.17 C and D respectively).

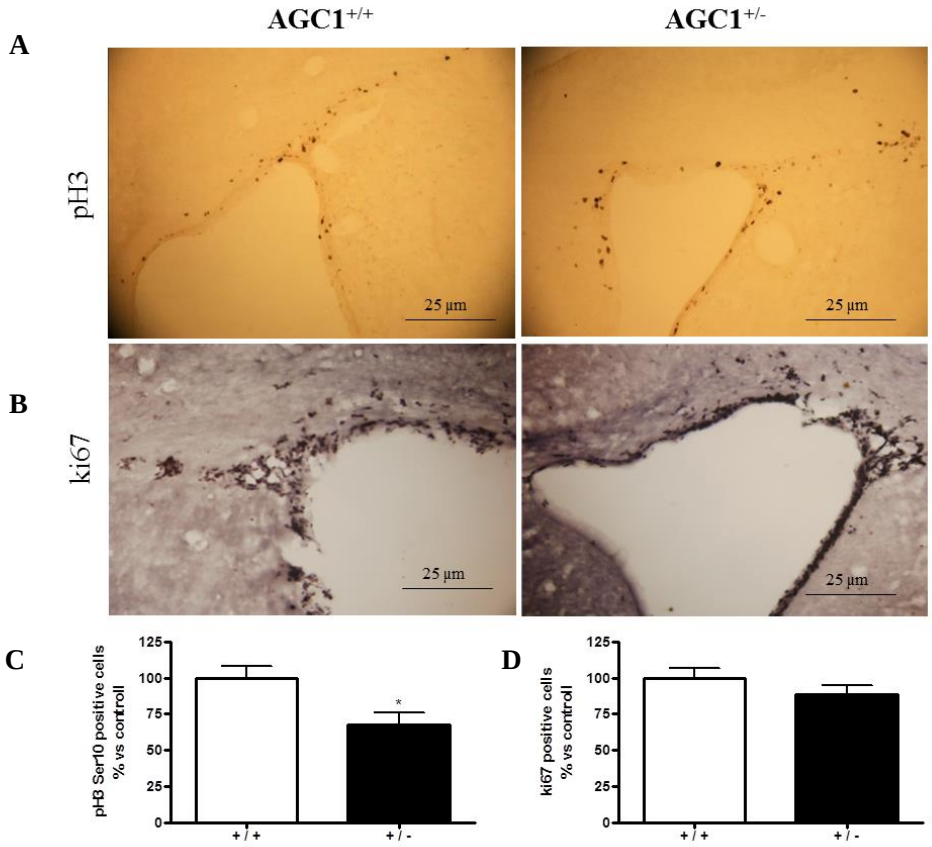

Figure 4.17: *Optical microscopy images (20X). Immunohistochemical analysis of pH3* ***(A)*** *and Ki67* ***(B)*** *proliferation markers in the corpus callosum and subventricular zone of 21 day-old AGC1$^{+/+}$ and AGC1$^{+/-}$ mice.* ***(C)*** *Cell count analysis showed a significant reduction in pH3^{+} cell number in AGC1$^{+/-}$ (1.09472 x 10^{-5} cells / µm ^ 3) mice compared to AGC1$^{+/+}$ mice (1.60714 x 10^{-5} cells / µM ^ 3). Similar results were obtained for Ki67^{+} cells however data were not statistically significant (AGC1$^{+/-}$ 6.90994 x 10^{-5} cells / µm ^ 3 compared to AGC1$^{+/+}$ mice 7.72516 x 10^{-5} cells / µm ^ 3)* ***(D)****. Bars represent the mean ± SE of three experiments. * P <0.05 compared to wild-type mice. Student T-Test.*

4.2.3.2. Proliferation and differentiation of OPCs

Since pH3 and Ki67 staining showed a reduction in proliferating cells in the SVZ and corpus callosum, immunohistochemistry was performed to confirm whether this could be due to reduced OPC proliferation. 21-day old AGC1 $^{+/+}$ and AGC1 $^{+/-}$ mouse brain sections were incubated with an anti-Olig2 antibody, a bHLH (basic helix-loop-helix) transcription factor essential for the differentiation of ventricular neuroectodermal cell progenitors into oligodendrocytes[156]. Following cell count analysis in the corpus callosum, a significantly reduced number of Olig2^{+} cells was determined in AGC1 $^{+/-}$ mice compared to AGC1 $^{+/+}$ mice (fig. 4.18).

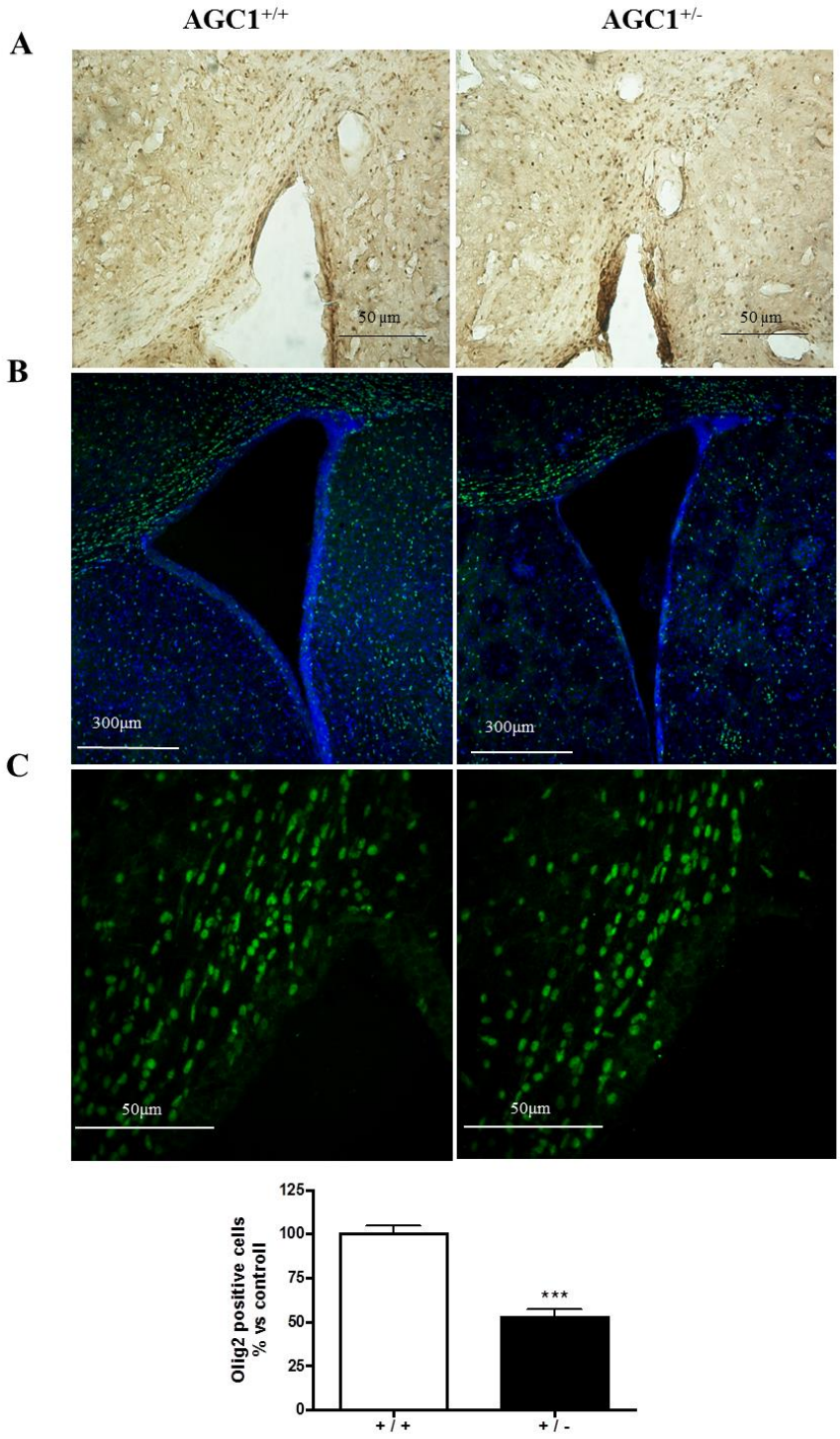

Figure 4.18: (A) *Immunohistochemical analysis of Olig2^{+} cells in 21 day-old AGC1 $^{+/+}$ (n = 3) and AGC1 $^{+/-}$ (n = 3) mouse brain sections. Optical microscopy images (20X).* ***(B)*** *Confocal microscopy images (10X) of Olig2^{+} cells (green) and Hoechst-labeled nuclei (blue) in the corpus callosum of 21 day-old AGC1 $^{+/+}$ and AGC1 $^{+/-}$ mice.* ***(C)*** *Confocal microscopy images (40X) of Olig2^{+} cells (green) and Hoechst-labeled nuclei (blue) in the corpus callosum of 21 day-old AGC1 $^{+/+}$ and AGC1 $^{+/-}$ mice.* ***(D)*** *Cell count analysis showed a significantly reduced number of Olig2^{+} cells in AGC1 $^{+/-}$ (3.381 x 10^{-3} cells / µm ^ 3) mice compared to AGC1 $^{+/+}$ (4.536 x 10^{-3} cells / µm ^ 3) mice; bars represent the mean ± SE of three experiments. *** P <0.001 compared to wild type tissues. Student T-Test.*

Immunohistochemical analyses of 21 day-old AGC1 $^{+/+}$ and AGC1 $^{+/-}$ mouse brain sections with anti-MBP and anti-CNPase antibodies were performed to study whether reduced AGC1 expression had any effect on OPCs differentiation into mature oligodendrocytes and consequently on myelination. MBP (myelin basic protein) is a myelination marker since it is the most prominent protein of the myelin sheath where it constitutes up to 30% of total protein content and participates in maintaining myelin fiber structure[157]. On the other hand, CNPase constitutes about 4% of total protein content of the myelin sheath in the CNS, and is mainly localized at the myelin-axon interface; its distribution matches exactly that of myelin[142]. Neither MBP$^+$ nor CNPase$^+$ cell count was performed, however through immunohistochemistry and optical microscopy, no macroscopic differences in the corpus callosum of 21 day-old AGC1 $^{+/+}$ and AGC1 $^{+/-}$ mice were observed (fig. 4.19), thus indicating that, similarly to *in vitro*, a reduction in AGC1 expression and activity does not affect oligodendrocyte differentiation and therefore myelination.

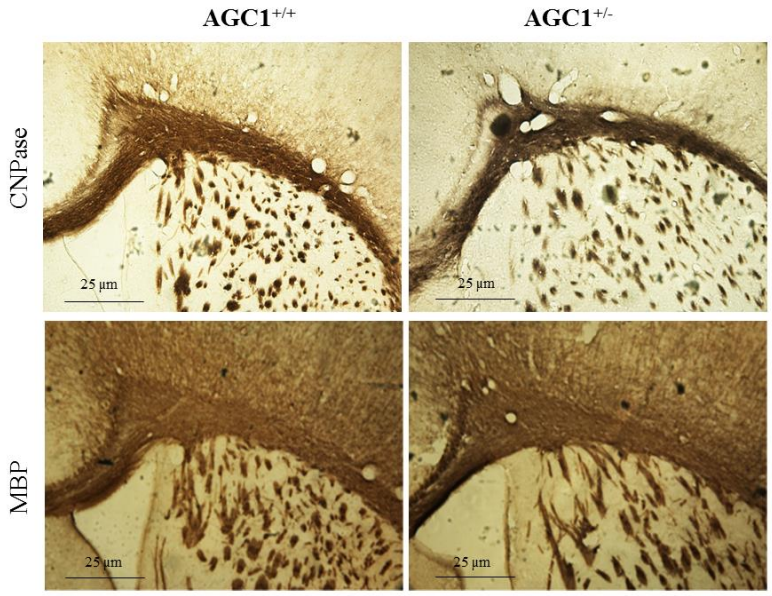

Figure 4.19: *Optical microscopy images (20X). MBP and CNPase immunohistochemical analysis in brain sections of 21 day-old AGC1 $^{+/+}$ (n = 3) and AGC1 $^{+/-}$ (n = 3) mice. Neither MBP$^+$ nor CNPase$^+$ cell count was performed, however through optical microscopy no macroscopic differences in MBP$^+$ and CNPase$^+$ cells were observed between 21 day-old AGC1 $^{+/+}$ and AGC1 $^{+/-}$ mice.*

To further confirm these results, CNPase activity was measured in mouse brain tissue homogenates; for 21-day old mice, cortex and cerebellum were analyzed while for adult mice the same areas and also the hippocampus were studied. No statistically significant differences in CNPase activity between 21-day old (fig. 4.20 A) and adult (fig. 4.20 B) AGC1 $^{+/+}$ and AGC1 $^{+/-}$ mice were detected.

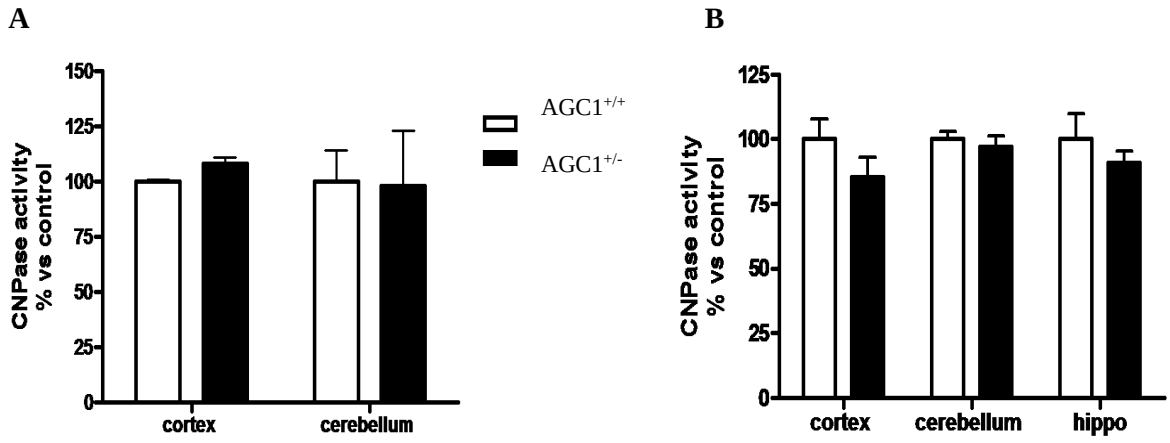

Figure 4.20: *CNPase activity analysis in 21-day old* ***(A)*** *and adult* ***(B)*** *AGC1 $^{+/+}$ (n = 8) and AGC1 $^{+/-}$ (n = 8) mice. Bars represent the mean ± SE of two experiments, Student's t-test.*

4.2.3.3. Neuronal and astroglial proliferation and differentiation

To analyze the effect of AGC1 reduced activity not only on the proliferation and differentiation of oligodendrocytes, but also of neurons and astrocytes, which all derive from the same neural stem cells, 21 day-old AGC1 $^{+/+}$ and AGC1 $^{+/-}$ mouse brain sections were incubated with an anti-doublecortin (DCX) antibody, which is an immature neuronal marker and an essential protein in the early phases of neuronal migration and lamination during cortical development[158], and an anti-GFAP antibody, which is an intermediate type III intermediate filament protein and specific marker for astrocytes[159]. For quantitative evaluation, given that cell count was not possible to perform, DCX^{+} fluorescence signal intensity was evaluated with ImageJ2 (Fiji) software (fig. 4.21). After fluorescence intensity analysis, DCX^{+} signal in brain sections of AGC1 $^{+/-}$ mice was 40% lower than AGC1 $^{+/+}$ mice (100% AGC1 $^{+/+}$ vs 60% AGC1 $^{+/-}$).

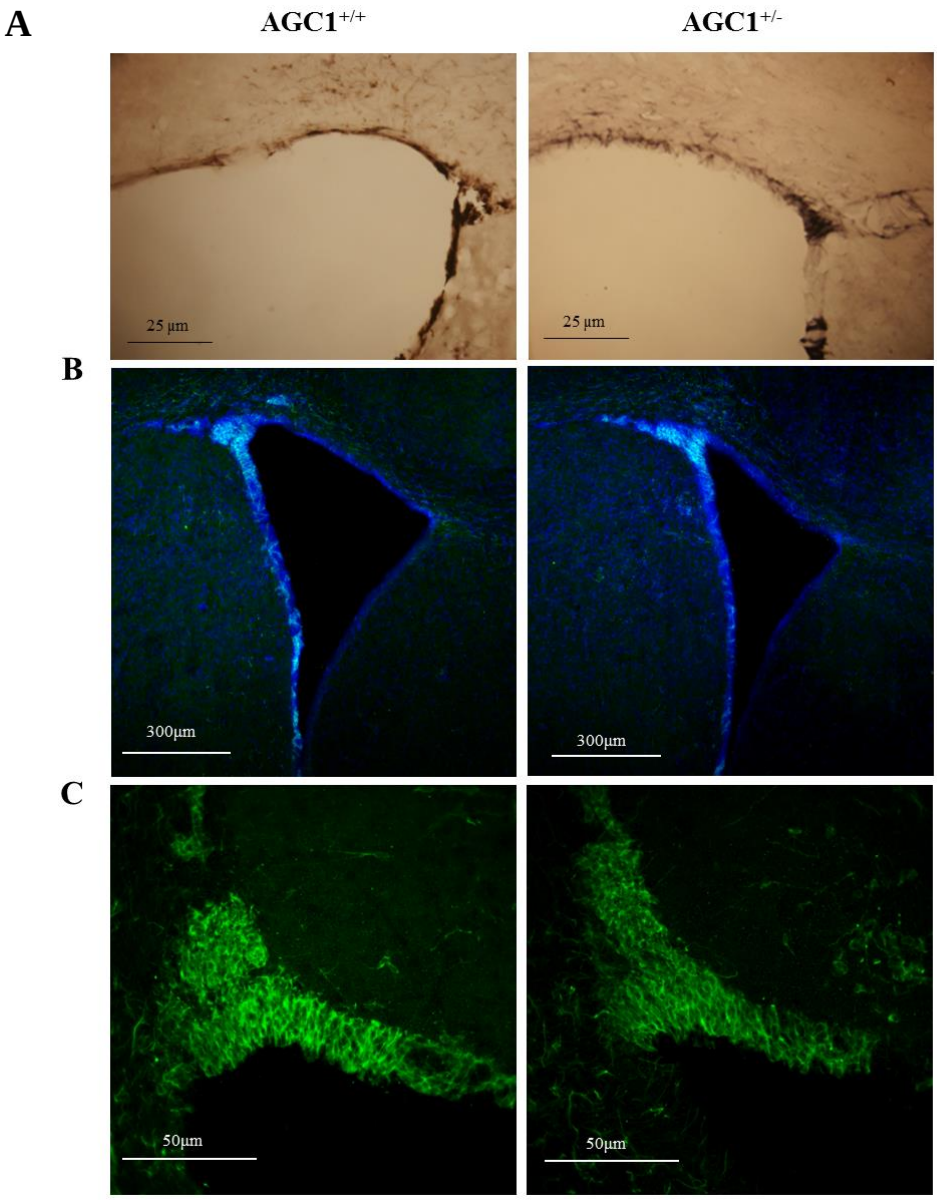

Figure 4.21: (A) *Immunohistochemical analysis of DCX$^+$ cells in brain sections of 21 day-old AGC1 $^{+/+}$ (n = 2) and AGC1 $^{+/-}$ (n = 2) mice. Image acquired by optical microscope (20X).* ***(B)*** *Confocal microscope image (10X) of DCX$^+$ labeled cells (green) and Hoechst-labeled nuclei (blue).* ***(C)*** *Confocal microscope images (40X) of DCX$^+$ labeled cells (green) and Hoechst-labeled nuclei (blue). DCX+ fluorescence signal intensity was evaluated by the ImageJ Fiji program; DCX+ signal in brain sections of AGC1 $^{+/-}$ mice was 40% lower than AGC1 $^{+/+}$ mice (100% AGC1 $^{+/+}$ VS 60% AGC1 $^{+/-}$).*

To study the proliferation and differentiation of astrocytes, 21-day old AGC1 $^{+/+}$ and AGC1 $^{+/-}$ mouse brain sections were incubated with an anti-GFAP antibody. For quantitative evaluation, since cell count was not possible to perform, GFAP$^+$ fluorescence signal intensity was evaluated with ImageJ2 (Fiji) software (fig. 4.22). After fluorescence intensity analysis, GFAP$^+$ signal in brain sections of AGC1 $^{+/-}$ mice was around 20% higher than AGC1 $^{+/+}$ mice (100% AGC1 $^{+/+}$ vs 123% AGC1 $^{+/-}$).

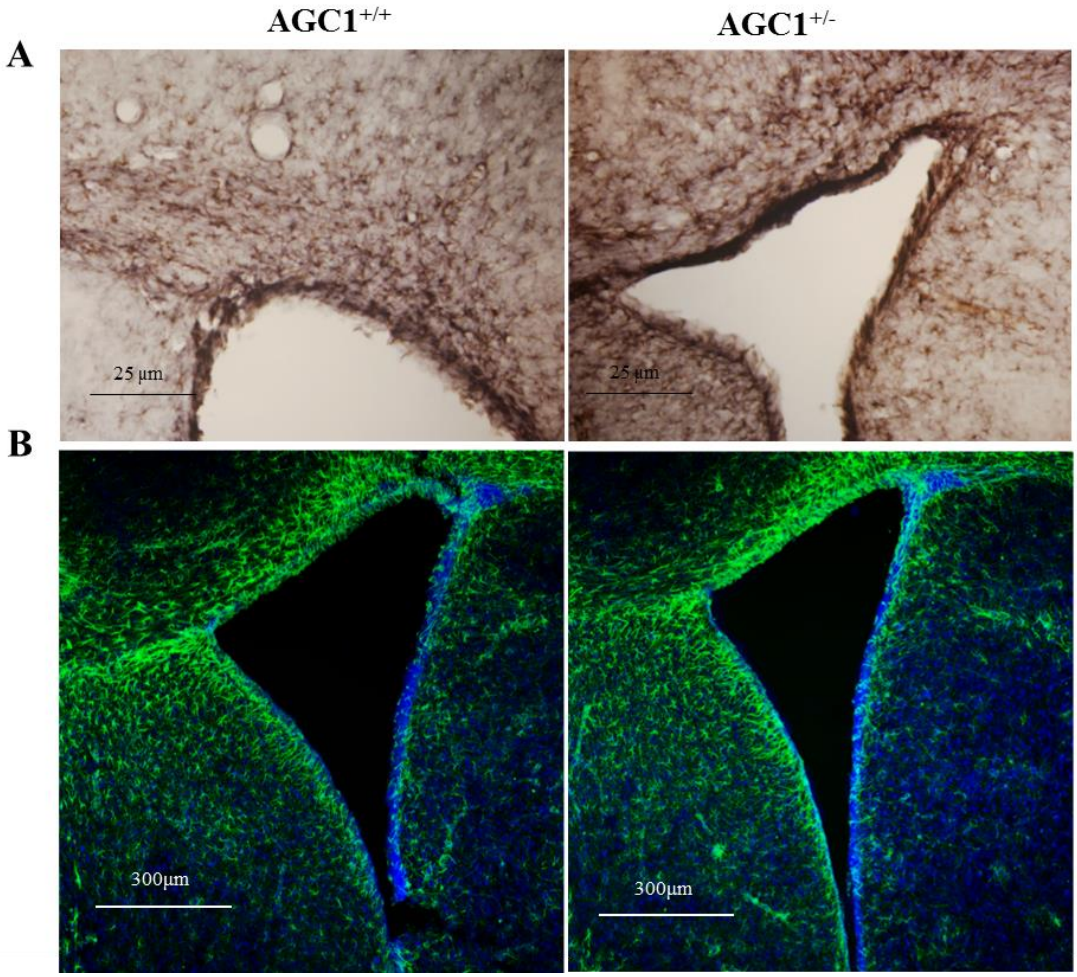

Figure 4.22: (A) *Immunohistochemical analysis of GFAP$^+$ cells in 21-day old brain sections of AGC1 $^{+/+}$ (n = 2) and AGC1 $^{+/-}$ (n = 2) mice. Optical microscopy images (20X).* ***(B)*** *Confocal microscopy images (10X) of GFAP$^+$ labeled cells (green) and Hoechst-labeled nuclei (blue). GFAP+ fluorescence signal intensity was evaluated with ImageJ2 (Fiji) software; GFAP+ signal in brain sections of AGC1 $^{+/-}$ mice was around 20% higher than AGC1 $^{+/+}$ mice (100% AGC1 $^{+/+}$ VS 123% AGC1 $^{+/-}$).*

4.2.3.4. Effect of AGC1 silencing on PDGFα and TGFβ pathways in AGC1 $^{+/+}$ and AGC1 $^{+/-}$ mice

Previous *in vivo* results seem to indicate that, at least in the SVZ at 21 days after birth, reduction in AGC1 expression and activity determines a general proliferation reduction, which mainly affects OPCs and neuronal precursors, while inducing an increase in astrocyte staining and no change in oligodendrocyte differentiation and in myelination. These data are in agreement with data obtained in Oli-Neu cells, therefore, to study the possible dysregulation of the PDGFα and TGFβ pathways, we performed Western Blot analysis in 21 day-old and adult AGC1 $^{+/+}$ and AGC1 $^{+/-}$ mice. As shown in figure 4.23, PDGFα was less expressed in both 21-day old and adult AGC1 $^{+/-}$ mice compared to AGC1 $^{+/+}$ mice

(respectively 21-day old mice fig 4.23 A and adult mice fig 4.23 B), this reduction was statistically significant only in adult AGC1 $^{+/-}$ mice (fig 4.23 B). A lower expression of PDGFα suggests impaired oligodendrocyte precursor proliferation due to reduced AGC1 activity. However, a statistically significant increase in PDGFα receptor expression in 21-day old (fig. 4.23 C) and adult (fig. 4.23 D) AGC1 $^{+/-}$ mice compared to AGC1 $^{+/+}$ mice was observed.

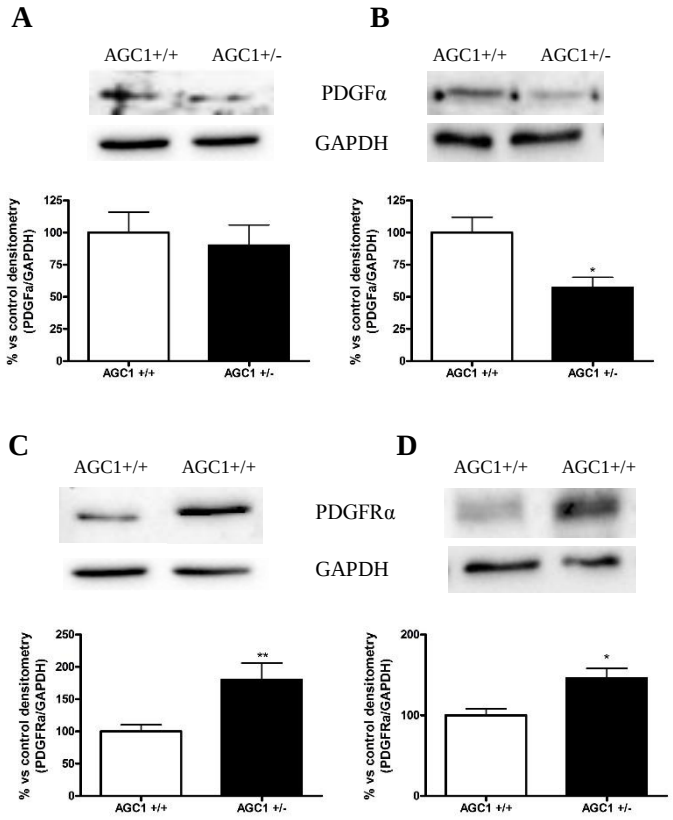

Figure 4.23: *Western blot analysis of PDGFα and PDGFRα expression in 21 day-old* ***(A, C)*** *and adult* ***(B, D)*** *AGC1 $^{+/+}$ (n = 6) and AGC1 $^{+/-}$ (n = 6) mice and respective densitometric analyses. A reduction of PDGFα and an increase of PDGFRα expression was observed. GAPDH was used as an endogenous control to normalize data. Bars represent the mean ± SE of three experiments, Student's t-test.*

Regarding the TGFβ pathway, only immature (precursor) TGFβ1 and 2 forms were expressed, whereas no mature (cleaved) forms were detected. TGFβ1 precursor expression was increased in 21-day old (fig. 4.24 A) and adult (fig 4.24 B) AGC1 $^{+/-}$ mice compared to AGC1 $^{+/+}$ mice; in AGC1 $^{+/-}$ adult mice this difference was statistically significant (* P <0.05). Similarly, TGFβ2 precursor expression was significantly increased in 21-day old AGC1 $^{+/-}$ mice compared to AGC1 $^{+/+}$ mice (* P <0.05; fig. 4.24 C), while adult mice pre-TGFβ2 expression was decreased in AGC1 $^{+/-}$ mice compared to AGC1 $^{+/+}$ mice (fig. 4.24 D).

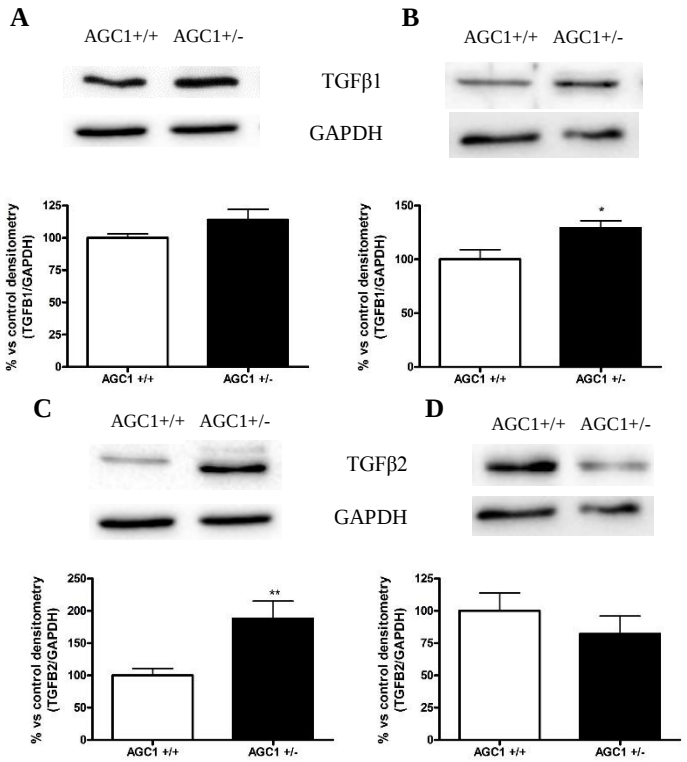

Figure 4.24: *Western blot analysis of TGFβ1 and TGFβ2 expression in AGC1 $^{+/+}$ (n = 6) and AGC1 $^{+/-}$ (n = 6) mice, in 21-day old (A, C) and in adult (B, D) mice and respective densitometric analyses. An increase of pre-TGFβ1 was observed in AGC1 $^{+/-}$ mice compared to AGC1 $^{+/+}$ mice both in 21-day old and adult mice while pre-TGFβ2 was more expressed in 21-day old AGC1 $^{+/-}$ mice and less expressed in adult AGC1 $^{+/-}$ mice compared to their AGC1 $^{+/+}$ counterpart. GAPDH was used as an endogenous control to normalize data. Bars represent the mean ± SE of three experiments, * P <0.05, compared to the wild type, Student's t-test.*

Lastly, TGFβ receptor 1 and 2 (TGFβR1 and TGFβR2) expression was evaluated. While TGFβR2 expression was increased in both 21 day-old (fig. 4.25 A, C) and adult (fig 4.25 B) AGC1 $^{+/-}$ mice compared to AGC1 $^{+/+}$ mice, TGFβR1 expression was significantly reduced in 21-day old AGC1 $^{+/-}$ mice compared to AGC1 $^{+/+}$ mice (fig 4.25C) and increased in adult AGC1 $^{+/-}$ mice (fig 4.25 D) compared to AGC1 $^{+/+}$ mice.

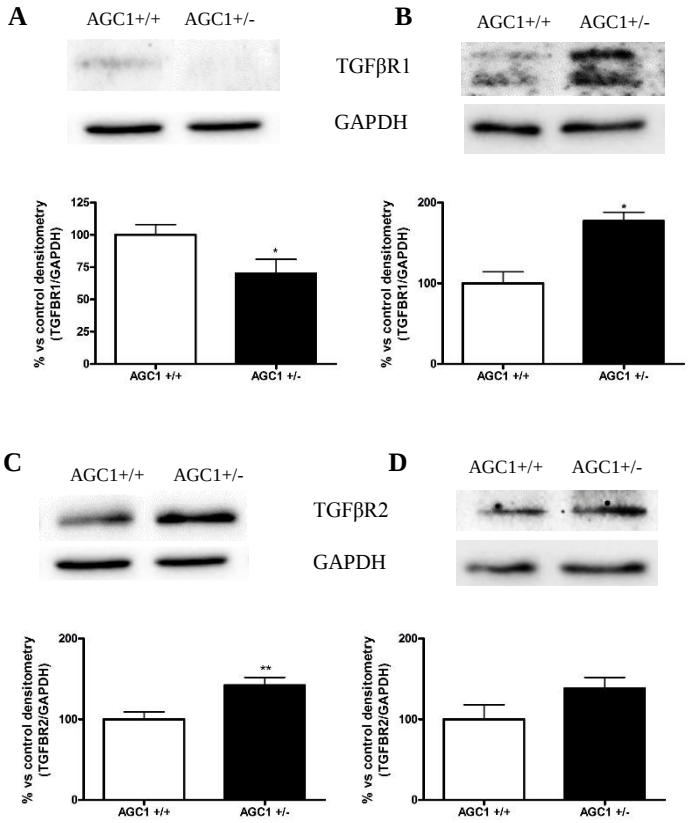

Figure 4.25: *Western blot analysis of TGFβR1 and TGFβR2 expression in 21 day-old (A, C) and adult (B, D) mice AGC1 $^{+/+}$ (n = 6) and AGC1 $^{+/-}$ (n = 6) mice and respective densitometric analyses. Western blot analysis showed that TGFβR1 expression was significantly increased in 21-day old AGC1 $^{+/-}$ compared to AGC1 $^{+/+}$ mice but less expressed in adult AGC1 $^{+/-}$ mice compared to AGC1 $^{+/+}$ mice (data not statistically significant). TGFβR2 expression was increased in both 21-day old and adult AGC1 $^{+/-}$ mice compared to AGC1 $^{+/+}$ mice. GAPDH was used as an endogenous control to normalize data. Bars represent the mean ± SE of three experiments, * P <0.05, compared to the wild type, Student's t-test.*

4.2.3.5. Neural Stem Cell proliferation in AGC1$^{+/+}$ and AGC1$^{+/-}$ SVZ-derived neurospheres

In order to further confirm the alteration of proliferation/differentiation in brain cell-precursors, we produced SVZ-derived neurospheres from adult AGC1$^{+/+}$ and AGC1$^{+/-}$ mice. Firstly, to validate the *in vitro* model, performed Western blot analysis showed that AGC1 expression was reduced approximately by 65-70% in AGC1 $^{+/-}$ neurospheres compared to AGC1$^{+/+}$ ones, as previously observed in the *in vivo* model (fig. 4.26 A). For proliferation assays, AGC1$^{+/+}$ and AGC1$^{+/-}$ neurospheres were plated as single cells at a density of 5 x 10^3 cells/cm^2. After 4 days of incubation, the number of newly formed neurospheres was counted and proliferation was evaluated by using Fiji ImageJ2 software. After counting analysis,

AGC1$^{+/-}$ neurosphere size was significantly lower (* p<0.05) compared to AGC1$^{+/+}$ neurospheres (fig. 4.26 B). On the other hand, AGC1$^{+/-}$ neurosphere cell number was significantly higher (***p<0.001) compared to AGC1$^{+/+}$ neurospheres (fig. 4.26 B). AGC1 $^{+/-}$ neurospheres appeared also morphologically more heterogeneous, irregularly shaped and presented pseudopod-like cytoplasmic processes (fig. 4.26 C).

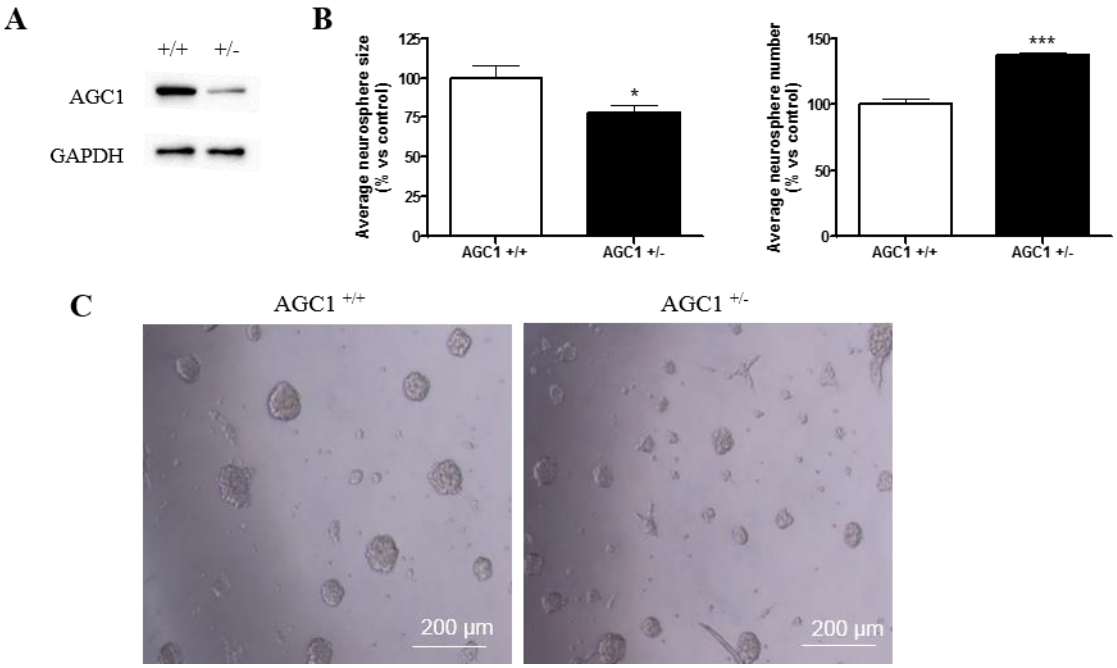

Figure 4.26: (A) *WB analysis confirmed reduced AGC1 expression in AGC1 +/- neurospheres compared to AGC1 $^{+/+}$ neurospheres (about 65-70% reduction). GAPDH was used as an endogenous control to normalize data.* ***(B)*** *Newly formed AGC1 $^{+/+}$ and AGC1 $^{+/-}$ neurosphere size (left) and number (right) analysis after 4 days of incubation. * P <0.05, *** P <0.001 compared to AGC1 $^{+/+}$ neurospheres. Student's t-test.* ***(C)*** *Bright field microscopy images (10X) of AGC1 $^{+/+}$ and AGC1 $^{+/-}$ neurospheres. AGC1 $^{+/-}$ neurospheres (right) showed heterogeneous morphology and appeared smaller than AGC1 $^{+/+}$ neurospheres. AGC1 $^{+/-}$ neurosphere cell number was also higher than AGC1 $^{+/+}$ neurospheres. Bars represent the mean ± SE of three experiments.*

To further analyze AGC1$^{+/+}$ and AGC $^{+/-}$ neurosphere proliferation rate, BrdU incorporation (labeling index = BrdU positive cells/total cells) was quantified after a 24-hour pulse through confocal microscopy. A lower labeling index was observed in AGC1$^{+/-}$ neurospheres compared to AGC1$^{+/+}$ neurospheres, suggesting a lower proliferation rate in AGC1$^{+/-}$ neurospheres as shown in representative 3D confocal microscopy images (fig. 4.27 A) and confirmed by BrdU positive cell count analysis (fig. 4.27 B).

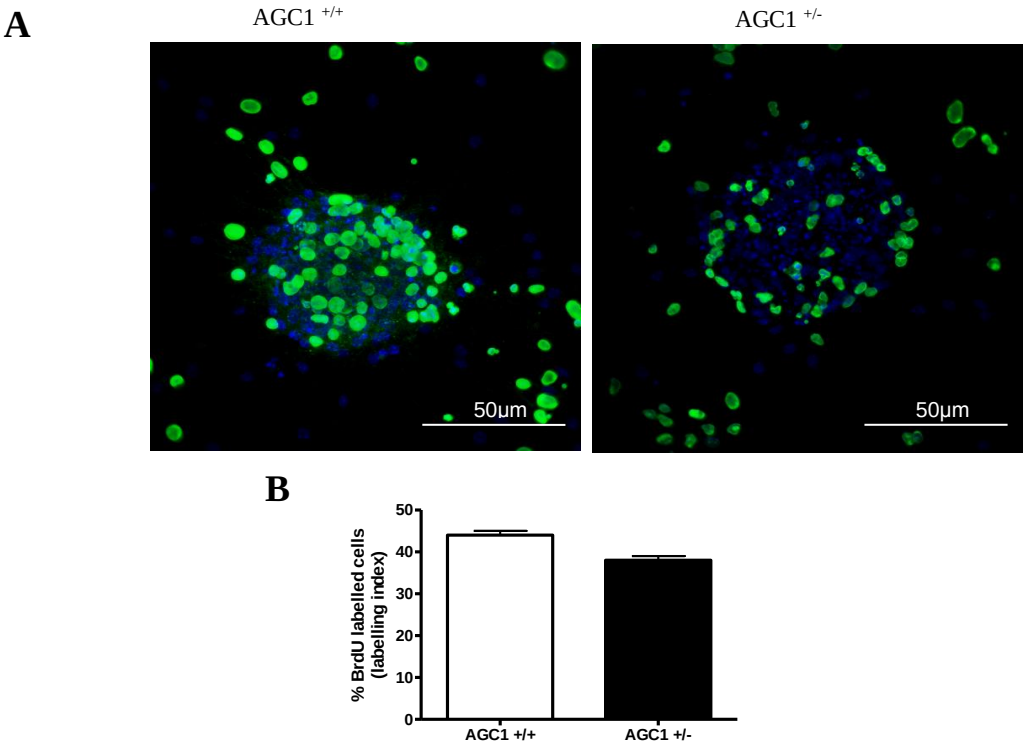

Figure 4.27: ***(A)*** *BrdU immunofluorescence 3D confocal microscopy images (40X) on AGC1 $^{+/+}$ and AGC1 $^{+/-}$ neurospheres; BrdU (green), nuclei (blue).* ***(B)*** *BrdU positive cell count showed a reduced number of BrdU^{+} cells in AGC1 $^{+/-}$ neurospheres compared to AGC1 $^{+/+}$ neurospheres; data were not statistically significant. Bars represent the mean ± SE of three experiments.*

To study the effect of AGC1 deficiency on NSC differentiation, neurospheres obtained from AGC1$^{+/+}$ and AGC1$^{+/-}$ adult mice were plated on fibronectin and PFA-fixed after 1 or 7 days of spontaneous differentiation. In order to verify their neural stem nature, 1-day differentiated AGC1$^{+/+}$ and AGC1$^{+/-}$ neurospheres were characterized by double-labeling immunofluorescence with an anti-Ki67 antibody (proliferation marker) and an anti-Nestin antibody (intermediate filament protein and NSC marker). Proliferating cells (Ki67^{+}) and neural stem cells (Nestin^{+}) were observed in both AGC1$^{+/+}$ and AGC $^{+/-}$ neurospheres (fig. 4.28 A). Then, 1-day differentiated neurospheres were incubated with specific antibodies for 3 brain cell lineages: anti-Olig2 for OPCs; anti-DCX for neural precursors; anti-GFAP for astrocytes (respectively fig. 4.28 B, C, D). Immunofluorescence analysis showed a reduced number of Olig2^{+} cells in AGC1$^{+/-}$ neurospheres compared to AGC1$^{+/+}$ neurospheres, confirmed by positive cell count (fig. 4.28 E), whereas no significant differences in DCX^{+} cells (immature neurons) were found. Interestingly, after labeling with an anti-GFAP antibody specific for astrocytes and radial glia cells, GFAP^{+} labeling was homogeneous in

neurospheres from AGC1$^{+/+}$ mice whereas in AGC1$^{+/-}$ neurospheres GFAP^{+} labeling was localized mainly in outer layer cells.

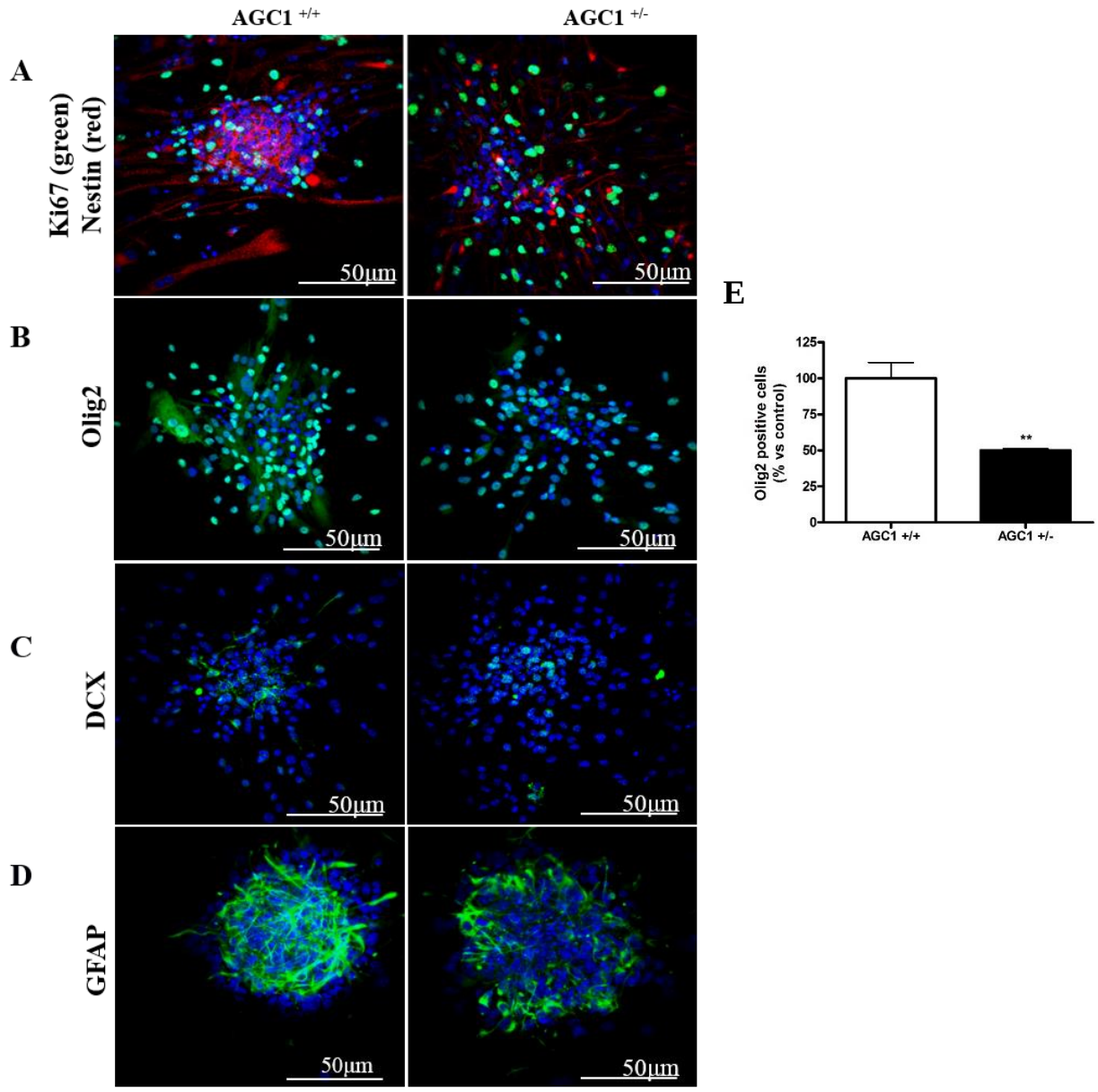

Figure 4.28: *1-day differentiated AGC1 $^{+/+}$ and AGC1 $^{+/-}$ neurosphere confocal microscopy images (40X).* ***(A)*** *Proliferation marker Ki67 (green) and NSC-specific marker Nestin (red) staining;* ***(B, C, D)*** *Immunofluorescence labeling for three brain cell lineages: oligodendrocyte precursors (Olig2), immature neurons (DCX) and astrocytes (GFAP). While a reduced number of Olig2^{+} cells was observed in AGC1 +/- neurospheres compared to AGC1 +/+ neurospheres, no significant differences in DCX^{+} cells (immature neurons) were found. Interestingly, GFAP staining, specific for astrocytes and radial glia cells, was more pronounced and homogeneous in neurospheres from AGC1 $^{+/+}$ mice whereas in AGC1 $^{+/-}$ neurospheres, GFAP^{+}signal was localized only in peripheral layers cells.* ***(E)*** *Cell count showed a significantly reduced number of Olig2^{+} cells in AGC1 $^{+/-}$ neurospheres compared to AGC1 $^{+/+}$ neurospheres; ** P <0.01. T-Test Student. Bars represent the mean ± SE of three experiments.*

Similar analyses were performed on 7-day differentiated neurospheres, labeled with anti-Olig2, anti-DCX, anti-GFAP and anti-CNPase (mature oligodendrocyte marker) antibodies. $Olig2^+$ cell number, indicative of oligodendrocyte precursor number, was lower in $AGC1^{+/-}$ neurospheres compared to $AGC1^{+/+}$ neurospheres (fig. 4.29A), as observed by positive cell count (fig. 4.29 E), while no difference in mature oligodendrocyte number was observed ($CNPase^+$ cells; fig. 4.29 B). On the other hand, a higher number of DCX^+ (fig. 4.29 F) and $GFAP^+$ cells (fig. 4.29 G) was observed in $AGC1^{+/-}$ neurospheres compared to $AGC1^{+/+}$ neurospheres suggesting a higher spontaneous differentiation into neuronal or astroglial cells (fig. 4.29 C, D).

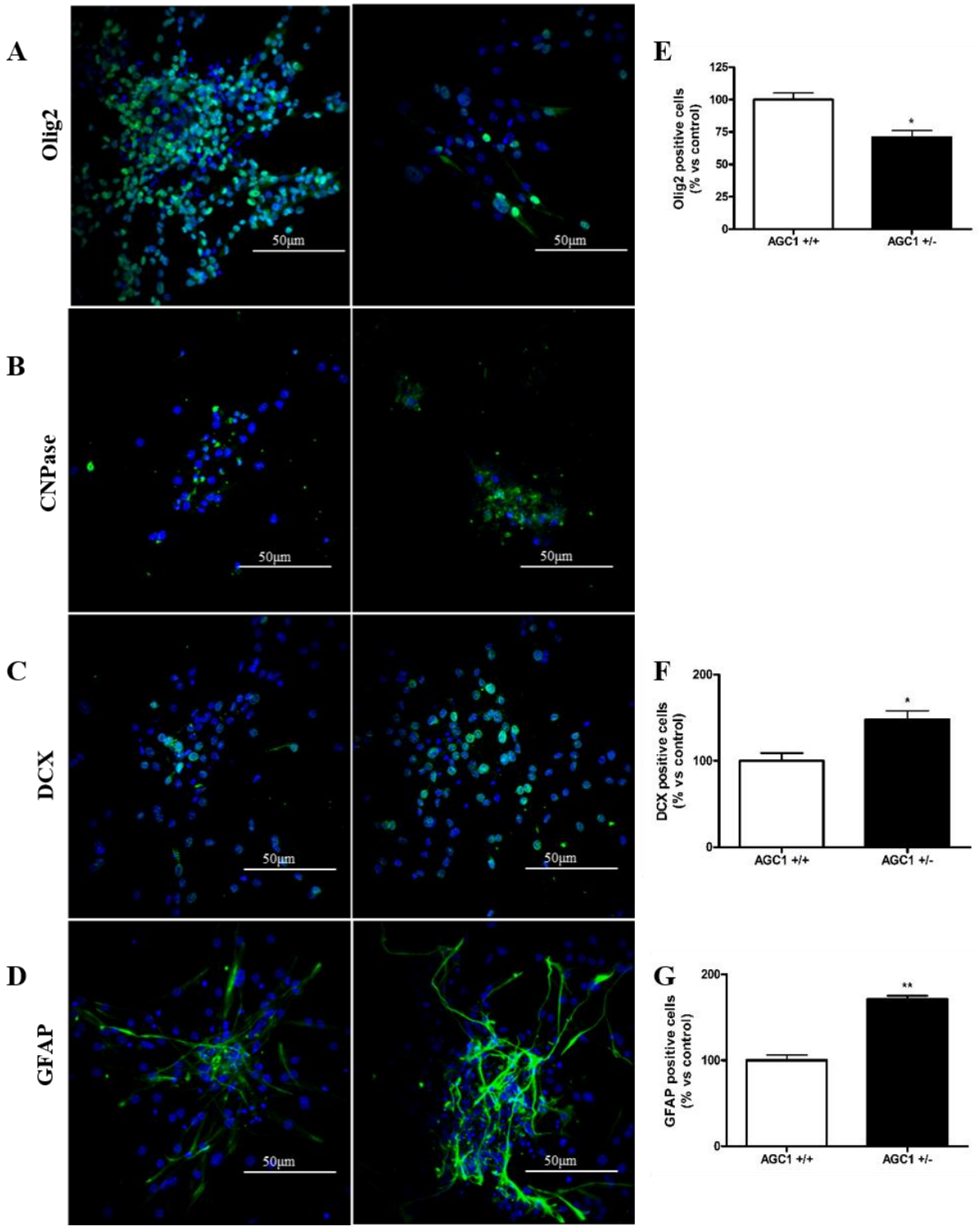

Figure 4.29: *7-day old AGC1 $^{+/+}$ and AGC1 $^{+/-}$ neurosphere confocal microscopy images (40X). Immunofluorescence labeling for oligodendrocyte precursors (Olig2)* ***(A)****, mature oligodendrocytes (CNPase)* ***(B)****, immature neurons (DCX)* ***(C)****, and astrocytes (GFAP)* ***(D)*** *Significant differences in Olig2^{+} cell number between AGC1 $^{+/+}$ and AGC1 $^{+/-}$ neurospheres were observed whereas no differences in mature oligodendrocyte number (CNPase^{+} cells) were observed, similarly to what observed in vivo. GFAP^{+} and DCX^{+} labeling, however, was particularly intense in AGC1 $^{+/-}$ neurospheres, suggesting a higher spontaneous neuronal or astroglial differentiation.* ***(E, F, G)*** *Cell count respectively of Olig2^{+}, DCX^{+} and GFAP^{+}. Bars represent the mean ± SE of three experiments.*

These results obtained from SVZ-derived neurospheres seem to confirm our *in vivo* results; in fact, neurospheres from AGC1$^{+/-}$ mice show a general decrease in cell proliferation and a specific reduction in OPCs number, with a parallel increase in neural and astrocytic cells and no change in oligodendrocytes. Furthermore, these data are in agreement with previous observations made in Oli-Neu cells, thus indicating that a decrease in AGC1 activity could affect myelin formation not through a direct effect on oligodendrocytes, but more probably on oligodendrocyte precursor cell proliferation and therefore affecting remyelination.

4.3. Effect of AGC1-deficiency on brain cells derived from human induced pluripotent (hiPS) cells: preliminary results

As shown in paragraph 4.1 and 4.2, results from mouse cell lines and a mouse animal model, both *in vivo* and in neurospheres, seem to indicate that a reduction in AGC1 activity due to its reduced expression determines a decrease in OPCs proliferation and a shift of NSCs differentiation towards a neural and an astrocytic phenotype. To further confirm the translational validity of these results into humans, we decided to perform preliminary experiments on Neural Stem Cells derived from iPS cells obtained from healthy controls and AGC1-deficiency patients fibroblasts (in collaboration with Prof. S. Anderson, Children's Hospital of Philadelphia, UPenn School of Medicine, Philadelphia, PA in the framework of a project from Italian Ministry of Foreign Affair and International Cooperation, MAECI Italia-USA 2016-2018).

4.3.1. human iPS cell characterization

The pluripotency of hiPSs (human induced Pluripotent Stem Cells) was characterized by double immunofluorescence labeling for Nestin (neural stem marker) and SSEA-4 (glycolipid expressed in early stages of embryonic development and by pluripotent stem cells, used also as a human embryonic stem cell marker[160]. Analyses were conducted both in healthy controls and AGC1-deficiency patient iPS cells. Since no differences were observed between control and patient iPS cells, only control data are shown.

Human iPS cells were Ki67^{+} confirming their active proliferation (fig. 4.30 A), SSEA-4^{+} (fig. 4.30 B) and Nestin^{-} (fig. 4.30 C) confirming their cellular pluripotency and DCX^{-} (fig. 4.30 D), confirming the absence of neuronal phenotype.

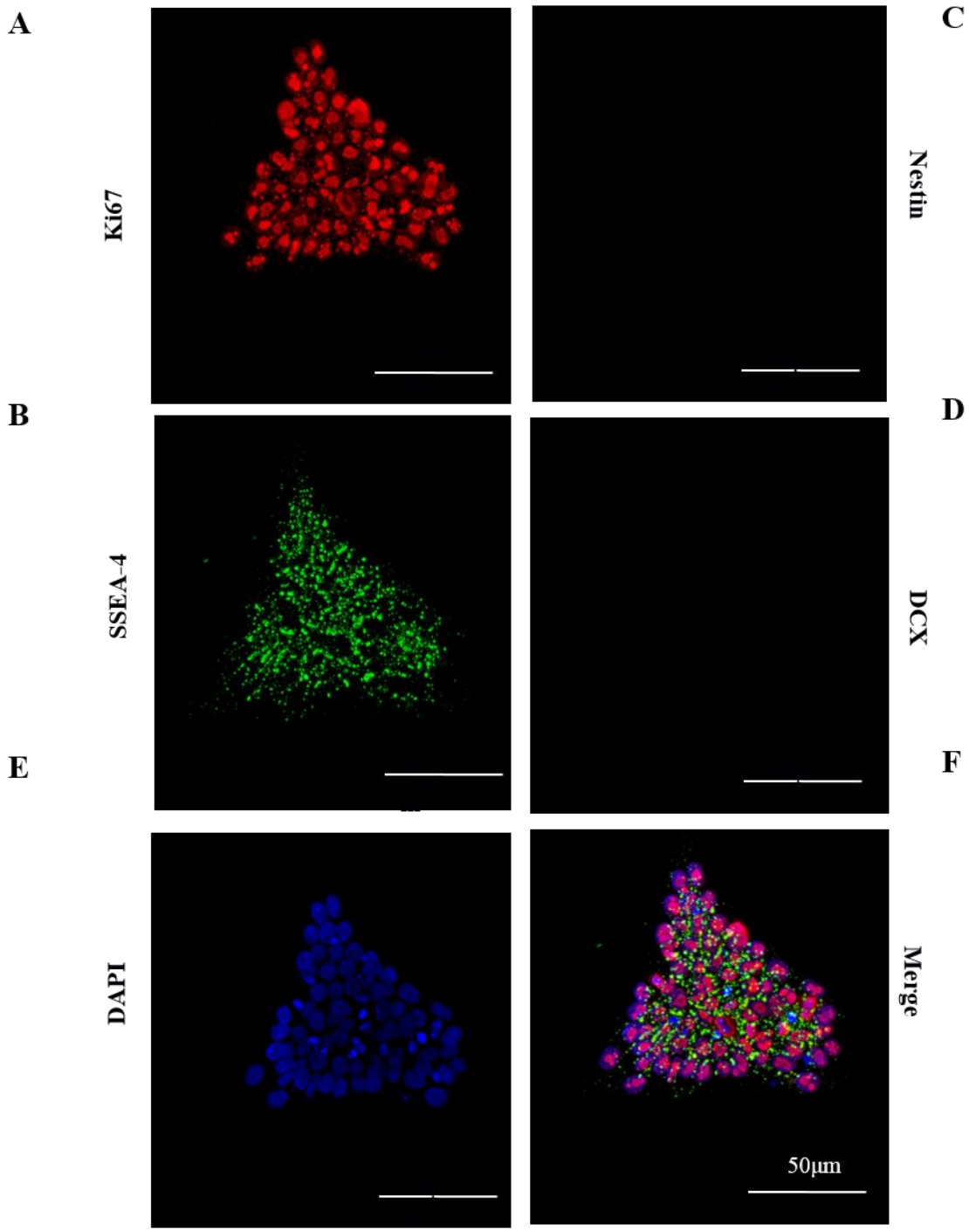

Figure 4.30: *Ki67* ***(A)****, marker of active proliferation, SSEA-4 embryonic stem cell marker* ***(B)****, Nestin neural stem cells marker* ***(C)*** *and DCX immature neurons marker* ***(D)*** ***c****onfocal microscopy images (40X) of control hiPS. Control hiPSs appeared SSEA-4^{+} and Nestin^{-} confirming their cellular pluripotency, high level of proliferation (Ki67^{+}), typical of stem cells. Furthermore, hiPSs appeared DCX^{-} confirming the absence of neuronal phenotype.*

4.3.2. Characterization of NSCs obtained by hiPSCs

Following characterization, healthy control and AGC1-deficiency patient iPS cells were induced to differentiate into NSCs (Neural Stem Cells) according to a published protocol[121] (fig. 4.31).

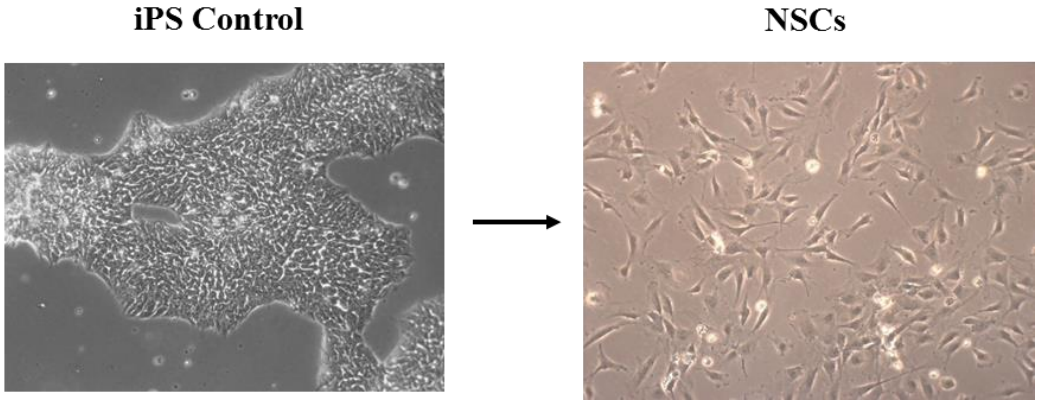

Figure 4.31: *Bright field microscopy images (10X). NSCs (right panel) derived from control iPS cells (left panel) with a published differentiation protocol[121].*

Effective NSC differentiation was verified by immunofluorescence against SSEA-4 and DCX, a differentiation index into a neuronal phenotype. Also in this case, analyses were conducted both in healthy control and AGC1-deficiency patient NSCs. Since no differences were observed between control and patient NSCs, only control data are shown No SEEA-4^{+} signal was detected, confirming the loss of cell pluripotency, while NSCs resulted DCX^{+}, confirming the acquisition of a neuronal phenotype (fig. 4.32).

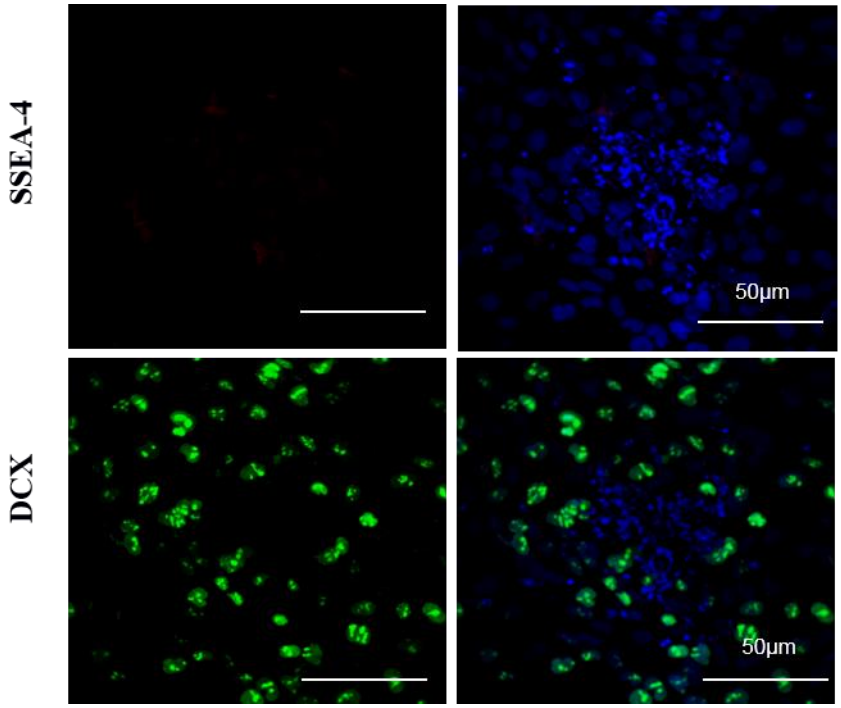

Figure 4.32: *Confocal microscopy images (40X); NSC characterization according to a published differentiation protocol[121] by immunofluorescence analysis. No SEEA-4$^+$ signal was detected, confirming the loss of cellular pluripotency, while NSCs were resulted DCX+, confirming the acquisition of a neuronal phenotype.*

4.3.3. Proliferation of NSCs

To analyze the proliferation rate between control NSCs and NSCs derived from an AGC1-deficiency patient, Ki67$^+$ cells were quantified after immunofluorescence staining. Preliminary results (fig. 4.33) showed a decrease of Ki67$^+$ cells in patient NSCs compared to control NSCs suggesting, also in this model, a proliferation deficit caused by AGC1 deficiency. However, this data will need to be confirmed with further experiments.

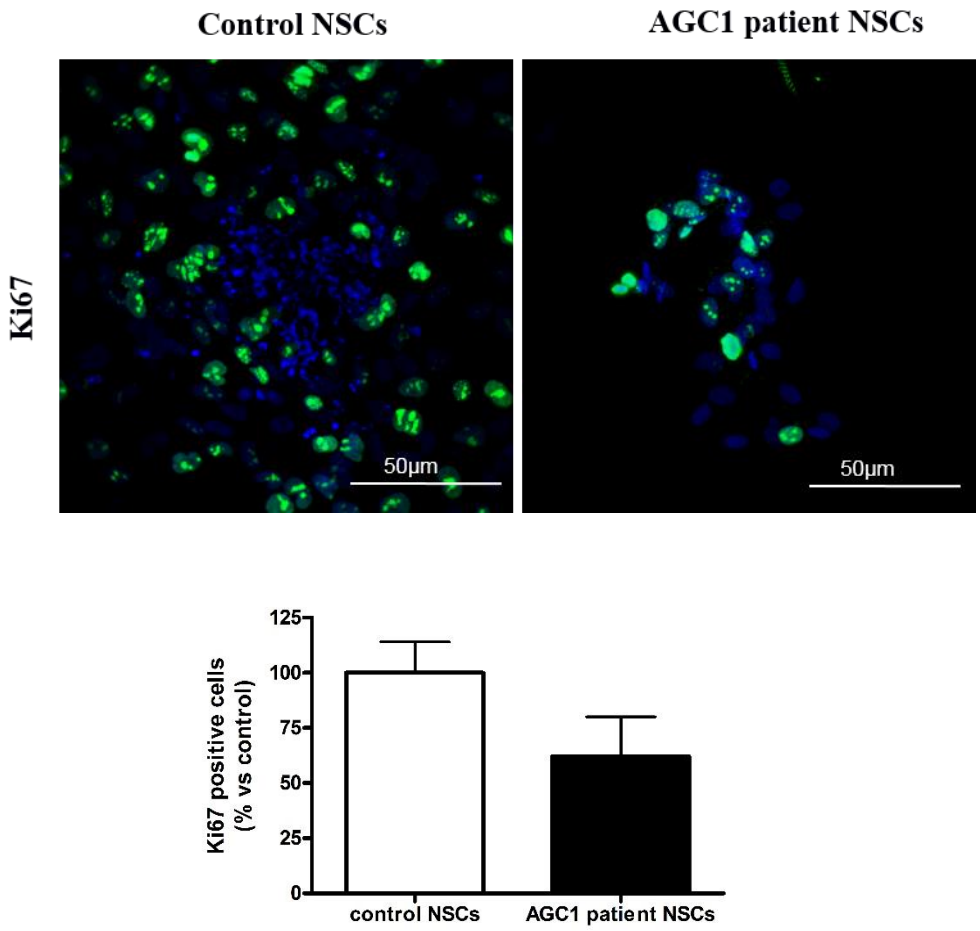

Figure 4.33: *Confocal microscopy images (40X) of immunofluorescence labeling for proliferation marker Ki67 (green) in control and AGC1-deficiency patient NSCs. Cell count showed a reduced number of Ki67$^+$ cells in patient NSCs compared to control NSCs. Bars represent the mean ± SE of three experiments.*

5. DISCUSSION AND CONCLUSION

AGC1 deficiency is a rare neurodegenerative disease caused by AGC1 carrier activity reduction, which results in cerebral hypomyelination and low levels of N-acetyl aspartate (NAA). Although the role of AGC1 in biochemical pathways such as MAS is well known, its direct role in NAA synthesis and myelin formation in the CNS remains largely unknown.

In vitro, AGC1 partial silencing in undifferentiated N2A mouse neuronal cell lines (which display reduced mitochondrial carrier activity down to about 30% compared to controls), show reduced growth and NAA production[124]. This result could explain the main clinical phenotypes observed in AGC1-deficiency patients, such as cerebral atrophy and demyelination with reduced NAA levels[1,2]. In the CNS, NAA is generated in neurons and used for aspartate acetylation through aspartate-N-acetyltransferase and then transferred into oligodendrocytes where it provides acetyl groups for myelin lipid synthesis. From previously obtained data[124], it was hypothesized that in normally proliferating neurons, AGC1 activity could support mitochondrial pyruvate oxidation leading to acetyl-CoA production, which enters the TCA cycle and is also necessary for lipid and NAA synthesis. Few data on the role of oligodendrocytes in this rare disease are currently available; Ramos and collaborators observed hypomyelination in the cerebral cortex of AGC1$^{-/-}$ mice with a parallel increase in the number of immature oligodendrocytes, thus suggesting a defect in oligodendrocyte maturation. However, the same authors observed no defects in oligodendrocyte maturation in *in vitro* cultures[36]. Moreover, no studies have been performed on oligodendrocyte precursor cells (OPCs) and on Neural Stem Cells (NSCs), from which OPCs derive. Given the importance of oligodendrocytes in myelin synthesis and their cross-talk with neurons, it was hypothesized that the pathological mechanism could involve an alteration of OPC and/or NSC proliferation and/or differentiation mechanisms.

For this purpose, three different models were used:

1) An *in vitro* model represented by the Oli-Neu cell line (immortalized mouse oligodendrocyte precursor cells), in which AGC1 expression was partially silenced, in order to obtain a reduction in carrier activity down to about 30-40% compared to controls;

2) An *in vivo* model, represented by SLC25A12 heterozygous knockout mice (AGC1 $^{+/-}$ C57BL6/N background) and neurospheres derived from the subventricular zone of the same mice;

3) Neural stem cells (NSCs) derived from AGC1-deficiency patients iPS cells.

Through *in vitro* studies, it was found that reduction of AGC1 expression is not essential for Oli-Neu cell differentiation, since no evident morphological and biochemical differences were found between control and silenced cells suggesting that AGC1 deficiency development may be influenced by functional alteration of undifferentiated cells. Both undifferentiated and differentiated control and silenced Oli-Neu cells express AGC1 but surprisingly, AGC1 was detected not only in mitochondria, but also in the nucleus. The nuclear/mitochondrial AGC1 colocalization is an interesting result that deserves further investigation; currently, no role for nuclear localization of a mitochondrial carrier has been elucidated.

Following cell proliferation studies (cell count and BrdU incorporation assays), we observed that AGC1-silenced Oli-Neu cells proliferated less than control cells, which was also confirmed by flow cytometry. Considering that AGC1 silencing reduced Oli-Neu cell proliferation, whereas it did not affect cAMP-induced differentiation, we decided to evaluate whether AGC1 silencing could induce by itself Oli-Neu cell differentiation. We therefore evaluated first the effect of AGC1 silencing on cell morphology. AGC1-silenced Oli-Neu cells showed a more elongated and branched morphology compared to control cells, a decrease in cell and process number and an increase in average process length, suggesting premature cell differentiation.

Based on data obtained in collaboration with Dr. Lasorsa (IBIOM, CNR Bari) and Prof. Pinton (University of Ferrara), no differences between control and AGC1-silenced Oli-Neu cells were observed at the mitochondrial level. In particular, AGC1 silencing i) did not reduce glucose oxidation rate in Oli-Neu cells; ii) did not modify mitochondrial morphology or membrane potential, suggesting that AGC1 silencing did not affect the mitochondrial network and OXPHOS activity; ii) induced a slight, but significant increase of ROS production in the cytosol, when compared to control cells, while no difference in mitochondrial ROS production and in mitochondrial [Ca^{2+}] was measured.

We therefore thought the observed proliferation deficit could not be due to mitochondrial biochemical alterations, but rather associated with an alteration of trophic factors essential for maintaining the balance between oligodendrocyte proliferation and differentiation[3]. In fact, Western blot analysis showed a lower expression of PDGFα (involved in the proliferation process) and a significant increase of TFGβ1/2 (crucial for cell differentiation) in AGC1-silenced Oli-Neu cells, supporting the hypothesis that AGC1 reduced expression could lead to OPCs proliferation impairment, thus favoring premature differentiation. While PDGFα receptor expression did not change, TGFβ receptors 1 and 2 were more expressed in AGC1-silenced Oli-Neu cells, especially TGFβR2. This last result was unexpected since TGFβR2

deletion in oligodendrocyte progenitors caused hypomyelination preventing their development into mature myelinating oligodendrocytes[100]. Therefore, AGC1-silenced Oli-Neu cells seem to express TGFβR2 because they may already be in a pre-differentiated state.

Our *in vitro* results were also validated in an *in vivo* AGC1 deficiency model represented by SLC25A12 heterozygous knockout mice (AGC1 $^{+/-}$ C57BL6/N background). AGC1 $^{+/-}$ mice have a reduced AGC1 carrier expression of about 60% compared to AGC1 $^{+/+}$ control mice. Moreover, AGC1 knockout mice (AGC1 $^{-/-}$) have previously been described in the literature as an AGC1-deficiency model. AGC1 $^{-/-}$ mice showed growth retardation, epileptic seizures and reduced myelination (typical AGC1-deficiency patient symptoms), as well as global cerebral atrophy, neurofilament distribution alteration in cortical neurons and Purkinje cell abnormalities in the cerebellum, though they all died at weaning[35,36,161]. Unlike the AGC1 deficiency *in vivo* models reported in the literature, in our mouse model, AGC1 knockout (AGC1 $^{-/-}$) appeared to be embryonic lethal, since no AGC1 $^{-/-}$ mice were born alive whereas Jalil and Sakurai reported the use of live AGC1 $^{-/-}$ mice. This could be due to the presence of a truncated AGC1 protein containing one catalytic site for aspartate, resulting in a mutant protein with residual activity produced (Jalil's model)[35], and a different mouse background represented by a C57BL/6 and C57BL/6Tac chimera (Sakurai's model)[24]. Since currently identified AGC1 mutations determine a reduction of activity down to 20-30% compared to wild-type AGC1 and not the total absence of mitochondrial carrier activity[1], AGC1 $^{+/-}$ mice are considered a good disease model. AGC1 $^{+/-}$ mouse did not show any suffering phenotype, presenting only slight changes in social behavior that did not compromise normal physiological and behavioral functions. Furthermore, AGC1 $^{+/-}$ mice were not distinguishable from AGC1 $^{+/+}$; however, they showed a reduction in brain structure size, particularly the subventricular zone (SVZ) and overall brain ventricle size.

We performed studies on 21-day and adult AGC1 $^{+/+}$ and AGC1 $^{+/-}$ mice, but in this PhD thesis we focused on 21-day old mice, since this stage represents the peak of OPCs proliferation. Significant number reduction of proliferating cells (positive for proliferation markers, such as phosphorylated histone H3 on serine 10 and Ki67) in the subventricular zone (SVZ) and the corpus callosum (CC) as well as a reduction of Olig2 (OPC marker) and DCX (immature neuron marker) positive cell number were observed in AGC1 $^{+/-}$ mice. DCX^{+} cell number reduction was a very interesting result, since DCX is known to be essential for neuronal migration, cell proliferation during neurogenesis and for the development of a functional brain[162]; this result could explain the difference in the subventricular zone and overall brain ventricle size observed in AGC1 $^{+/-}$ mice compared to AGC1 $^{+/+}$ mice. All these data suggest

that proliferation defects affected mainly oligodendrocyte precursor cells, in agreement with our *in vitro* results. Moreover, reduced AGC1 expression had not effects on mature oligodendrocytes and myelination, since no significant differences in MBP^+ and $CNPase^+$ cells were observed through immunohistochemical and biochemical analysis. As in our *in vitro* model, an imbalance in PDGFα and TGFβ pathways was also observed in our *in vivo* mouse model; PDGFα reduced expression confirmed OPCs reduced proliferation in AGC1 $^{+/-}$ mice whereas TGFβ1 and TGFβ2 increased expression, which correlated with reduced PDGFα expression, confirmed that oligodendrocyte precursor cells proliferated less because they differentiated prematurely. PDGFα receptor was more expressed in AGC1 $^{+/-}$ mice compared to AGC1 $^{+/+}$ mice in agreement with literature data showing that PDGFRα expression is a key event in OPC ontogenesis[163,164]. On the other hand, TGFβR2 was more expressed in AGC1 $^{+/-}$ mice as observed in AGC1 silenced Oli-Neu cells indicating that OPCs differentiated earlier into mature oligodendrocytes[100]. All these results confirmed our *in vitro* data, supporting that alterations induced by AGC1 reduced activity could impair the physiological cross-talk through growth factors between neurons and OPCs necessary for OPC proliferation and neuronal survival. These data not only are in agreement with data previously obtained by Ramos and collaborators[36], who observed no alteration in oligodendrocyte maturation in both *in vitro* and *in vivo* models, but could also contribute to explain their results.

In addition, the effect of AGC1 reduced expression on proliferation and differentiation was also evaluated in neural stem cells (NSCs) derived from neurospheres[103], which represent a nearly perfect system able to provide a consistent and self-renewable source of CNS undifferentiated precursors for cell replacement therapies and *in vitro* studies for neural stem cell analysis/characterization. Defined as an "environmental adaptation", NSCs could be clustered to survive in the non-physiological conditions of *in vitro* cell culture by optimizing their cell-cell interactions and acquiring a thermodynamically favorable sphere shape[104]. Once plated as single NSCs and allowed to grow in culture for 4 days in the absence of an adhesion matrix, neo-formed neurospheres from AGC1 $^{+/+}$ adult mice were larger in size and showed a more regular spherical morphology compared to AGC1 $^{+/-}$ cells. AGC1 $^{+/-}$ neurospheres, on the other hand, displayed a higher number compared to AGC1 $^{+/+}$ neurospheres, meaning that while they may be able to organize themselves more easily into suspended clusters, which would explain the greater observed number, they presented proliferation defects and thus remained smaller. Proliferation defects in AGC1 $^{+/-}$ neurospheres were further confirmed through BrdU incorporation. In addition, AGC1 $^{+/-}$ neurospheres also appeared

morphologically more heterogeneous, irregularly shaped and presented pseudopod-like cytoplasmic processes suggesting a possible tendency to differentiate much more easily, similarly to what previously observed in Oli-Neu cells. AGC1 $^{+/-}$ neurospheres allowed to differentiate for 1 and 7 days in culture showed a significantly reduced number of Olig2^{+} cells compared to AGC1 $^{+/+}$ neurospheres, while no differences were found in mature oligodendrocytes (CNPase^{+} cells) at 7 days of differentiation, in agreement with our *in vivo* immunohistochemical analysis. However, after 7 days of differentiation, AGC1 $^{+/-}$ neurospheres showed more intense DCX^{+} and GFAP^{+} labeling, suggesting a "shift" of neural stem cells towards neuronal or astroglial differentiation.

Our last model examined was represented by neural stem cells (NSCs) derived from AGC1-deficiency patient iPS cells (harboring the R353Q mutation). After iPS cell differentiation into NSCs by using a published protocol[121], neural stem cells were characterized; immunofluorescence analysis confirmed the successful differentiation into NSCs, as shown by loss of pluripotency (SSEA4^{-}) with acquisition of typical characteristics of neural phenotype cells (DCX^{+}). Preliminary data also showed reduced proliferation of AGC1-deficiency patient-derived NSCs compared to control cells, after Ki67^{+} cell count. Besides proliferation and differentiation studies, it would be extremely important to differentiate NSCs into oligodendrocyte precursors and mature oligodendrocytes to better understand disease mechanisms underlying hypomyelination. Figure 5.1 summarizes our *in vitro* (Oli-Neu, neurospheres and NSCs) and *in vivo* (AGC1 deficiency mouse model) results.

Since AGC1 is an important component of the malate-aspartate shuttle system (MAS), we can hypothesize that the reduced activity of this mitochondrial carrier, and consequently MAS shuttle reduced functionality, is involved in decreased acetyl group availability. This hypothesis is indirectly supported by data reported in the literature according to which treatment of an AGC1 deficiency patient with a ketogenic diet[125] improves the pathological phenotype; in fact, reduced glycolysis could compensate the metabolic defect and allow myelination recovery in AGC1 deficiency. We hypothesize that decreased acetyl group availability could be involved in impaired NAA and/or N-acetyl-CoA synthesis in neurons, but it could also lead to a reduction of histone acetylation, possibly explaining gene expression alterations. To indirectly support our hypothesis, it has been observed that a ketogenic diet, which is often used in the treatment of epilepsy, has positive effects against neurodegeneration, by providing ketone bodies and fatty acids[165]. However, the biochemical, molecular and cellular mechanisms underlying this nutritional approach have not yet been completely clarified[126]. We think that a ketogenic diet could provide sufficient levels of

ketone bodies (for example β-OH-butyrate) as an alternative source of mitochondrial acetyl groups, thus improving NAA deficiency in neurons and favoring myelination in AGC1-deficiency patients, though these acetyl groups could also contribute to gene expression regulation. Therefore, studying and eventually confirming a possible histone acetylation dysregulation in AGC1-deficiency OPCs, could contribute to understanding the role of AGC1 in health and disease. Overall, these data could be useful to clarify biochemical and molecular mechanisms underlying proliferation deficits of neuronal and oligodendrocyte precursors, responsible for demyelination and consequent neurodegeneration in the rare genetic disease AGC1-deficiency, but possibly involved in other demyelinating and neurodegenerative diseases. It is well known that the interaction between neurons and oligodendrocytes is crucial for neuronal maturation and myelin sheath formation during brain development and also in the adult brain in order to guarantee proper brain functioning. Moreover studying the effect of supplementation with different metabolic substrates (glucose, pyruvate or lactate in absence/presence of glutamine or other acetyl group precursors such as leucine) or pharmacological treatment with histone deacetylase inhibitors such as valproic acid or lithium[166-168] (which inhibit histone deacetylases such as HDAC1) on proliferation/differentiation of different brain cells could provide additional data for AGC1-deficiency therapeutic strategies.

The identification of AGC1 interactions through high throughput proteomic approaches[169] with transcription factors, such as c-myc, which is known to play a crucial role in regulating OPCs proliferation and differentiation[100], support a possible nuclear role for AGC1. We have also confirmed this interaction in our laboratory from preliminary co-immunoprecipitation experiments. However, whether AGC1 has a biological role in the nucleus and how much this could influence disease mechanisms stills needs to be understood. Lastly, while AGC1-deficiency remains a rare disease, data obtained from this study could be translated to other demyelinating and neurodegenerative and/or neurodevelopmental diseases with similar mechanisms, such as other pediatric diseases (rare genetic diseases, metabolic diseases and orphan diseases) or adult onset diseases such as multiple sclerosis. These diseases are not only extremely disabling due to the neurological deficits they cause, but also exert high social and economic impact.

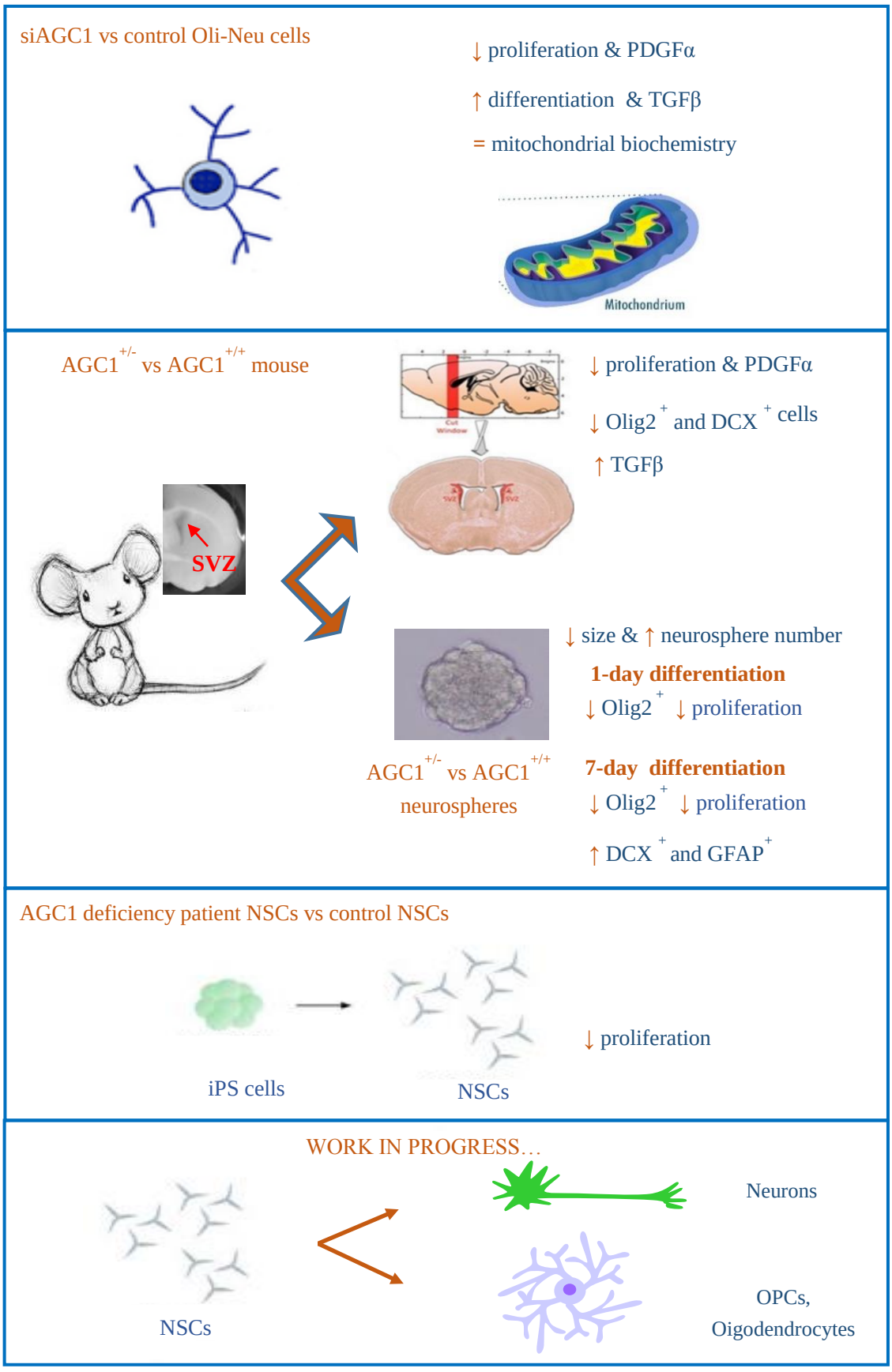

Figure 5.1: *Summary of our in vitro (Oli-Neu, neurospheres and NSCs) and in vivo (AGC1 deficiency mouse model) results.*

ACKNOWLEDGMENTS

I am very grateful to the Italian Ministry for Foreign Affairs and International Cooperation (MAECI) for fully funding this PhD project within the framework of the Italy-USA (2016-2018) research project *"Biochemical changes in the rare genetic demyelinating and neurodegenerative disease AGC1 deficiency: a study on the different brain cells derived from human iPS".*

I am also very grateful to Comitato Telethon Fondazione Onlus for fully funding the project *"Mitochondrial Aspartate/Glutamate Carrier 1 Deficiency: Pathogenetic Mechanisms and Mutational Analysis"* (2011-2014).

I also thank Prof. Stewart Anderson (Children's Hospital of Philadelphia, University of Pennsylvania, USA) for kindly hosting me and providing training on iPS culture during my stay as a visiting PhD student and for donating control and AGC1-deficiency patient iPS cells.

I thank Prof. Ferdinando Palmieri (University of Bari, Italy) as a coordinator of the Telethon project *"Mitochondrial Aspartate/Glutamate Carrier 1 Deficiency: Pathogenetic Mechanisms and Mutational Analysis"* (2011-2014).

A special thank you goes to Dr. Massimo Lasorsa and his research group (IBIOM, CNR, Bari, Italy) for actively contributing to the development and progress of this PhD project as well as for performing a great amount of biochemical experiments discussed in this PhD thesis.

I wish to thank Prof. Paolo Pinton and his research group (University of Ferrara, Italy) for their precious suggestions during the development of this PhD project and for performing mitochondrial analysis experiments.

I thank Dr. Miriam Capri and Dr. Rita Ostan (University of Bologna, Italy) for kindly performing flow cytometry experiments.

I am also grateful to Prof. Natalia Calonghi and Dr. Francesco Formaggio (University of Bologna) for kindly and patiently providing confocal microscopy assistance.

I deeply thank my supervisor Barbara Monti for her valuable and unconditional support, mentoring and assistance during my PhD and the development of this PhD thesis.

And last but not least, a special thank you goes to my current laboratory colleagues Dr. Luis Emiliano Pena Altamira, Prof. Antonio Contestabile, Prof. Marco Virgili, Miss Monia Bentivogli and Miss Eleonora Poeta, for always supporting me.

BIBLIOGRAPHY

1. Falk MJ, Li D, Gai X, et al. AGC1 Deficiency Causes Infantile Epilepsy, Abnormal Myelination, and Reduced N-Acetylaspartate. *JIMD Rep.* 2014;14:77-85.
2. Wibom R, Lasorsa FM, Tohonen V, et al. AGC1 deficiency associated with global cerebral hypomyelination. *N Engl J Med.* 2009;361(5):489-495.
3. Diemel LT, Jackson SJ, Cuzner ML. Role for TGF-beta1, FGF-2 and PDGF-AA in a myelination of CNS aggregate cultures enriched with macrophages. *J Neurosci Res.* 2003;74(6):858-867.
4. Campbell GR, Mahad DJ. Metabolic support of axons by oligodendrocytes: Implications for multiple sclerosis. *Mult Scler Relat Disord.* 2014;3(1):28-30.
5. Morato L, Bertini E, Verrigni D, et al. Mitochondrial dysfunction in central nervous system white matter disorders. *Glia.* 2014;62(11):1878-1894.
6. Witte ME, Mahad DJ, Lassmann H, van Horssen J. Mitochondrial dysfunction contributes to neurodegeneration in multiple sclerosis. *Trends Mol Med.* 2014;20(3):179-187.
7. Pebay-Peyroula E, Brandolin G. Nucleotide exchange in mitochondria: insight at a molecular level. *Curr Opin Struct Biol.* 2004;14(4):420-425.
8. del Arco A, Satrustegui J. Molecular cloning of Aralar, a new member of the mitochondrial carrier superfamily that binds calcium and is present in human muscle and brain. *J Biol Chem.* 1998;273(36):23327-23334.
9. Kobayashi K, Sinasac DS, Iijima M, et al. The gene mutated in adult-onset type II citrullinaemia encodes a putative mitochondrial carrier protein. *Nat Genet.* 1999;22(2):159-163.
10. Del Arco A, Agudo M, Satrustegui J. Characterization of a second member of the subfamily of calcium-binding mitochondrial carriers expressed in human non-excitable tissues. *Biochem J.* 2000;345 Pt 3:725-732.
11. Sanz R, del Arco A, Ayuso C, Ramos C, Satrustegui J. Assignment of the calcium-binding mitochondrial carrier Aralar1 gene (SLC25A12) to human chromosome band 2q31 by in situ hybridization. *Cytogenet Cell Genet.* 2000;89(3-4):143-144.
12. Sinasac DS, Crackower MA, Lee JR, et al. Genomic structure of the adult-onset type II citrullinemia gene, SLC25A13, and cloning and expression of its mouse homologue. *Genomics.* 1999;62(2):289-292.
13. Cavero S, Vozza A, del Arco A, et al. Identification and metabolic role of the mitochondrial aspartate-glutamate transporter in Saccharomyces cerevisiae. *Mol Microbiol.* 2003;50(4):1257-1269.
14. Amoedo ND, Punzi G, Obre E, et al. AGC1/2, the mitochondrial aspartate-glutamate carriers. *Biochim Biophys Acta.* 2016;1863(10):2394-2412.
15. Ramos M, del Arco A, Pardo B, et al. Developmental changes in the Ca2+-regulated mitochondrial aspartate-glutamate carrier aralar1 in brain and prominent expression in the spinal cord. *Brain Res Dev Brain Res.* 2003;143(1):33-46.
16. LaNoue KF, Schoolwerth AC. Metabolite transport in mitochondria. *Annu Rev Biochem.* 1979;48:871-922.

17. Palmieri L, Pardo B, Lasorsa FM, et al. Citrin and aralar1 are Ca(2+)-stimulated aspartate/glutamate transporters in mitochondria. *EMBO J.* 2001;20(18):5060-5069.
18. Urenjak J, Williams SR, Gadian DG, Noble M. Proton nuclear magnetic resonance spectroscopy unambiguously identifies different neural cell types. *J Neurosci.* 1993;13(3):981-989.
19. Bjartmar C, Battistuta J, Terada N, Dupree E, Trapp BD. N-acetylaspartate is an axon-specific marker of mature white matter in vivo: a biochemical and immunohistochemical study on the rat optic nerve. *Ann Neurol.* 2002;51(1):51-58.
20. Ariyannur PS, Moffett JR, Manickam P, et al. Methamphetamine-induced neuronal protein NAT8L is the NAA biosynthetic enzyme: implications for specialized acetyl coenzyme A metabolism in the CNS. *Brain Res.* 2010;1335:1-13.
21. Wiame E, Tyteca D, Pierrot N, et al. Molecular identification of aspartate N-acetyltransferase and its mutation in hypoacetylaspartia. *Biochem J.* 2009;425(1):127-136.
22. Huang W, Wang H, Kekuda R, et al. Transport of N-acetylaspartate by the Na(+)-dependent high-affinity dicarboxylate transporter NaDC3 and its relevance to the expression of the transporter in the brain. *J Pharmacol Exp Ther.* 2000;295(1):392-403.
23. Moffett JR, Ross B, Arun P, Madhavarao CN, Namboodiri AM. N-Acetylaspartate in the CNS: from neurodiagnostics to neurobiology. *Prog Neurobiol.* 2007;81(2):89-131.
24. Sakurai T, Ramoz N, Barreto M, et al. Slc25a12 disruption alters myelination and neurofilaments: a model for a hypomyelination syndrome and childhood neurodevelopmental disorders. *Biol Psychiatry.* 2010;67(9):887-894.
25. Ramoz N, Reichert JG, Smith CJ, et al. Linkage and association of the mitochondrial aspartate/glutamate carrier SLC25A12 gene with autism. *Am J Psychiatry.* 2004;161(4):662-669.
26. Segurado R, Conroy J, Meally E, Fitzgerald M, Gill M, Gallagher L. Confirmation of association between autism and the mitochondrial aspartate/glutamate carrier SLC25A12 gene on chromosome 2q31. *Am J Psychiatry.* 2005;162(11):2182-2184.
27. Turunen JA, Rehnstrom K, Kilpinen H, Kuokkanen M, Kempas E, Ylisaukko-Oja T. Mitochondrial aspartate/glutamate carrier SLC25A12 gene is associated with autism. *Autism Res.* 2008;1(3):189-192.
28. Palmieri L, Papaleo V, Porcelli V, et al. Altered calcium homeostasis in autism-spectrum disorders: evidence from biochemical and genetic studies of the mitochondrial aspartate/glutamate carrier AGC1. *Mol Psychiatry.* 2010;15(1):38-52.
29. Rabionet R, McCauley JL, Jaworski JM, et al. Lack of association between autism and SLC25A12. *Am J Psychiatry.* 2006;163(5):929-931.
30. Blasi F, Bacchelli E, Carone S, et al. SLC25A12 and CMYA3 gene variants are not associated with autism in the IMGSAC multiplex family sample. *Eur J Hum Genet.* 2006;14(1):123-126.
31. Steen RG, Hamer RM, Lieberman JA. Measurement of brain metabolites by 1H magnetic resonance spectroscopy in patients with schizophrenia: a systematic review and meta-analysis. *Neuropsychopharmacology.* 2005;30(11):1949-1962.
32. Tsai SJ. Central N-acetyl aspartylglutamate deficit: a possible pathogenesis of schizophrenia. *Med Sci Monit.* 2005;11(9):HY39-45.
33. Flynn SW, Lang DJ, Mackay AL, et al. Abnormalities of myelination in schizophrenia detected in vivo with MRI, and post-mortem with analysis of oligodendrocyte proteins. *Mol Psychiatry.* 2003;8(9):811-820.

34. Harrison PJ, Weinberger DR. Schizophrenia genes, gene expression, and neuropathology: on the matter of their convergence. *Mol Psychiatry.* 2005;10(1):40-68; image 45.
35. Jalil MA, Begum L, Contreras L, et al. Reduced N-acetylaspartate levels in mice lacking aralar, a brain- and muscle-type mitochondrial aspartate-glutamate carrier. *J Biol Chem.* 2005;280(35):31333-31339.
36. Ramos M, Pardo B, Llorente-Folch I, Saheki T, Del Arco A, Satrustegui J. Deficiency of the mitochondrial transporter of aspartate/glutamate aralar/AGC1 causes hypomyelination and neuronal defects unrelated to myelin deficits in mouse brain. *J Neurosci Res.* 2011;89(12):2008-2017.
37. Satrustegui J, Pardo B, Del Arco A. Mitochondrial transporters as novel targets for intracellular calcium signaling. *Physiol Rev.* 2007;87(1):29-67.
38. Pino A, Fumagalli G, Bifari F, Decimo I. New neurons in adult brain: distribution, molecular mechanisms and therapies. *Biochem Pharmacol.* 2017;141:4-22.
39. Haston KM, Finkbeiner S. Clinical Trials in a Dish: The Potential of Pluripotent Stem Cells to Develop Therapies for Neurodegenerative Diseases. *Annu Rev Pharmacol Toxicol.* 2016;56:489-510.
40. Wilson SI, Edlund T. Neural induction: toward a unifying mechanism. *Nat Neurosci.* 2001;4 Suppl:1161-1168.
41. Kriegstein AR, Gotz M. Radial glia diversity: a matter of cell fate. *Glia.* 2003;43(1):37-43.
42. Sauer ME, Walker BE. Radioautographic study of interkinetic nuclear migration in the neural tube. *Proc Soc Exp Biol Med.* 1959;101(3):557-560.
43. Hayes NL, Nowakowski RS. Exploiting the dynamics of S-phase tracers in developing brain: interkinetic nuclear migration for cells entering versus leaving the S-phase. *Dev Neurosci.* 2000;22(1-2):44-55.
44. Spear PC, Erickson CA. Apical movement during interkinetic nuclear migration is a two-step process. *Dev Biol.* 2012;370(1):33-41.
45. Hochstim C, Deneen B, Lukaszewicz A, Zhou Q, Anderson DJ. Identification of positionally distinct astrocyte subtypes whose identities are specified by a homeodomain code. *Cell.* 2008;133(3):510-522.
46. Brunet JF, Ghysen A. Deconstructing cell determination: proneural genes and neuronal identity. *Bioessays.* 1999;21(4):313-318.
47. Noctor SC, Martinez-Cerdeno V, Ivic L, Kriegstein AR. Cortical neurons arise in symmetric and asymmetric division zones and migrate through specific phases. *Nat Neurosci.* 2004;7(2):136-144.
48. Noctor SC, Martinez-Cerdeno V, Kriegstein AR. Distinct behaviors of neural stem and progenitor cells underlie cortical neurogenesis. *J Comp Neurol.* 2008;508(1):28-44.
49. Kriegstein A, Alvarez-Buylla A. The glial nature of embryonic and adult neural stem cells. *Annu Rev Neurosci.* 2009;32:149-184.
50. Pringle NP, Richardson WD. A singularity of PDGF alpha-receptor expression in the dorsoventral axis of the neural tube may define the origin of the oligodendrocyte lineage. *Development.* 1993;117(2):525-533.
51. Spassky N, Goujet-Zalc C, Parmantier E, et al. Multiple restricted origin of oligodendrocytes. *J Neurosci.* 1998;18(20):8331-8343.
52. Tekki-Kessaris N, Woodruff R, Hall AC, et al. Hedgehog-dependent oligodendrocyte lineage specification in the telencephalon. *Development.* 2001;128(13):2545-2554.

53. Kessaris N, Fogarty M, Iannarelli P, Grist M, Wegner M, Richardson WD. Competing waves of oligodendrocytes in the forebrain and postnatal elimination of an embryonic lineage. *Nat Neurosci.* 2006;9(2):173-179.
54. Gorski JA, Talley T, Qiu M, Puelles L, Rubenstein JL, Jones KR. Cortical excitatory neurons and glia, but not GABAergic neurons, are produced in the Emx1-expressing lineage. *J Neurosci.* 2002;22(15):6309-6314.
55. Altman J. Are new neurons formed in the brains of adult mammals? *Science.* 1962;135(3509):1127-1128.
56. Batiz LF, Castro MA, Burgos PV, et al. Exosomes as Novel Regulators of Adult Neurogenic Niches. *Front Cell Neurosci.* 2015;9:501.
57. Urban N, Guillemot F. Neurogenesis in the embryonic and adult brain: same regulators, different roles. *Front Cell Neurosci.* 2014;8:396.
58. Bayraktar OA, Fuentealba LC, Alvarez-Buylla A, Rowitch DH. Astrocyte development and heterogeneity. *Cold Spring Harb Perspect Biol.* 2014;7(1):a020362.
59. Capdevila C, Rodriguez Vazquez L, Marti J. Glioblastoma Multiforme and Adult Neurogenesis in the Ventricular-Subventricular Zone: A Review. *J Cell Physiol.* 2017;232(7):1596-1601.
60. Marti J, Santa-Cruz MC, Hervas JP. Generation and vulnerability of deep cerebellar nuclei neurons in the weaver condition along the anteroposterior and mediolateral axes. *Int J Dev Neurosci.* 2016;49:37-45.
61. Alvarez-Buylla A, Seri B, Doetsch F. Identification of neural stem cells in the adult vertebrate brain. *Brain Res Bull.* 2002;57(6):751-758.
62. Altman J, Das GD. Autoradiographic and histological evidence of postnatal hippocampal neurogenesis in rats. *J Comp Neurol.* 1965;124(3):319-335.
63. Kosaka T, Hama K. Three-dimensional structure of astrocytes in the rat dentate gyrus. *J Comp Neurol.* 1986;249(2):242-260.
64. Seri B, Garcia-Verdugo JM, Collado-Morente L, McEwen BS, Alvarez-Buylla A. Cell types, lineage, and architecture of the germinal zone in the adult dentate gyrus. *J Comp Neurol.* 2004;478(4):359-378.
65. Steiner B, Klempin F, Wang L, Kott M, Kettenmann H, Kempermann G. Type-2 cells as link between glial and neuronal lineage in adult hippocampal neurogenesis. *Glia.* 2006;54(8):805-814.
66. Palmer TD, Willhoite AR, Gage FH. Vascular niche for adult hippocampal neurogenesis. *J Comp Neurol.* 2000;425(4):479-494.
67. Filippov V, Kronenberg G, Pivneva T, et al. Subpopulation of nestin-expressing progenitor cells in the adult murine hippocampus shows electrophysiological and morphological characteristics of astrocytes. *Mol Cell Neurosci.* 2003;23(3):373-382.
68. Fukuda S, Kato F, Tozuka Y, Yamaguchi M, Miyamoto Y, Hisatsune T. Two distinct subpopulations of nestin-positive cells in adult mouse dentate gyrus. *J Neurosci.* 2003;23(28):9357-9366.
69. Gould E, Cameron HA, Daniels DC, Woolley CS, McEwen BS. Adrenal hormones suppress cell division in the adult rat dentate gyrus. *J Neurosci.* 1992;12(9):3642-3650.
70. Cameron HA, Tanapat P, Gould E. Adrenal steroids and N-methyl-D-aspartate receptor activation regulate neurogenesis in the dentate gyrus of adult rats through a common pathway. *Neuroscience.* 1998;82(2):349-354.

71. Monster TB, Janssen WM, de Jong PE, de Jong-van de Berg LT. Corticosteroid use and its association with microalbuminuria in the adult population. *Pulm Pharmacol Ther.* 2003;16(6):349-353.
72. Santarelli L, Saxe M, Gross C, et al. Requirement of hippocampal neurogenesis for the behavioral effects of antidepressants. *Science.* 2003;301(5634):805-809.
73. Emery B. Regulation of oligodendrocyte differentiation and myelination. *Science.* 2010;330(6005):779-782.
74. Tomassy GS, Dershowitz LB, Arlotta P. Diversity Matters: A Revised Guide to Myelination. *Trends Cell Biol.* 2016;26(2):135-147.
75. Ninomiya Y, Sugahara-Yamashita Y, Nakachi Y, Tokuzawa Y, Okazaki Y, Nishiyama M. Development of a rapid culture method to induce adipocyte differentiation of human bone marrow-derived mesenchymal stem cells. *Biochem Biophys Res Commun.* 2010;394(2):303-308.
76. Balsamo J, Leung T, Ernst H, Zanin MK, Hoffman S, Lilien J. Regulated binding of PTP1B-like phosphatase to N-cadherin: control of cadherin-mediated adhesion by dephosphorylation of beta-catenin. *J Cell Biol.* 1996;134(3):801-813.
77. Thibault RA, Scott Baggett L, Mikos AG, Kasper FK. Osteogenic differentiation of mesenchymal stem cells on pregenerated extracellular matrix scaffolds in the absence of osteogenic cell culture supplements. *Tissue Eng Part A.* 2010;16(2):431-440.
78. Fruttiger M, Karlsson L, Hall AC, et al. Defective oligodendrocyte development and severe hypomyelination in PDGF-A knockout mice. *Development.* 1999;126(3):457-467.
79. Sugimoto Y, Taniguchi M, Yagi T, Akagi Y, Nojyo Y, Tamamaki N. Guidance of glial precursor cell migration by secreted cues in the developing optic nerve. *Development.* 2001;128(17):3321-3330.
80. Frost EE, Zhou Z, Krasnesky K, Armstrong RC. Initiation of oligodendrocyte progenitor cell migration by a PDGF-A activated extracellular regulated kinase (ERK) signaling pathway. *Neurochem Res.* 2009;34(1):169-181.
81. Wang S, Sdrulla AD, diSibio G, et al. Notch receptor activation inhibits oligodendrocyte differentiation. *Neuron.* 1998;21(1):63-75.
82. Charles P, Hernandez MP, Stankoff B, et al. Negative regulation of central nervous system myelination by polysialylated-neural cell adhesion molecule. *Proc Natl Acad Sci U S A.* 2000;97(13):7585-7590.
83. Mi S, Miller RH, Lee X, et al. LINGO-1 negatively regulates myelination by oligodendrocytes. *Nat Neurosci.* 2005;8(6):745-751.
84. Brinkmann BG, Agarwal A, Sereda MW, et al. Neuregulin-1/ErbB signaling serves distinct functions in myelination of the peripheral and central nervous system. *Neuron.* 2008;59(4):581-595.
85. Fancy SP, Baranzini SE, Zhao C, et al. Dysregulation of the Wnt pathway inhibits timely myelination and remyelination in the mammalian CNS. *Genes Dev.* 2009;23(13):1571-1585.
86. Fu H, Cai J, Clevers H, et al. A genome-wide screen for spatially restricted expression patterns identifies transcription factors that regulate glial development. *J Neurosci.* 2009;29(36):11399-11408.
87. Demerens C, Stankoff B, Logak M, et al. Induction of myelination in the central nervous system by electrical activity. *Proc Natl Acad Sci U S A.* 1996;93(18):9887-9892.

88. Ishibashi T, Dakin KA, Stevens B, et al. Astrocytes promote myelination in response to electrical impulses. *Neuron.* 2006;49(6):823-832.
89. Bergles DE, Roberts JD, Somogyi P, Jahr CE. Glutamatergic synapses on oligodendrocyte precursor cells in the hippocampus. *Nature.* 2000;405(6783):187-191.
90. Lin SC, Bergles DE. Physiological characteristics of NG2-expressing glial cells. *J Neurocytol.* 2002;31(6-7):537-549.
91. Ziskin JL, Nishiyama A, Rubio M, Fukaya M, Bergles DE. Vesicular release of glutamate from unmyelinated axons in white matter. *Nat Neurosci.* 2007;10(3):321-330.
92. De Biase LM, Nishiyama A, Bergles DE. Excitability and synaptic communication within the oligodendrocyte lineage. *J Neurosci.* 2010;30(10):3600-3611.
93. Karadottir R, Hamilton NB, Bakiri Y, Attwell D. Spiking and nonspiking classes of oligodendrocyte precursor glia in CNS white matter. *Nat Neurosci.* 2008;11(4):450-456.
94. Wegner M. A matter of identity: transcriptional control in oligodendrocytes. *J Mol Neurosci.* 2008;35(1):3-12.
95. Ye F, Chen Y, Hoang T, et al. HDAC1 and HDAC2 regulate oligodendrocyte differentiation by disrupting the beta-catenin-TCF interaction. *Nat Neurosci.* 2009;12(7):829-838.
96. Shen S, Li J, Casaccia-Bonnefil P. Histone modifications affect timing of oligodendrocyte progenitor differentiation in the developing rat brain. *J Cell Biol.* 2005;169(4):577-589.
97. Zhao X, He X, Han X, et al. MicroRNA-mediated control of oligodendrocyte differentiation. *Neuron.* 2010;65(5):612-626.
98. Shin D, Shin JY, McManus MT, Ptacek LJ, Fu YH. Dicer ablation in oligodendrocytes provokes neuronal impairment in mice. *Ann Neurol.* 2009;66(6):843-857.
99. Budde H, Schmitt S, Fitzner D, Opitz L, Salinas-Riester G, Simons M. Control of oligodendroglial cell number by the miR-17-92 cluster. *Development.* 2010;137(13):2127-2132.
100. Palazuelos J, Klingener M, Aguirre A. TGFbeta signaling regulates the timing of CNS myelination by modulating oligodendrocyte progenitor cell cycle exit through SMAD3/4/FoxO1/Sp1. *J Neurosci.* 2014;34(23):7917-7930.
101. Siegel PM, Massague J. Cytostatic and apoptotic actions of TGF-beta in homeostasis and cancer. *Nat Rev Cancer.* 2003;3(11):807-821.
102. Reynolds BA, Weiss S. Generation of neurons and astrocytes from isolated cells of the adult mammalian central nervous system. *Science.* 1992;255(5052):1707-1710.
103. Tropepe V, Hitoshi S, Sirard C, Mak TW, Rossant J, van der Kooy D. Direct neural fate specification from embryonic stem cells: a primitive mammalian neural stem cell stage acquired through a default mechanism. *Neuron.* 2001;30(1):65-78.
104. Bez A, Corsini E, Curti D, et al. Neurosphere and neurosphere-forming cells: morphological and ultrastructural characterization. *Brain Res.* 2003;993(1-2):18-29.
105. Reynolds BA, Weiss S. Clonal and population analyses demonstrate that an EGF-responsive mammalian embryonic CNS precursor is a stem cell. *Dev Biol.* 1996;175(1):1-13.
106. Gritti A, Parati EA, Cova L, et al. Multipotential stem cells from the adult mouse brain proliferate and self-renew in response to basic fibroblast growth factor. *J Neurosci.* 1996;16(3):1091-1100.
107. Tropepe V, Sibilia M, Ciruna BG, Rossant J, Wagner EF, van der Kooy D. Distinct neural stem cells proliferate in response to EGF and FGF in the developing mouse telencephalon. *Dev Biol.* 1999;208(1):166-188.

108. Rietze RL, Valcanis H, Brooker GF, Thomas T, Voss AK, Bartlett PF. Purification of a pluripotent neural stem cell from the adult mouse brain. *Nature.* 2001;412(6848):736-739.
109. Uchida N, Buck DW, He D, et al. Direct isolation of human central nervous system stem cells. *Proc Natl Acad Sci U S A.* 2000;97(26):14720-14725.
110. Jensen JB, Parmar M. Strengths and limitations of the neurosphere culture system. *Mol Neurobiol.* 2006;34(3):153-161.
111. Babu H, Claasen JH, Kannan S, Runker AE, Palmer T, Kempermann G. A protocol for isolation and enriched monolayer cultivation of neural precursor cells from mouse dentate gyrus. *Front Neurosci.* 2011;5:89.
112. Azari H, Rahman M, Sharififar S, Reynolds BA. Isolation and expansion of the adult mouse neural stem cells using the neurosphere assay. *J Vis Exp.* 2010(45).
113. Campos LS, Leone DP, Relvas JB, et al. Beta1 integrins activate a MAPK signalling pathway in neural stem cells that contributes to their maintenance. *Development.* 2004;131(14):3433-3444.
114. Santa-Olalla J, Baizabal JM, Fregoso M, del Carmen Cardenas M, Covarrubias L. The in vivo positional identity gene expression code is not preserved in neural stem cells grown in culture. *Eur J Neurosci.* 2003;18(5):1073-1084.
115. Irvin DK, Dhaka A, Hicks C, Weinmaster G, Kornblum HI. Extrinsic and intrinsic factors governing cell fate in cortical progenitor cultures. *Dev Neurosci.* 2003;25(2-4):162-172.
116. Evans MJ, Kaufman MH. Establishment in culture of pluripotential cells from mouse embryos. *Nature.* 1981;292(5819):154-156.
117. Martin GR. Isolation of a pluripotent cell line from early mouse embryos cultured in medium conditioned by teratocarcinoma stem cells. *Proc Natl Acad Sci U S A.* 1981;78(12):7634-7638.
118. Takahashi K, Yamanaka S. Induction of pluripotent stem cells from mouse embryonic and adult fibroblast cultures by defined factors. *Cell.* 2006;126(4):663-676.
119. Robinton DA, Daley GQ. The promise of induced pluripotent stem cells in research and therapy. *Nature.* 2012;481(7381):295-305.
120. Wernig M, Zhao JP, Pruszak J, et al. Neurons derived from reprogrammed fibroblasts functionally integrate into the fetal brain and improve symptoms of rats with Parkinson's disease. *Proc Natl Acad Sci U S A.* 2008;105(15):5856-5861.
121. Choi HW, Hong YJ, Kim JS, et al. In vivo differentiation of induced pluripotent stem cells into neural stem cells by chimera formation. *PLoS One.* 2017;12(1):e0170735.
122. Chamberlain KA, Nanescu SE, Psachoulia K, Huang JK. Oligodendrocyte regeneration: Its significance in myelin replacement and neuroprotection in multiple sclerosis. *Neuropharmacology.* 2016;110(Pt B):633-643.
123. Bockbrader K, Feng Y. Essential function, sophisticated regulation and pathological impact of the selective RNA-binding protein QKI in CNS myelin development. *Future Neurol.* 2008;3(6):655-668.
124. Profilo E, Pena-Altamira LE, Corricelli M, et al. Down-regulation of the mitochondrial aspartate-glutamate carrier isoform 1 AGC1 inhibits proliferation and N-acetylaspartate synthesis in Neuro2A cells. *Biochim Biophys Acta.* 2017;1863(6):1422-1435.
125. Dahlin M, Martin DA, Hedlund Z, Jonsson M, von Dobeln U, Wedell A. The ketogenic diet compensates for AGC1 deficiency and improves myelination. *Epilepsia.* 2015;56(11):e176-181.
126. Baranano KW, Hartman AL. The ketogenic diet: uses in epilepsy and other neurologic illnesses. *Curr Treat Options Neurol.* 2008;10(6):410-419.

127. Nave KA. Myelination and support of axonal integrity by glia. *Nature.* 2010;468(7321):244-252.
128. Connor JR, Menzies SL, St Martin SM, Mufson EJ. Cellular distribution of transferrin, ferritin, and iron in normal and aged human brains. *J Neurosci Res.* 1990;27(4):595-611.
129. Connor JR, Menzies SL. Cellular management of iron in the brain. *J Neurol Sci.* 1995;134 Suppl:33-44.
130. Dixon SJ, Lemberg KM, Lamprecht MR, et al. Ferroptosis: an iron-dependent form of nonapoptotic cell death. *Cell.* 2012;149(5):1060-1072.
131. Dixon SJ, Patel DN, Welsch M, et al. Pharmacological inhibition of cystine-glutamate exchange induces endoplasmic reticulum stress and ferroptosis. *Elife.* 2014;3:e02523.
132. Schubert D, Chevion M. The role of iron in beta amyloid toxicity. *Biochem Biophys Res Commun.* 1995;216(2):702-707.
133. Liu B, Moloney A, Meehan S, et al. Iron promotes the toxicity of amyloid beta peptide by impeding its ordered aggregation. *J Biol Chem.* 2011;286(6):4248-4256.
134. Mi S, Hu B, Hahm K, et al. LINGO-1 antagonist promotes spinal cord remyelination and axonal integrity in MOG-induced experimental autoimmune encephalomyelitis. *Nat Med.* 2007;13(10):1228-1233.
135. Najm FJ, Madhavan M, Zaremba A, et al. Drug-based modulation of endogenous stem cells promotes functional remyelination in vivo. *Nature.* 2015;522(7555):216-220.
136. Wang S, Bates J, Li X, et al. Human iPSC-derived oligodendrocyte progenitor cells can myelinate and rescue a mouse model of congenital hypomyelination. *Cell Stem Cell.* 2013;12(2):252-264.
137. Contreras L. Role of AGC1/aralar in the metabolic synergies between neuron and glia. *Neurochem Int.* 2015;88:38-46.
138. Vozza A, Parisi G, De Leonardis F, et al. UCP2 transports C4 metabolites out of mitochondria, regulating glucose and glutamine oxidation. *Proc Natl Acad Sci U S A.* 2014;111(3):960-965.
139. Nusse M, Beisker W, Hoffmann C, Tarnok A. Flow cytometric analysis of G1- and G2/M-phase subpopulations in mammalian cell nuclei using side scatter and DNA content measurements. *Cytometry.* 1990;11(7):813-821.
140. Grove BD, Bruchey AK. Intracellular distribution of gravin, a PKA and PKC binding protein, in vascular endothelial cells. *J Vasc Res.* 2001;38(2):163-175.
141. Lasorsa FM, Pinton P, Palmieri L, Fiermonte G, Rizzuto R, Palmieri F. Recombinant expression of the Ca(2+)-sensitive aspartate/glutamate carrier increases mitochondrial ATP production in agonist-stimulated Chinese hamster ovary cells. *J Biol Chem.* 2003;278(40):38686-38692.
142. Brunner C, Lassmann H, Waehneldt TV, Matthieu JM, Linington C. Differential ultrastructural localization of myelin basic protein, myelin/oligodendroglial glycoprotein, and 2',3'-cyclic nucleotide 3'-phosphodiesterase in the CNS of adult rats. *J Neurochem.* 1989;52(1):296-304.
143. Prohaska JR, Clark DA, Wells WW. Improved rapidity and precision in the determination of brain 2',3'-cyclic nucleotide 3'-phosphohydrolase. *Anal Biochem.* 1973;56(1):275-282.
144. Walker TL, Kempermann G. One mouse, two cultures: isolation and culture of adult neural stem cells from the two neurogenic zones of individual mice. *J Vis Exp.* 2014(84):e51225.
145. Hagihara H, Toyama K, Yamasaki N, Miyakawa T. Dissection of hippocampal dentate gyrus from adult mouse. *J Vis Exp.* 2009(33).
146. Choudhry P. High-Throughput Method for Automated Colony and Cell Counting by Digital Image Analysis Based on Edge Detection. *PLoS One.* 2016;11(2):e0148469.

147. Nicaise AM, Banda E, Guzzo RM, et al. iPS-derived neural progenitor cells from PPMS patients reveal defect in myelin injury response. *Exp Neurol.* 2017;288:114-121.
148. Lowry OH, Rosebrough NJ, Farr AL, Randall RJ. Protein measurement with the Folin phenol reagent. *J Biol Chem.* 1951;193(1):265-275.
149. Bryan BA, Cai Y, Liu M. The Rho-family guanine nucleotide exchange factor GEFT enhances retinoic acid- and cAMP-induced neurite outgrowth. *J Neurosci Res.* 2006;83(7):1151-1159.
150. Hendzel MJ, Wei Y, Mancini MA, et al. Mitosis-specific phosphorylation of histone H3 initiates primarily within pericentromeric heterochromatin during G2 and spreads in an ordered fashion coincident with mitotic chromosome condensation. *Chromosoma.* 1997;106(6):348-360.
151. Chadee DN, Hendzel MJ, Tylipski CP, et al. Increased Ser-10 phosphorylation of histone H3 in mitogen-stimulated and oncogene-transformed mouse fibroblasts. *J Biol Chem.* 1999;274(35):24914-24920.
152. Crosio C, Fimia GM, Loury R, et al. Mitotic phosphorylation of histone H3: spatio-temporal regulation by mammalian Aurora kinases. *Mol Cell Biol.* 2002;22(3):874-885.
153. Li LT, Jiang G, Chen Q, Zheng JN. Ki67 is a promising molecular target in the diagnosis of cancer (review). *Mol Med Rep.* 2015;11(3):1566-1572.
154. Sturrock RR. Identification of mitotic oligodendrocytes in semithin sections of the developing mouse corpus callosum and hippocampal commissure. *J Anat.* 1983;137 (Pt 1):47-55.
155. Xing YL, Roth PT, Stratton JA, et al. Adult neural precursor cells from the subventricular zone contribute significantly to oligodendrocyte regeneration and remyelination. *J Neurosci.* 2014;34(42):14128-14146.
156. Takebayashi H, Nabeshima Y, Yoshida S, Chisaka O, Ikenaka K, Nabeshima Y. The basic helix-loop-helix factor olig2 is essential for the development of motoneuron and oligodendrocyte lineages. *Curr Biol.* 2002;12(13):1157-1163.
157. Baumann N, Pham-Dinh D. Biology of oligodendrocyte and myelin in the mammalian central nervous system. *Physiol Rev.* 2001;81(2):871-927.
158. Zhang J, Jiao J. Molecular Biomarkers for Embryonic and Adult Neural Stem Cell and Neurogenesis. *Biomed Res Int.* 2015;2015:727542.
159. Eng LF. Glial fibrillary acidic protein (GFAP): the major protein of glial intermediate filaments in differentiated astrocytes. *J Neuroimmunol.* 1985;8(4-6):203-214.
160. Lee S, Lee CM, Kim SC. Adult human pancreas-derived cells expressing stage-specific embryonic antigen 4 differentiate into Sox9-expressing and Ngn3-expressing pancreatic ducts in vivo. *Stem Cell Res Ther.* 2016;7(1):162.
161. Gomez-Galan M, Makarova J, Llorente-Folch I, et al. Altered postnatal development of cortico-hippocampal neuronal electric activity in mice deficient for the mitochondrial aspartate-glutamate transporter. *J Cereb Blood Flow Metab.* 2012;32(2):306-317.
162. Ayanlaja AA, Xiong Y, Gao Y, et al. Distinct Features of Doublecortin as a Marker of Neuronal Migration and Its Implications in Cancer Cell Mobility. *Front Mol Neurosci.* 2017;10:199.
163. Hart IK, Richardson WD, Bolsover SR, Raff MC. PDGF and intracellular signaling in the timing of oligodendrocyte differentiation. *J Cell Biol.* 1989;109(6 Pt 2):3411-3417.
164. Noble M, Murray K, Stroobant P, Waterfield MD, Riddle P. Platelet-derived growth factor promotes division and motility and inhibits premature differentiation of the oligodendrocyte/type-2 astrocyte progenitor cell. *Nature.* 1988;333(6173):560-562.

165. Heo G, Kim SH, Chang MJ. Effect of ketogenic diet and other dietary therapies on anti-epileptic drug concentrations in patients with epilepsy. *J Clin Pharm Ther.* 2017;42(6):758-764.
166. Phiel CJ, Klein PS. Molecular targets of lithium action. *Annu Rev Pharmacol Toxicol.* 2001;41:789-813.
167. Phiel CJ, Zhang F, Huang EY, Guenther MG, Lazar MA, Klein PS. Histone deacetylase is a direct target of valproic acid, a potent anticonvulsant, mood stabilizer, and teratogen. *J Biol Chem.* 2001;276(39):36734-36741.
168. Wu S, Zheng SD, Huang HL, et al. Lithium down-regulates histone deacetylase 1 (HDAC1) and induces degradation of mutant huntingtin. *J Biol Chem.* 2013;288(49):35500-35510.
169. Koch HB, Zhang R, Verdoodt B, et al. Large-scale identification of c-MYC-associated proteins using a combined TAP/MudPIT approach. *Cell Cycle.* 2007;6(2):205-217.